Discrete scale invariance and log-periodicity

in

Rupture, growth processes, Turbulence, finance…

TURBULENCE AND DISCRETE SCALE INVARIANCE

• *fully-developed turbulence* refers to a unique state of turbulent behavior believed to occur for sufficiently large but finite Reynolds number (Re).

• This state is characterised by local isotropy and homogeneity and associated universal behaviour of statistical properties, such as moments of the longitudinal velocity difference

$$v_r \equiv (\vec{v}(\vec{x}+\vec{r}) - \vec{v}(\vec{x})) \cdot \vec{r}/|\vec{r}| \ .$$

DIMENSIONAL ANALYSIS

Second order longitudinal structure function

$$D_{LL}(r) \equiv \left\langle (v_r)^2 \right\rangle \ .$$

- In K41, $D_{LL}(r)$ has the form

$$D_{LL}(r) = C_K(\bar{\epsilon} r)^{2/3} \ ,$$

where r lies in the inertial range, and $\bar{\epsilon}$ is the mean rate of energy dissipation per unit mass.

- Dimensional analysis shows

$$D_{LL}(r) = (\bar{\epsilon} r)^{2/3} F(\mathrm{Re}, r/L) \ ,$$

where $F(x, y)$ is a universal function to be determined, L is the external or integral scale and r is always considered to lie in the inertial range.

• Kolmogorov's assumption: $\mathrm{Re} \to \infty$ and $r/L \to 0$ leads to $F(x, y) \to C_K$.

Complete similarity of the first kind with respect to the variables Re and r/L.

Similarity of the second and third kinds

• The existence of the limit of

$$F(\mathrm{Re}, r/L \to 0)$$

has been questioned (L.D. Landau, A.M. Obukhov) due to intermittency — fluctuations of the energy dissipation rate about its mean value $\bar{\epsilon}$.

• Barenblatt's classification leads to the possibility of *Incomplete similarity* in the variable r/L. This would require the non-existence of a finite and non-zero limit of $F(\mathrm{Re}, r/L)$ as $r/L \to 0$, and leads in the simplest case to the form

$$D_{LL}(r) = C_K(\bar{\epsilon}r)^{2/3}\left(\frac{r}{L}\right)^{\alpha} ,$$

where α is the so-called intermittency exponent, believed to be small and non-negative.

1. if α is real $\to$ similarity of the second kind;
2. if α is complex,

$$D_{LL}(r) = C_K(\bar{\epsilon}r)^{2/3}\left(\frac{r}{L}\right)^{\alpha_R} \cos[\alpha_I \log(r/L)] .$$

There is no limit of $F(\mathrm{Re}, r/L)$ but rather accelerated oscillations. (Dubrulle, 1997)

D. Sornette, Discrete scale invariance in turbulence? U. Frisch (ed.), Advances in Turbulence VII, 251-254 (Kluwer Academic Publishers, The Netherlands, 1998) (http://xxx.lanl.gov/abs/cond-mat/9802121)

• To our knowledge, Novikov has been the first to point in 1966 that structure factors in turbulence should contain log-periodic oscillations
E.A. Novikov, Dokl.Akad.Nauk SSSR 168/6, 1279 (1966);
E.A. Novikov, The effect of intermittency on statistical characteristics of turbulence and scale similarity of breakdown coefficients, Phys.Fluids A 2, 814-820 (1990).

• if an unstable eddy in turbulent flow typically breaks up into two or three smaller eddies, but not into 10 or 20 eddies, then one can suspect the existence of a preferable scale factor, hence the log-periodic oscillations $\rightarrow$ existence of a prefered ratio in the cascade from large eddies to small ones.

Multi-scale descriptions are needed to understand complex systems

scaling laws, fractals and trees, renormalization, multi-grid...

Different physics at different scales?

Examples :

1. weather - patterns on all scales (cyclones, tornadoes, dust devils);
2. earthquakes and fault systems;
3. proteins - secondary, tertiary, quaternary structure;
4. physiology - molecules, cells, tissues, systems;
5. brain - hemispheres, lobes, functional regions, etc.;
6. economy/society : from currency blocks down to traders.

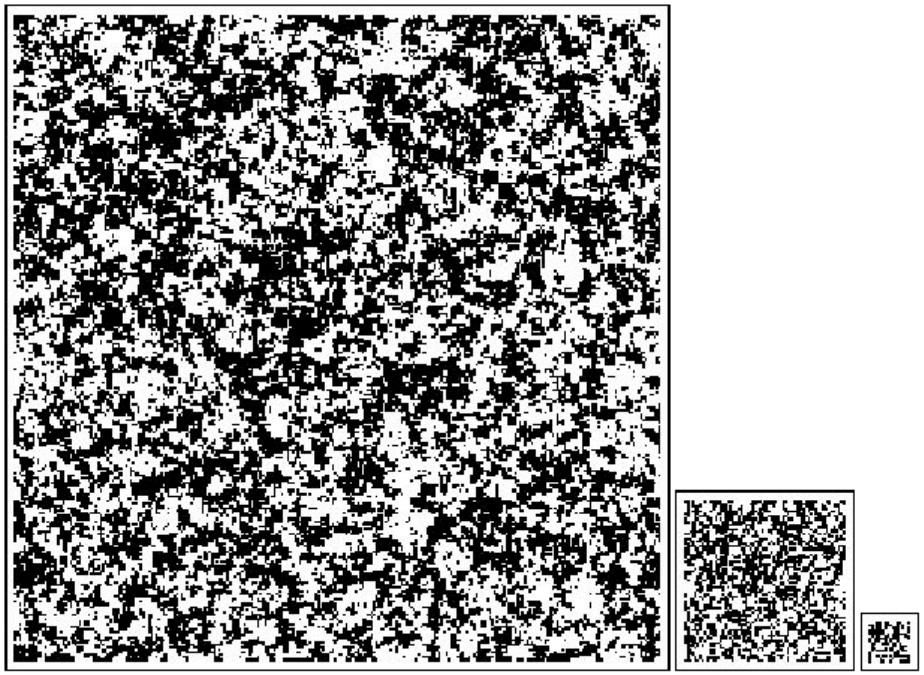

Disorder

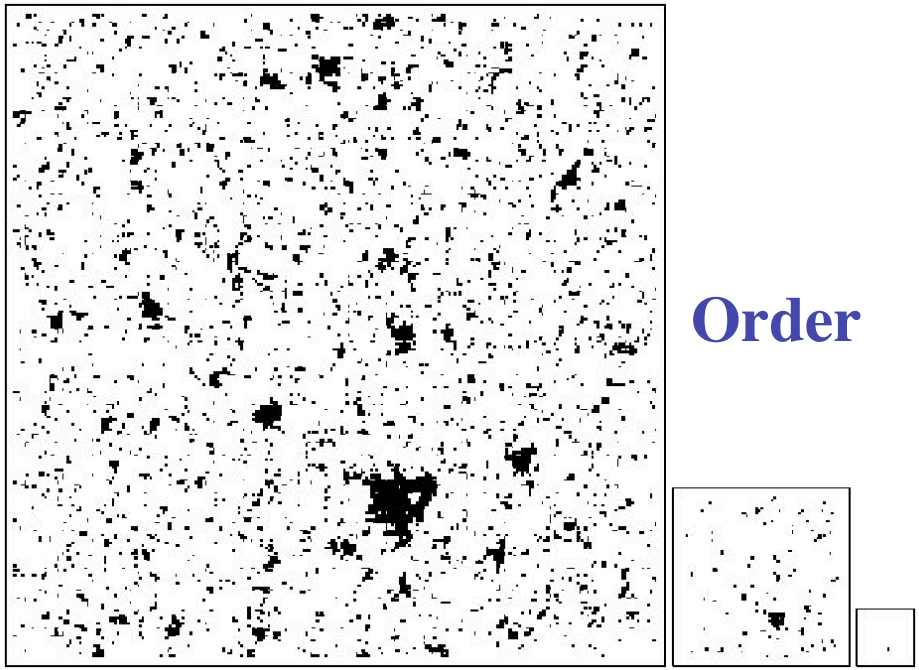

Order

Renormalization group:
Organization of the description scale by scale

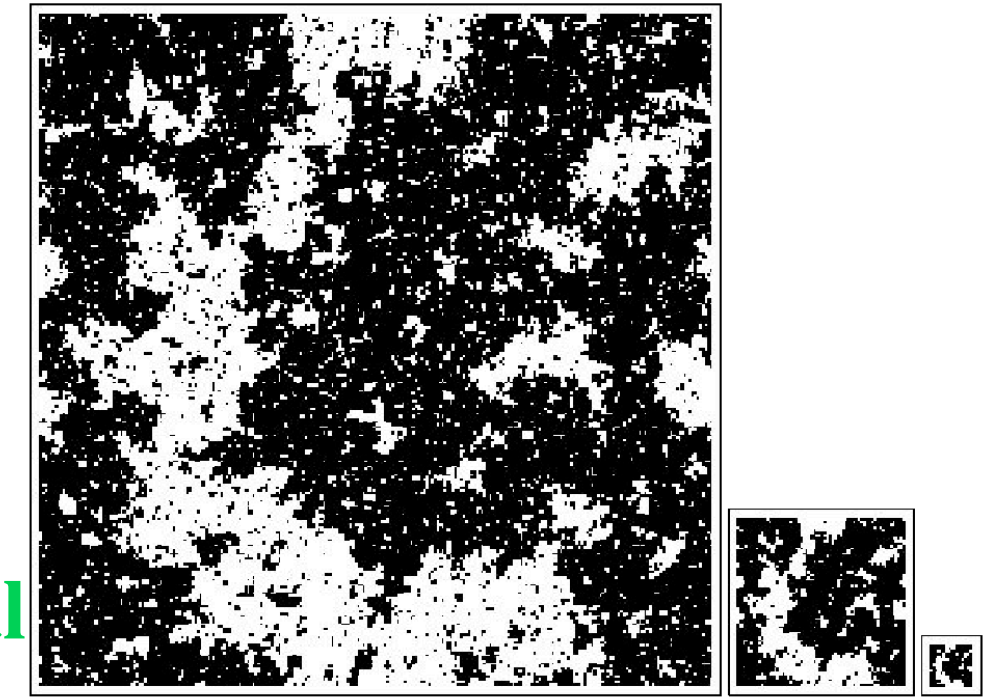

Critical

RG flow near a nontrivial fixed point

Scaling fields u_1 and u_2 are ***irrelevant***,
u_3 is a ***relevant*** scaling field:

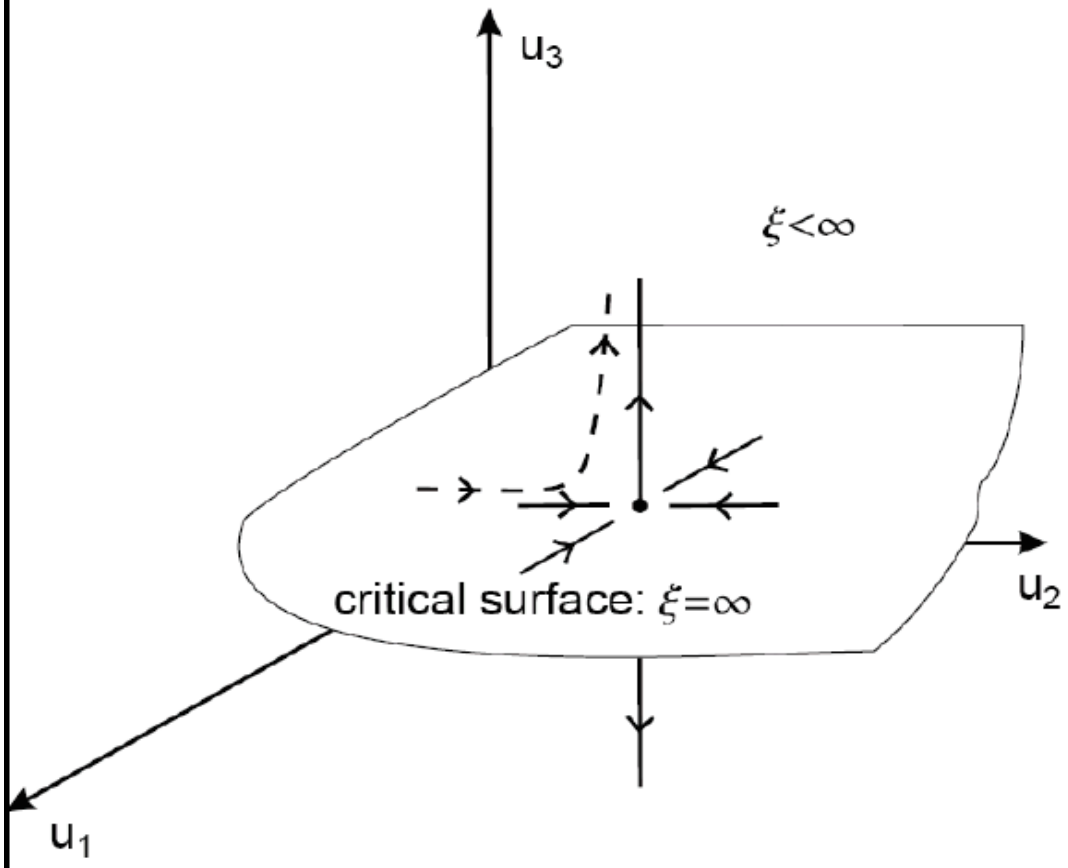

Surface of inflowing paths is the ***critical surface***. All models on critical surface are governed by nontrivial fixed point.

- All critical models are at a continuous phase transition with $\xi = \infty$, since $\xi = \infty$ asymptotically, and ξ can only decrease under RG, $\xi^{(n)} = b^{-n}\xi^{(0)}$, everywhere $\xi = \infty$ along any trajectory on critical surface.
  $\xi < \infty$ off critical surface.
- Phase transition exhibited by ***all*** critical models governed by $\mathcal{H}^\star$, with arbitrary values of irrelevant parameters.
  $\rightarrow$ ***Universality.***
- Critical surface acts as a separatrix dividing parameter space.

Hierarchies: different physics at different scales

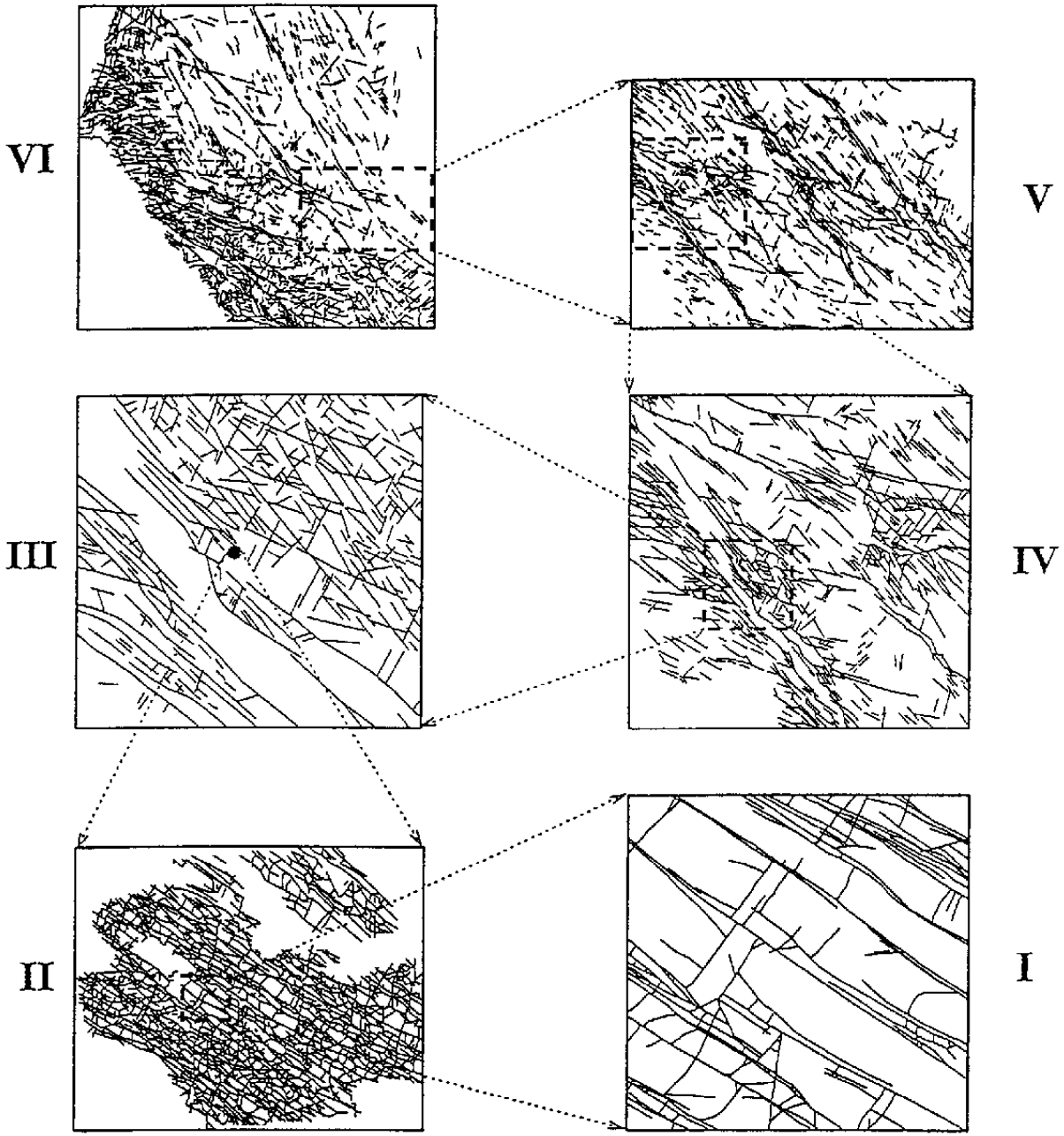

Series of fracture networks sampled from the field (1:1) (plate I of size about one meter across) to the continental scale (1:1,000,000) (plate VI of size about 400 km accross), based on field mapping, interpretation (checked on the ground) and digitization of photographs taken from a helicopter, classical aerial photography and satellite images on the western Arabian plate.

G. Ouillon, C. Castaing and D. Sornette, "Hierarchical scaling of faulting", J. Geophys. Res. 101, B3, 5477-5487, March 10 (1996)

Hierarchy of scales: FRACTALS

1) $d \in N$ Euclid (ca. 325-270 BC)

2) $d \in R$ Mandelbrot (1960-1980)

3) $d \in C$

Discrete scale invariance
Complex fractal dimension
Log-periodicity

Preferred scaling ratio is 3

$$D(n) = \ln 4/\ln 3 + i\, 2\pi n/\ln 3$$

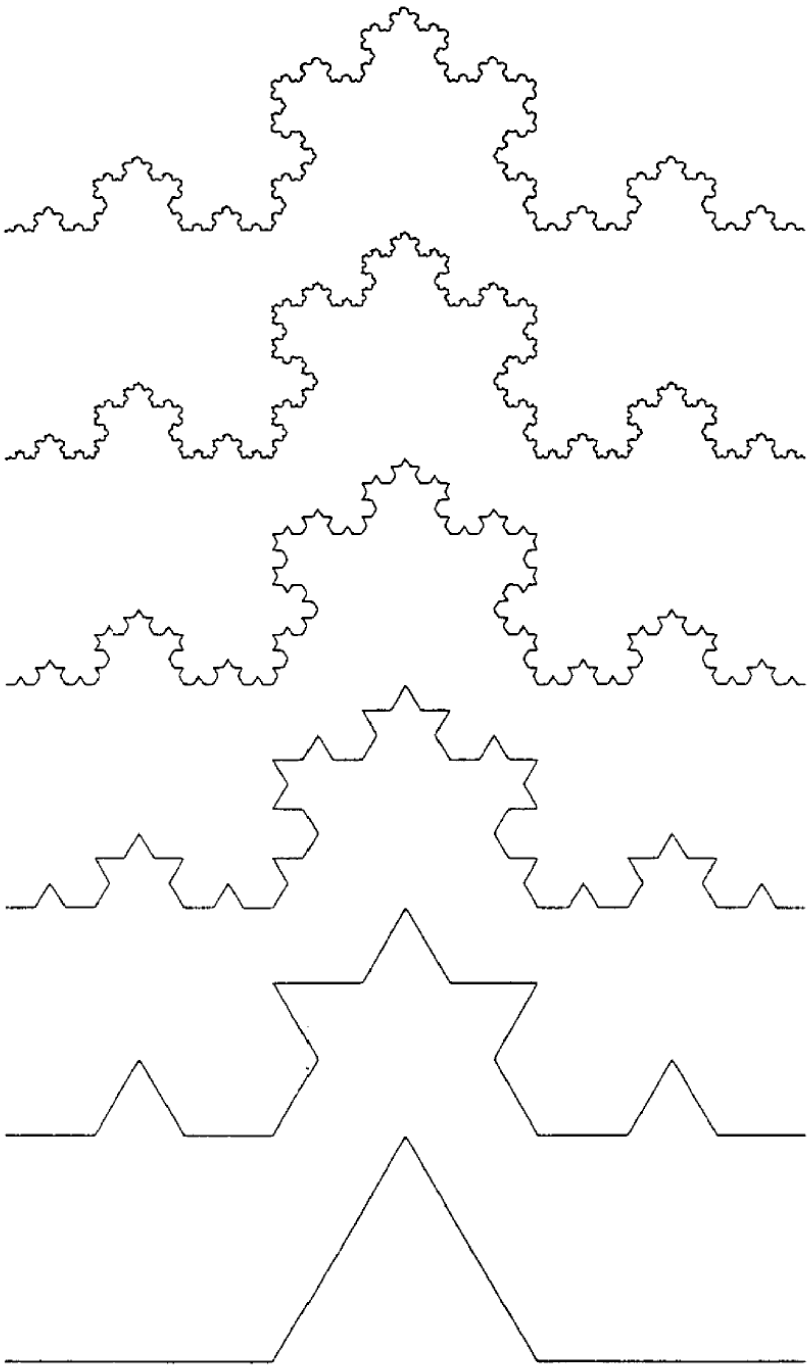

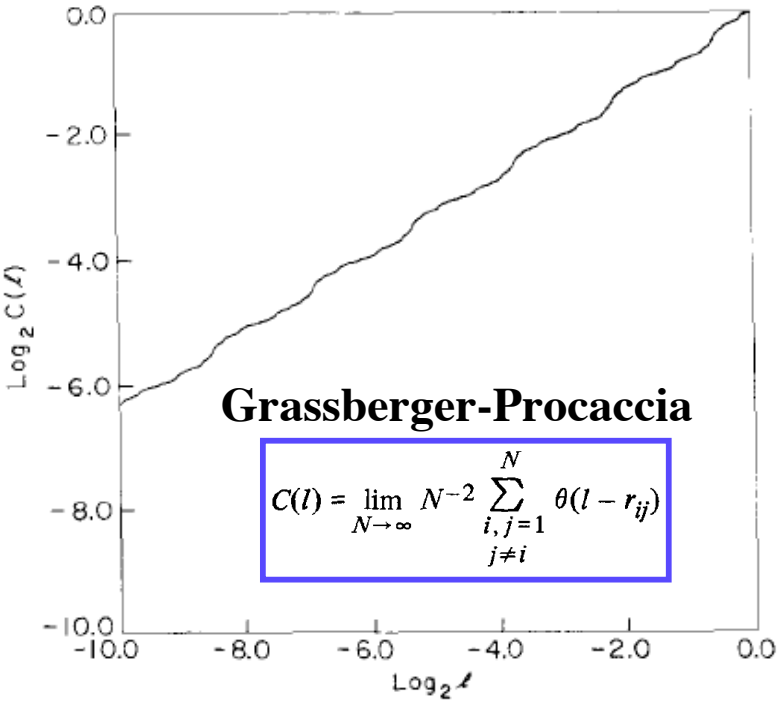

Grassberger-Procaccia

$$C(l) = \lim_{N\to\infty} N^{-2} \sum_{\substack{i,j=1 \\ j\neq i}}^{N} \theta(l - r_{ij})$$

Fig. 1. The correlation integral of (5) as a function of the separation. The original interval is the unit of length. The logarithms are base 2.

LACUNARITY AND INTERMITTENCY IN FLUID TURBULENCE ☆

L.A. SMITH [1]

NASA Goddard Space Flight Center, Institute for Space Studies, New York, NY 10025, USA

J.-D. FOURNIER [2,3] and E.A. SPIEGEL

Astronomy Department, Columbia University, New York, NY 10027, USA

CANTOR SETS

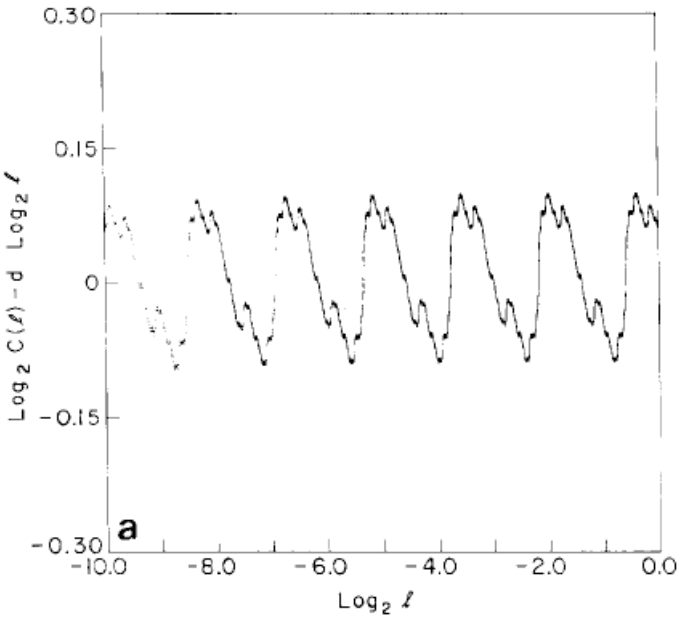

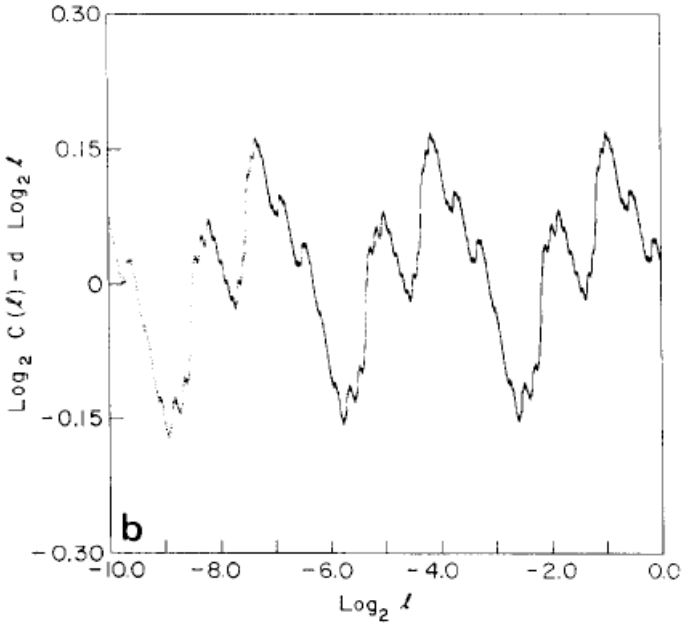

Two classes of mechanisms

Continuous scale invariance vs Discrete scale invariance

Pre-existing hierarchical geometry

-Ising, Potts and other models of statistical physics on Cayley trees, Diamond and other hierarchical lattices

-Shell models of turbulence

Dynamically generated DSI

-rupture in heterogenous media

-growth processes

-turbulence

-financial stock market prices

Fractal function

Discrete scale invariance

Complex fractal dimension

Log-periodicity

1) d ∈ N Euclid (6th BC)

2) d ∈ R Mandelbrot

3) d ∈ C

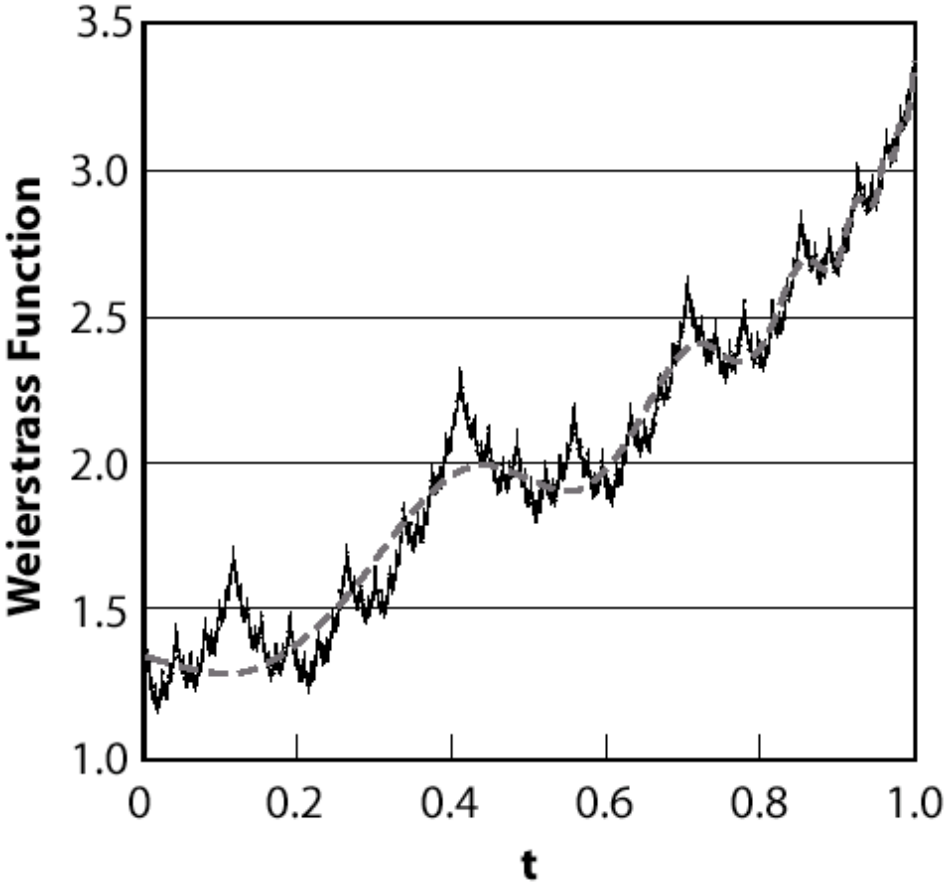

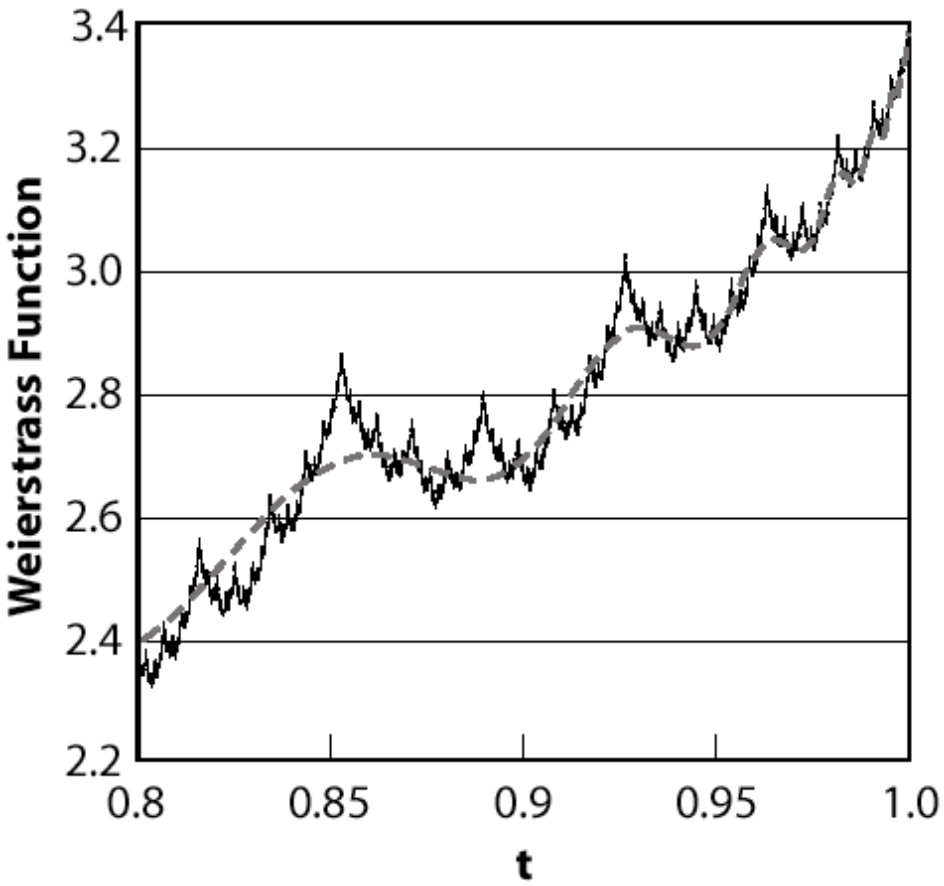

Log-periodic route to fractal functions

$$f(K) = g(K) + \frac{1}{\mu} f[R(K)]$$

$$f(K) = \sum_{n=0}^{\infty} \frac{1}{\mu^n} g[R^{(n)}(K)]$$

(Derrida, Eckmann, Erzan, 1983)

$$f(x) = \sum_{n=0}^{\infty} \frac{1}{\mu^n} g[\gamma^n x]$$

$$f_W = \sum_{n=0}^{\infty} b^n \cos[a^n \pi x]$$

$$f(x) = \frac{1}{2\pi i} \int_{c-i\infty}^{c+i\infty} \hat{f}(s) x^{-s} ds$$

Inverse Mellin transform

$$f(x) = f_s(x) + f_r(x)$$

$$f_s(x) = \sum_{n=0}^{\infty} A_n x^{-s_n} \qquad A_n = \frac{\hat{g}(s_n)}{\ln \gamma}$$

$$f_r(x) = \sum_{n=0}^{\infty} B_n x^n \qquad s_n = -m + i \frac{2\pi}{\ln \gamma} n$$

$$= -m + i\omega n$$

S. Gluzman and D. Sornette, Log-periodic route to fractal functions, art. no. 036142, Phys. Rev. E V6503 N3 PT2A:U418-U436 (2002)

TABLE I. Synthesis of the different classes of Weierstrass-type functions according to the general classification (21), $A_n \sim (1/n^p) e^{-\kappa n} e^{i\psi_n}$ of the expansion (18) in terms of a series of power laws x^{-s_n}. The parameters p, $\kappa \geq 0$, and ψ_n are determined by the form of $g(x)$ and the values of μ and γ. All numerical values given in this table correspond to $m=0.5, \omega=7.7$ corresponding to $\gamma=2.26$ and $\mu=\sqrt{\gamma}=1.5$. The last two columns quantify the amplitude of the log-periodic oscillations with respect to the leading real power law.

$g(x)$	p	κ	ψ_n	$\lvert A_{n=1}/A_{n=0}\rvert$	$\lvert A_{n=2}/A_{n=0}\rvert$
$\cos(x)$	$m+1/2$	0	$\omega n \ln(\omega n)$	0.065	0.032
$\exp(-x)$	$m+1/2$	$(\pi/2)\omega$	$\omega n \ln(\omega n)$	5.12×10^{-7}	1.432×10^{-12}
$\exp[-cx]\cos(xs)$[a]	$m+1/2$	$([\pi/2]-\alpha)\omega$	$\omega n \ln(\omega n)$		
$(1+x^2)^{-1}$	0	$(\pi/2)\omega$	$(\pi/2)m$	9.901×10^{-6}	4.414×10^{-11}
$\log(1+x)$	1	$\pi\omega$	$-\pi m$	4.045×10^{-12}	≈ 0
$\exp(-x^h)$	$m/h+1/2$	$(\pi/2h)\omega$	$[(\omega n)/h]\ln(\omega n)$	0.064 ($h=50$)	0.03 ($h=50$)
				4.386×10^{-4} ($h=2$)	6.177×10^{-7} ($h=2$)
$\sin(x)/x^\delta$	$m+\delta+1/2$	0	$-\omega n \ln(\omega n)$	0.044 ($\delta=0.1$)	0.021 ($\delta=0.1$)
				0.091 ($\delta=-0.1$)	0.049 ($\delta=-0.1$)
$\mathrm{Si}(x)$	$m+3/2$	0	$\omega n \ln(\omega n)$	4.199×10^{-3}	1.053×10^{-3}
$1-x^h$ $0<x<1$	2	0	π	0.064 ($h=50$)	0.031 ($h=50$)
				0.012 ($h=2$)	3.146×10^{-3} ($h=2$)

$c=\cos\alpha$ and $s=\sin\alpha$.

Mechanism for large log-periodic corrections to scaling:
The non-universal function g(K) must be either quasi-periodic or with compact support

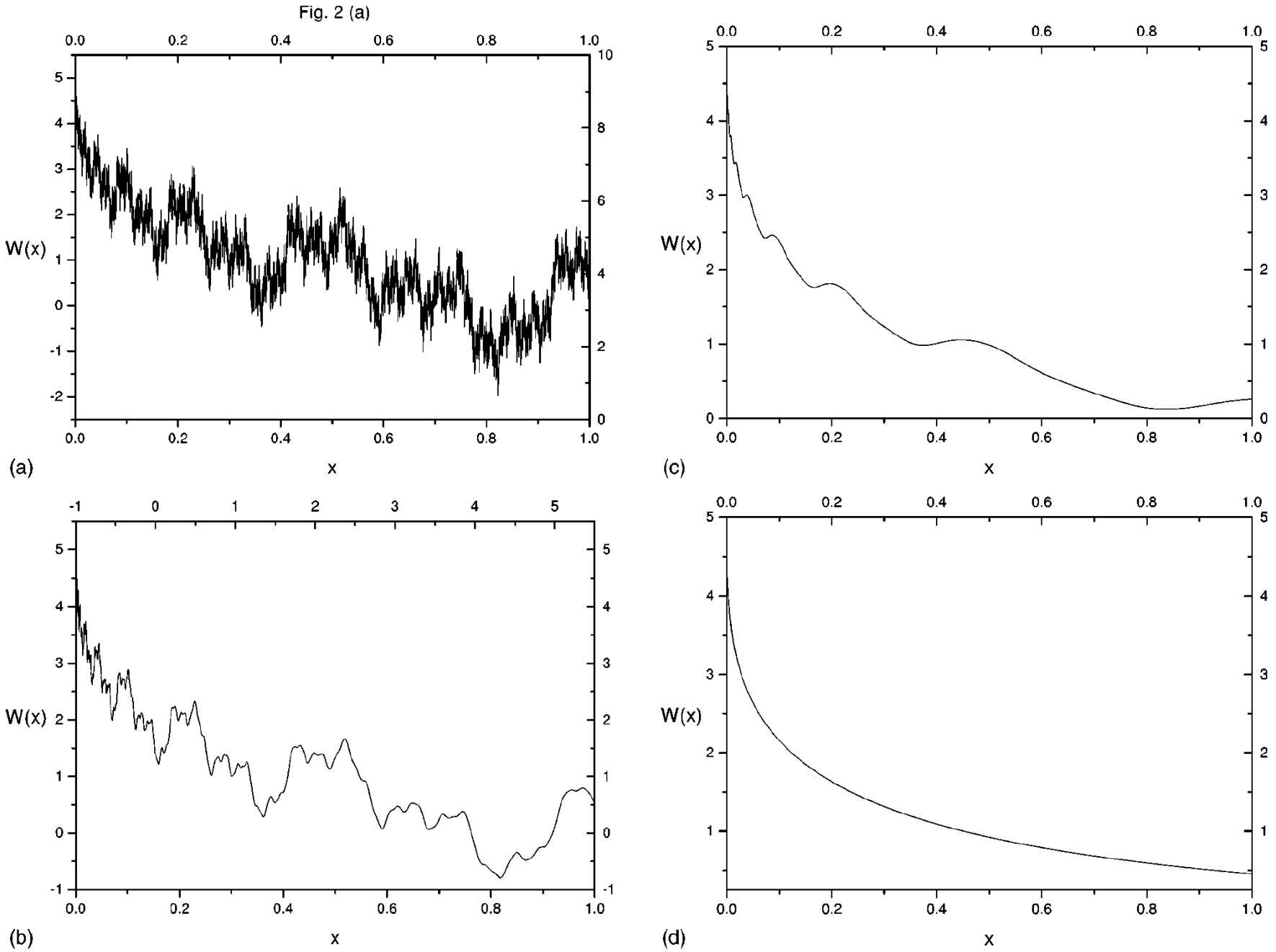

FIG. 2. Quasi-Weierstrass function for (a) $\alpha=\pi/2$, (b) $\alpha=0.993\pi/2=1.56$, (c) $\alpha=0.9\pi/2=1.414$, and (d) $\alpha=0$, for $m=0.25$,$\omega=7.7$, using $N=32$ terms to estimate the sums (51). Increasing N does not change the results.

$$S(x) = \sum_{n=1}^{\infty} n^{-m-(1/2)} e^{i\omega n \ln(\omega n)} x^{-s_n},$$

$$\psi_{n+1}^{(3)} = \psi_n^{(3)} + 2\pi R n.$$

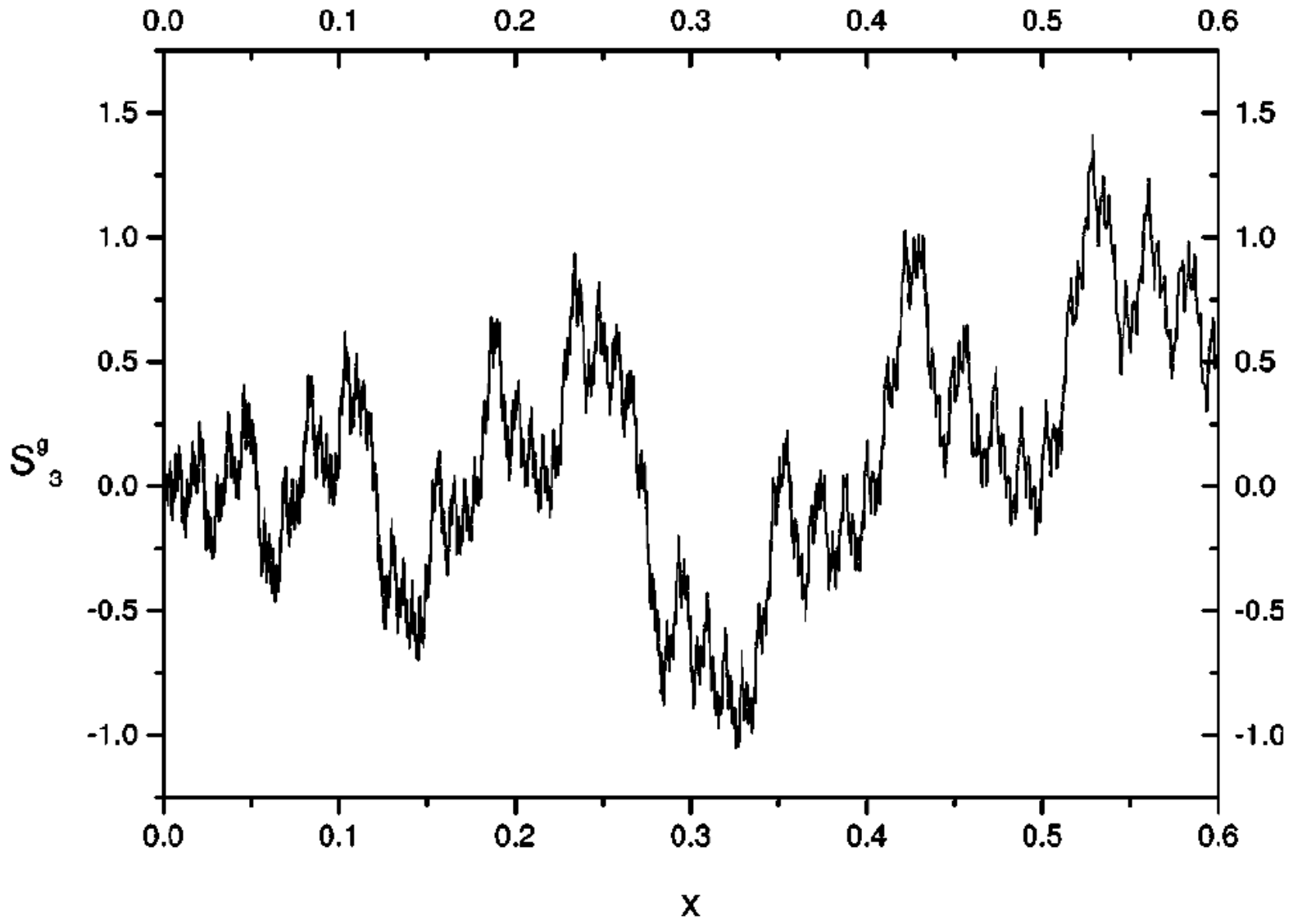

FIG. 8. "Golden-mean log-periodic Weierstrass function" $S_3^{(g)}(x)$ defined by Eq. (69) with Eq. (72) for $m=0.5,\omega=7.7,N=500$.

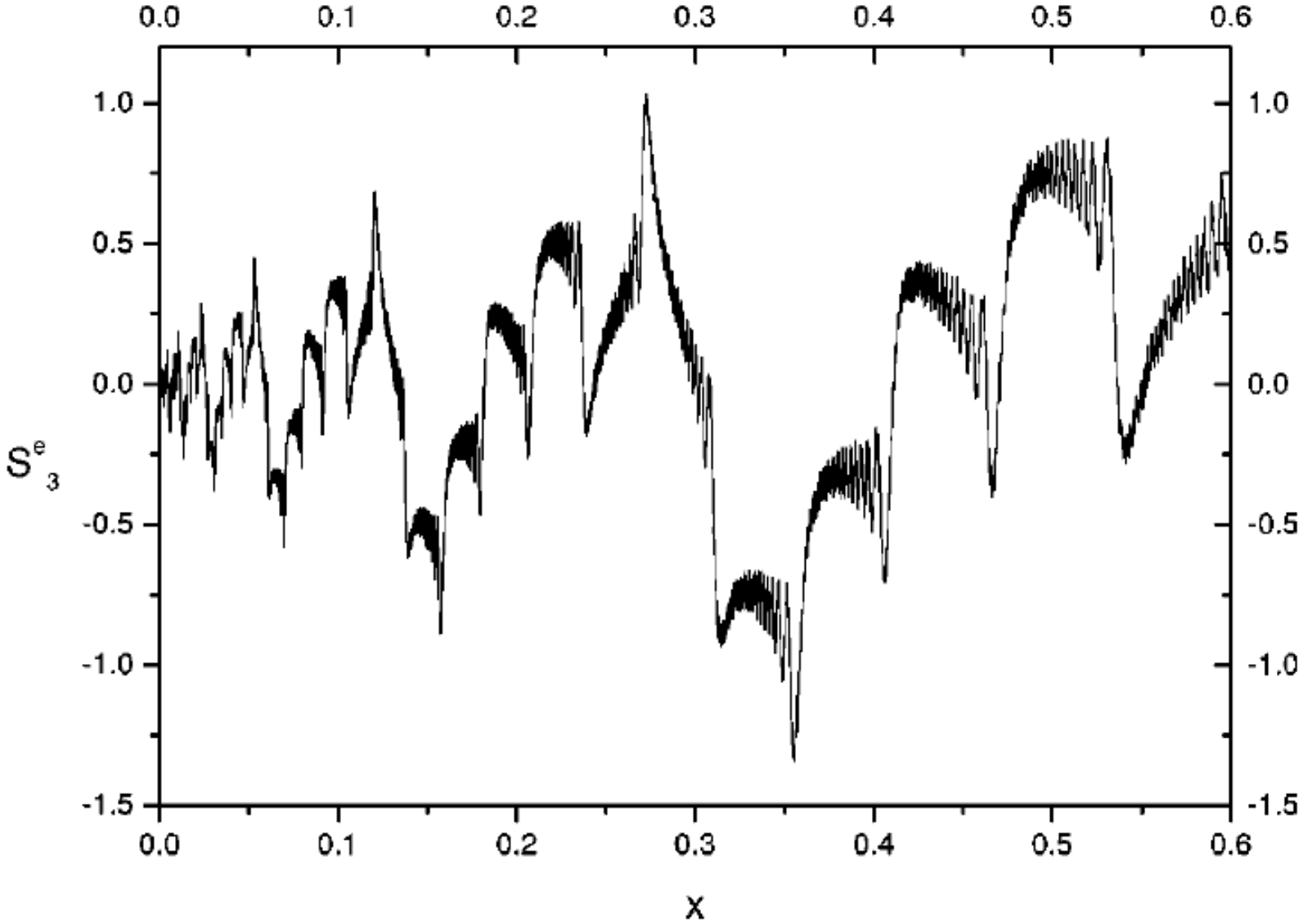

FIG. 10. "e-log-periodic Weierstrass function" $S_3^{(e)}$ defined by Eq. (69) with Eq. (72) and $R=e=2.718\ldots$ for $m=0.5,\omega=7.7,N=500$.

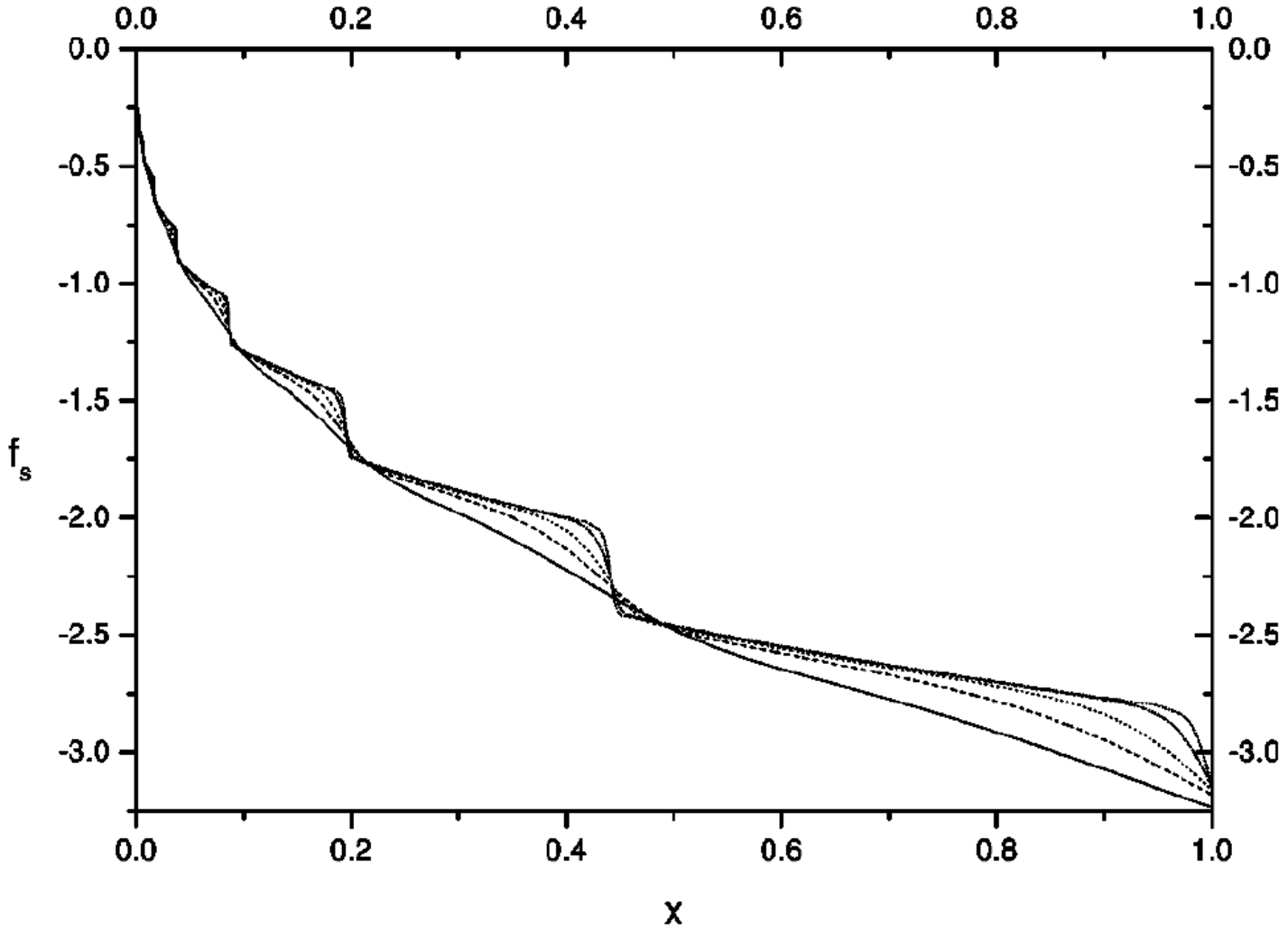

FIG. 11. Singular part $f_s(x)$ of the Weierstrass-like function for the regular function $g(x)$ equal to the stretched exponential (82) for $h=5$ (solid line), $h=10$ (dashed line), $h=20$ (dotted line), $h=50$ (dashed-dotted line), and $h=100$ (dashed-dot-dotted line), for $m=0.4, \omega=7.7, N=22$.

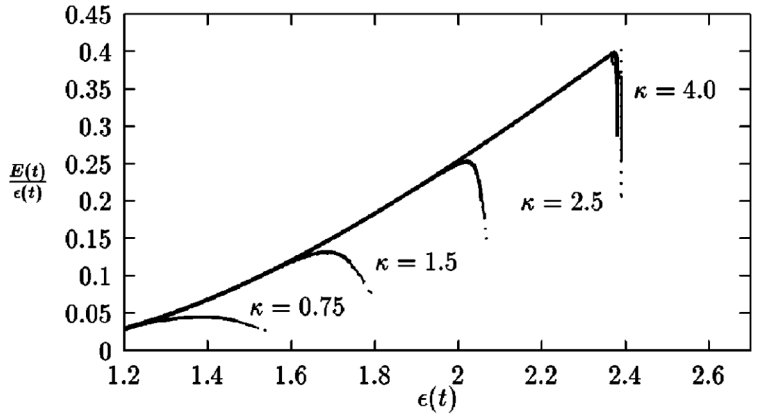

FIG. 1. Stress-strain curves for different values of κ and for different system sizes $L = 50$ (dotted line), 100 (thin bold line), and 200 (bold line). The fracturing is stopped at different $\epsilon(t)$ for different L in order to distinguish between the curves. (Notice that due to data collapse, the data for the various L become indistinguishable for $\kappa = 0.75, 1.5, 2.5$). One $L = 400$ simulation has been done for $\kappa = 4$ (thick bold line).

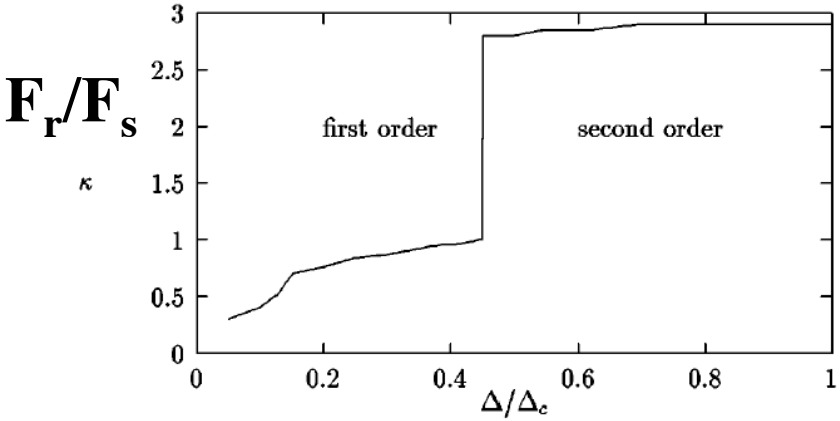

FIG. 3. Phase diagram for criticality of the fracturing. $\Delta/\Delta_c \to 0$ cannot be studied within the spring–block model since ambiguity in the updating rules for stress release affects the fracturing.

J.V. Andersen, D. Sornette and K.-T. Leung
Tri-critical behavior in rupture induced by disorder
Phys. Rev. Lett. 78, 2140-2143 (1997)

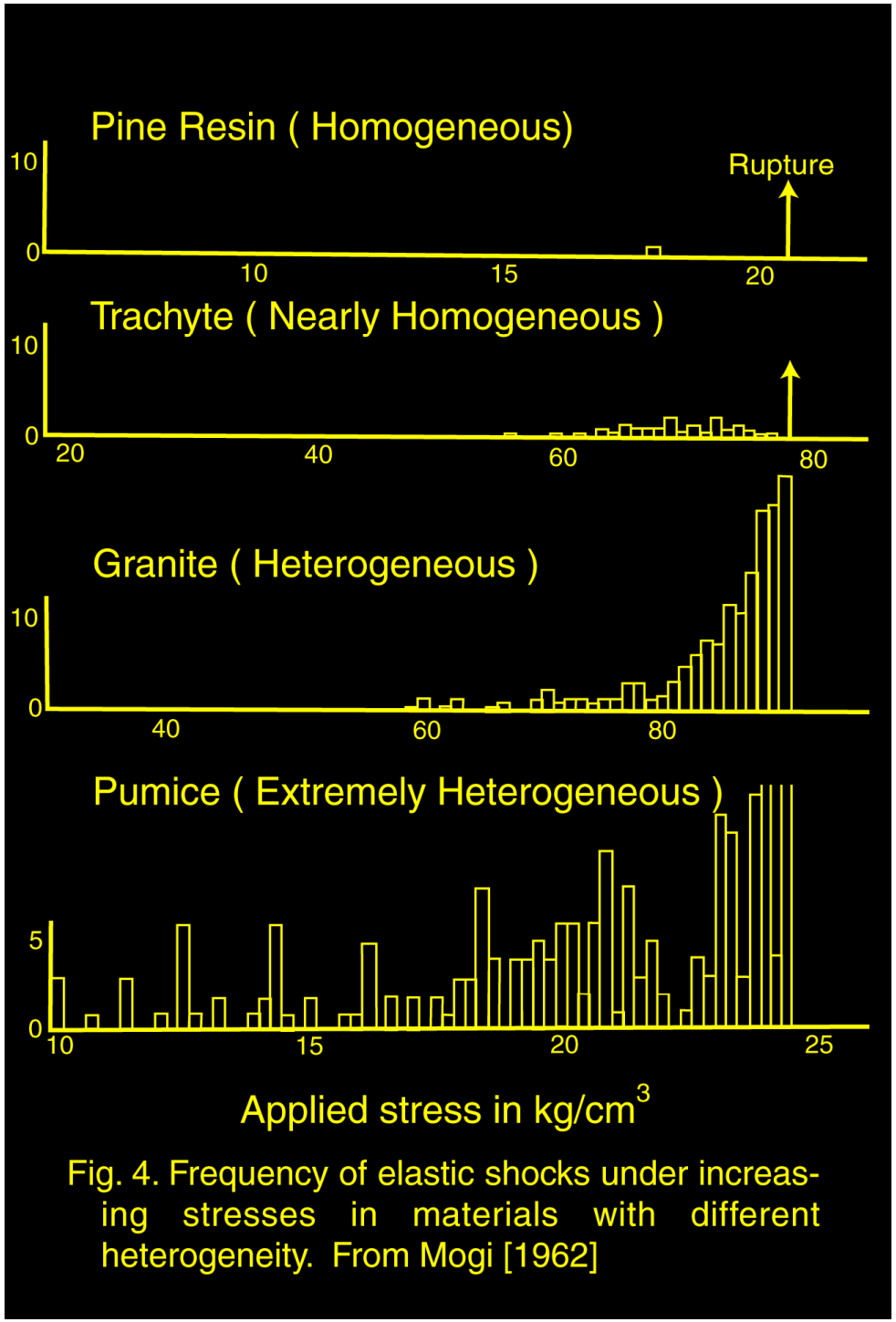

Fig. 4. Frequency of elastic shocks under increasing stresses in materials with different heterogeneity. From Mogi [1962]

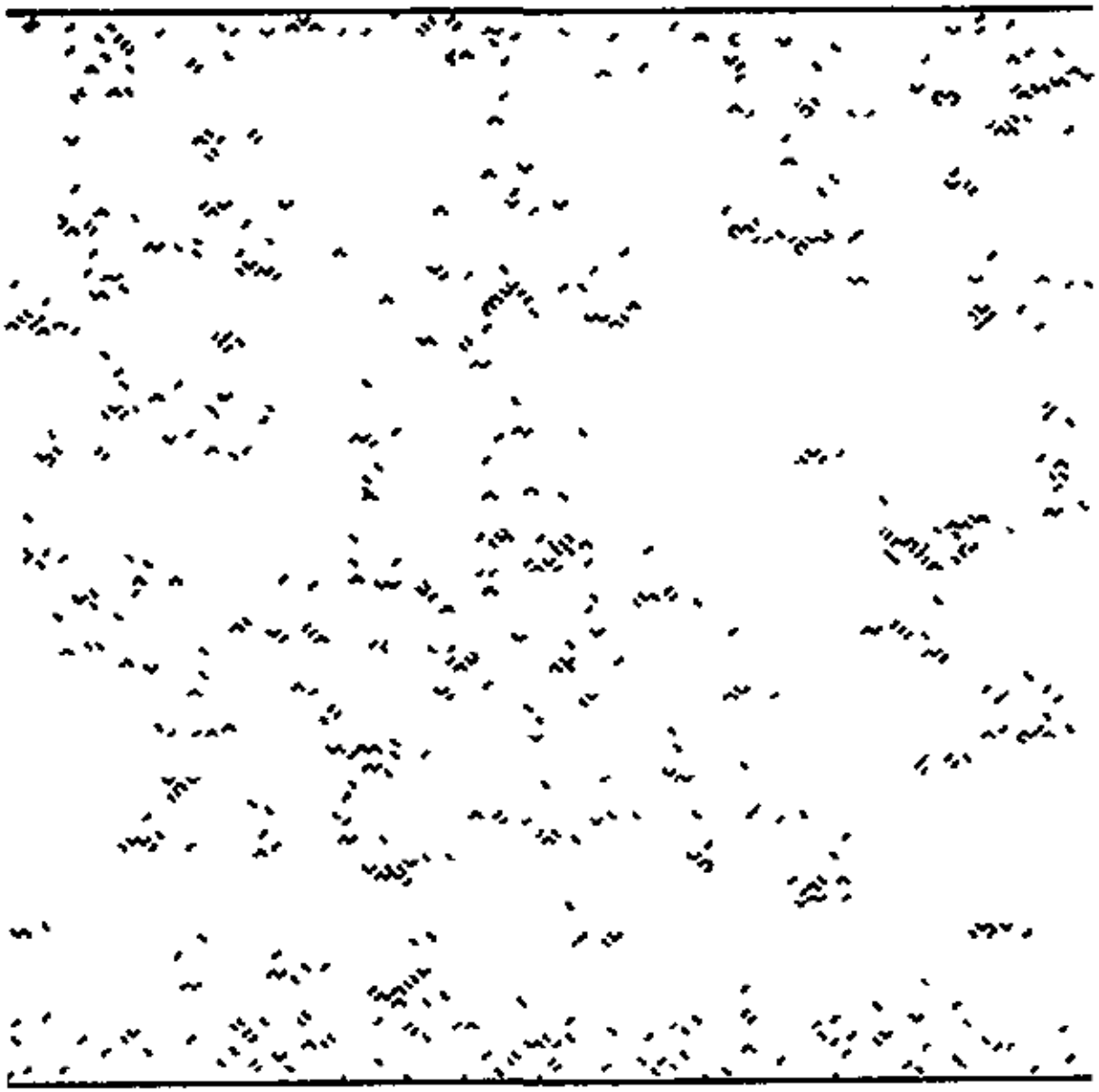

f=50% t/t_r=0.9912

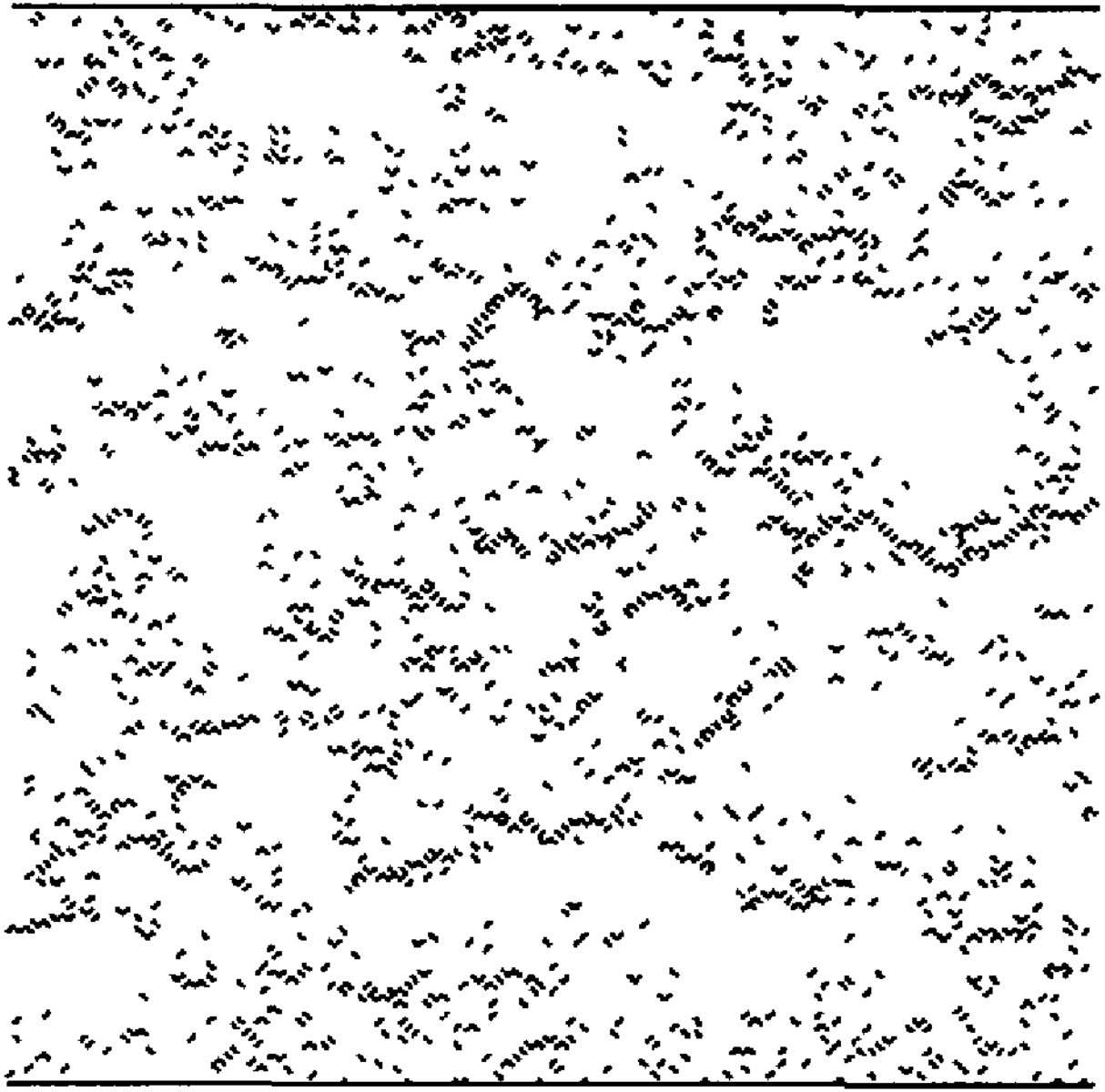

f=80% t/t_r=0.9982

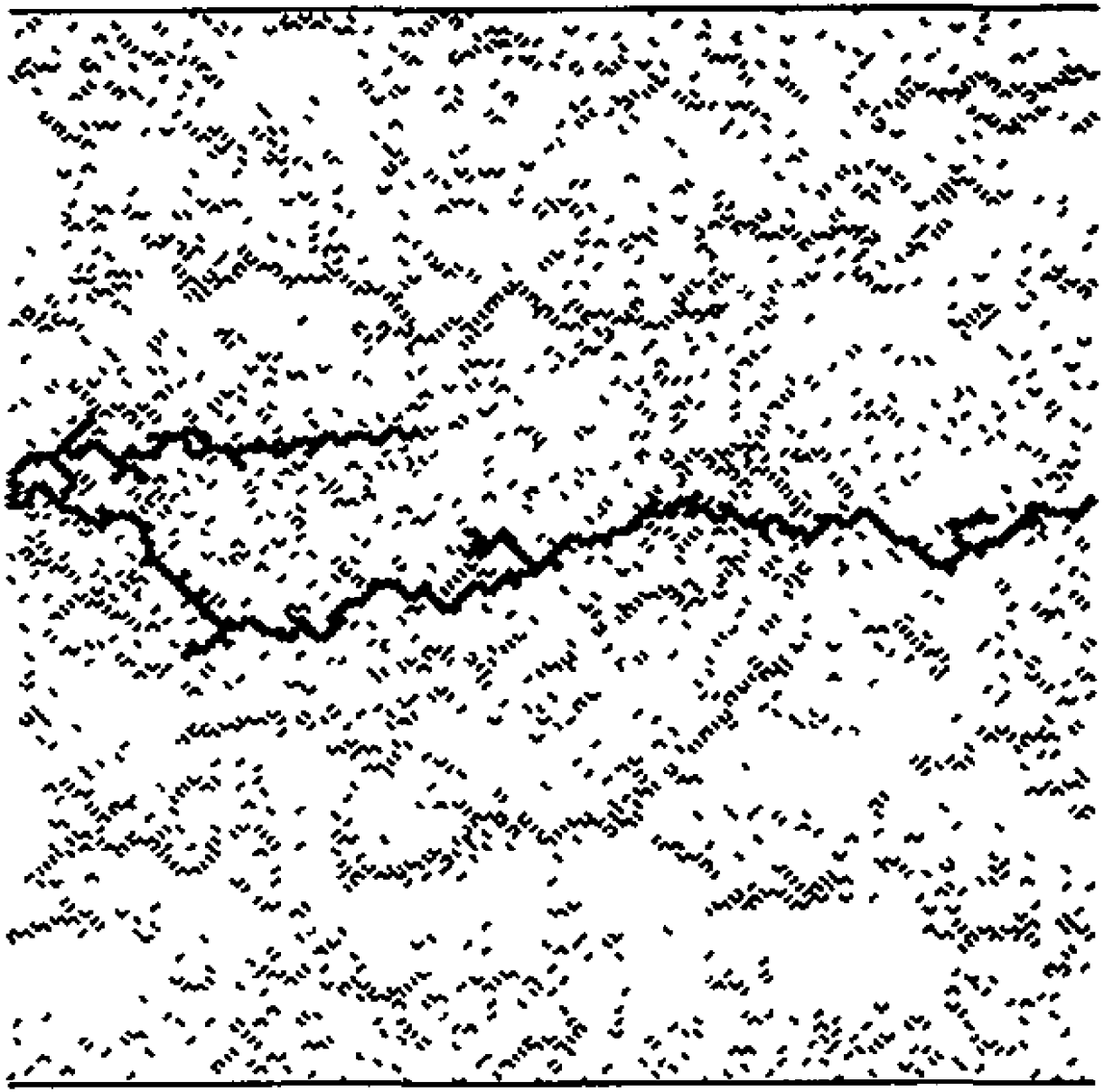

f=100% t/t_r=1.

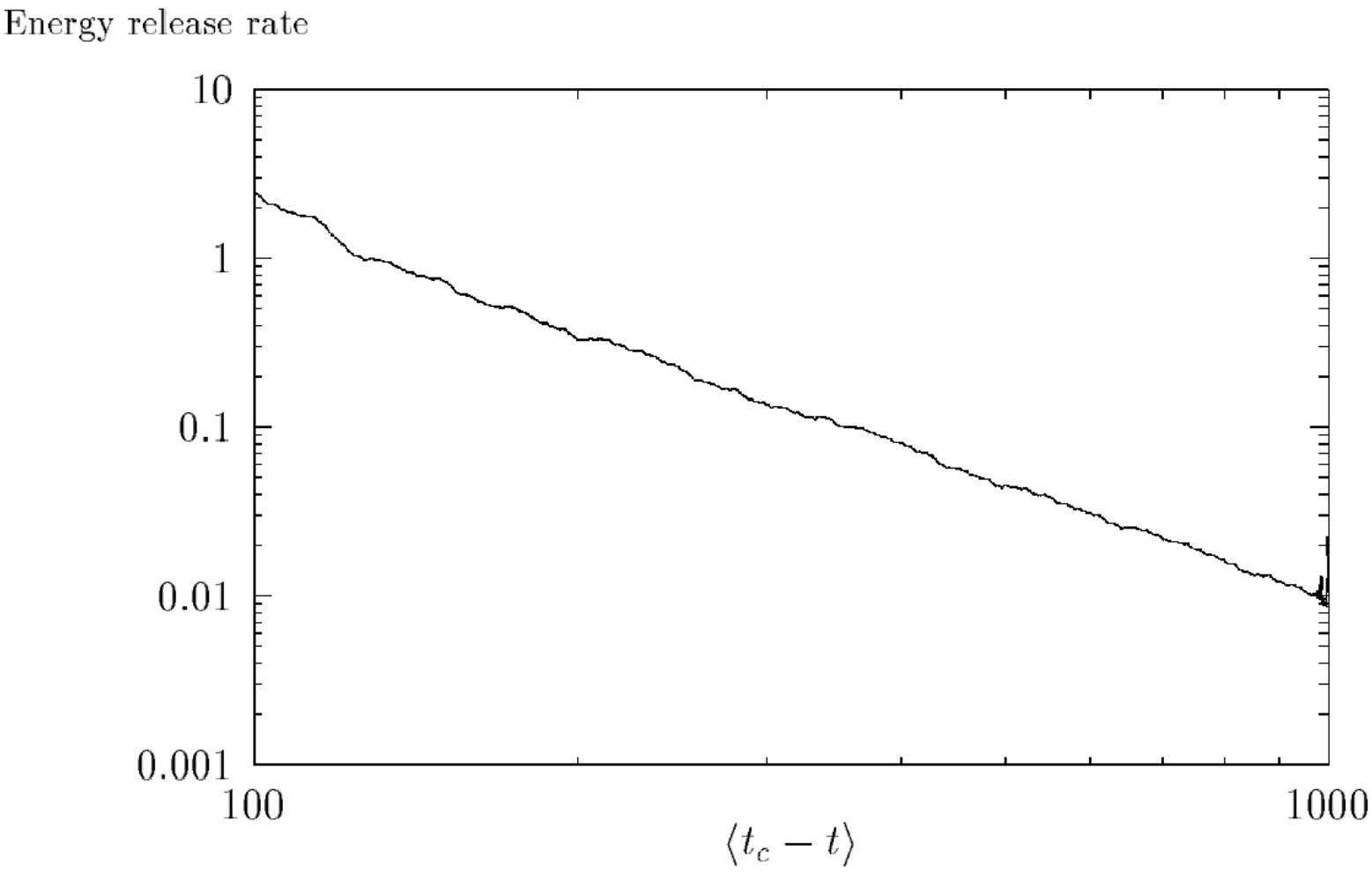

Figure 5: An average of the elastic energy release rate or rate of broken bonds as a function of time. The average is over 19 simulations of the thermal fuse model, using the standard ("grand canonical") averaging scheme, in terms of the time t from the beginning of the rupture process.

D. Sornette and C.Vanneste, Dynamics and memory effects in rupture of thermal fuse networks, Phys.Rev.Lett. 68, 612-615 (1992)

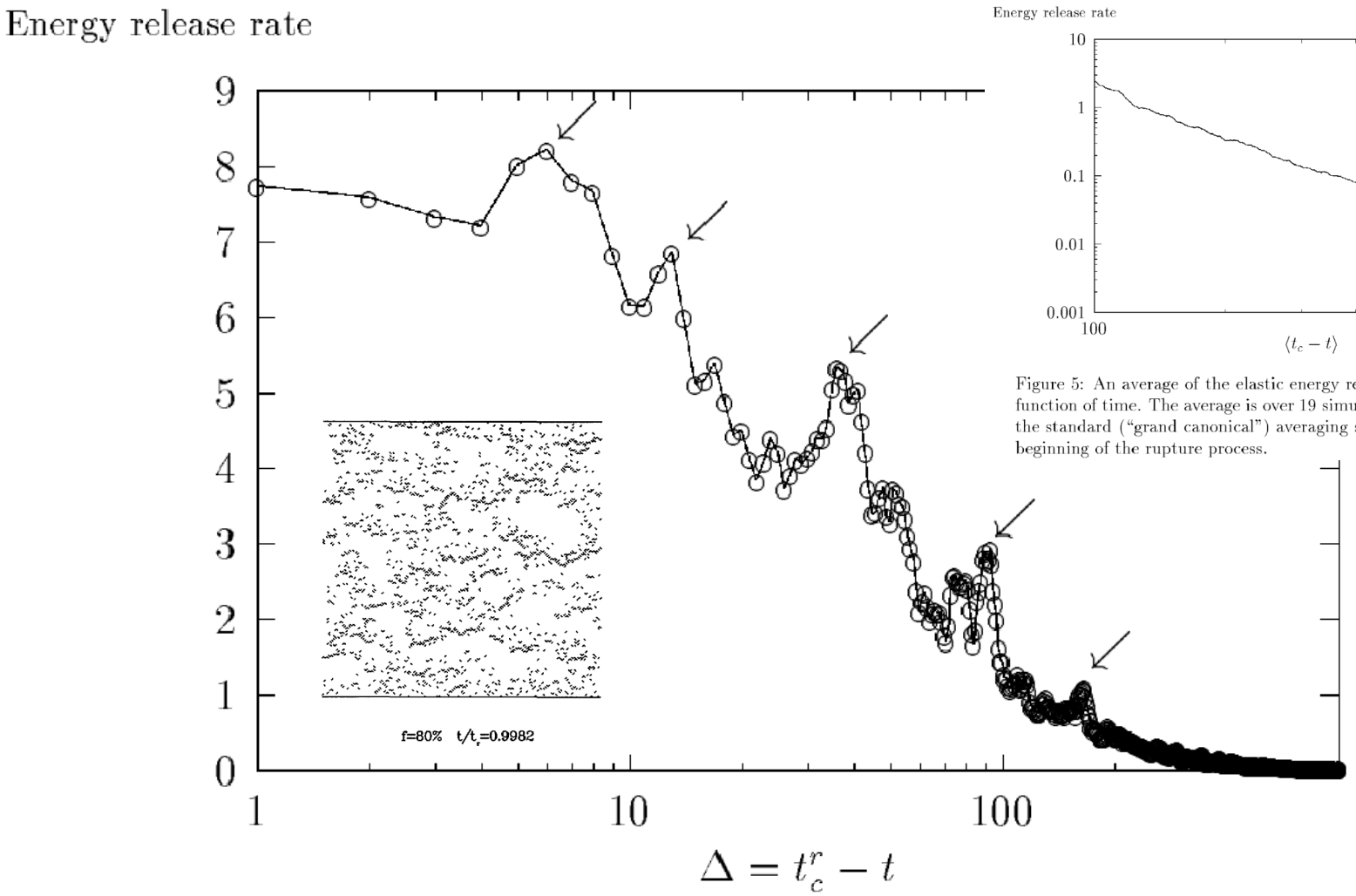

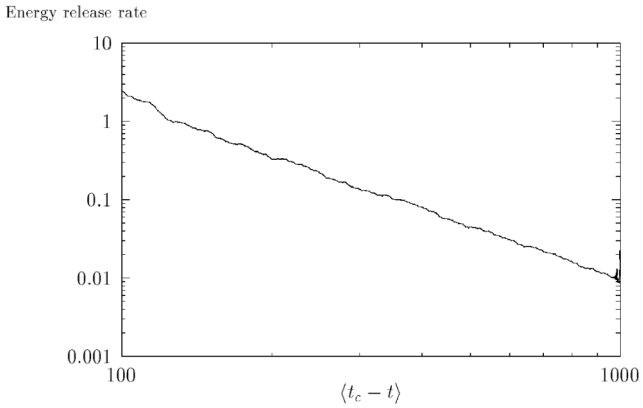

Figure 5: An average of the elastic energy release rate or rate of broken bonds as a function of time. The average is over 19 simulations of the thermal fuse model, using the standard ("grand canonical") averaging scheme, in terms of the time t from the beginning of the rupture process.

Figure 6: An average of the elastic energy release rate or rate of broken bonds as a function of time. The average is over the same 19 simulations of the thermal fuse model used in figure 5, but using the canonical averaging scheme described in the text, in terms of the effective time-to-failure measured by the sample specific susceptibility maximum.

A. Johansen and D. Sornette, Evidence of discrete scale invariance by canonical averaging, Int. J. Mod. Phys. C 9 (3), 433-447 (1998)

Spontaneous generation of discrete scale invariance in growth models

Y. Huang,[1] G. Ouillon,[2] H. Saleur,[1] and D. Sornette[2,3]

PHYSICAL REVIEW E VOLUME 55, NUMBER 6 JUNE 1997

The Mullins-Sekerka instability

$$\Delta\phi = 0,$$

$$v = \nabla\phi.$$

complex hodograph method

$$\Phi(z) = \phi(x,y) + i\psi(x,y)$$

Look for a parameterization of the interface in terms of z as a function of Φ and ψ

$$z_{\text{int}}(s,t) = C_0(t) + i\frac{s}{A} + \sum_{j=1}^{4} C_j(t) e^{-ijsa/A}.$$

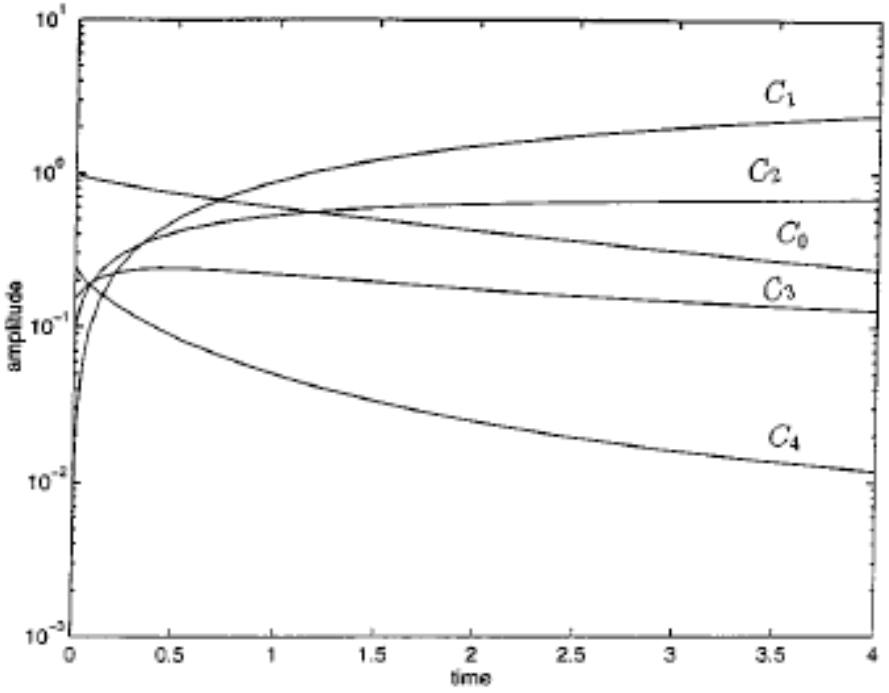

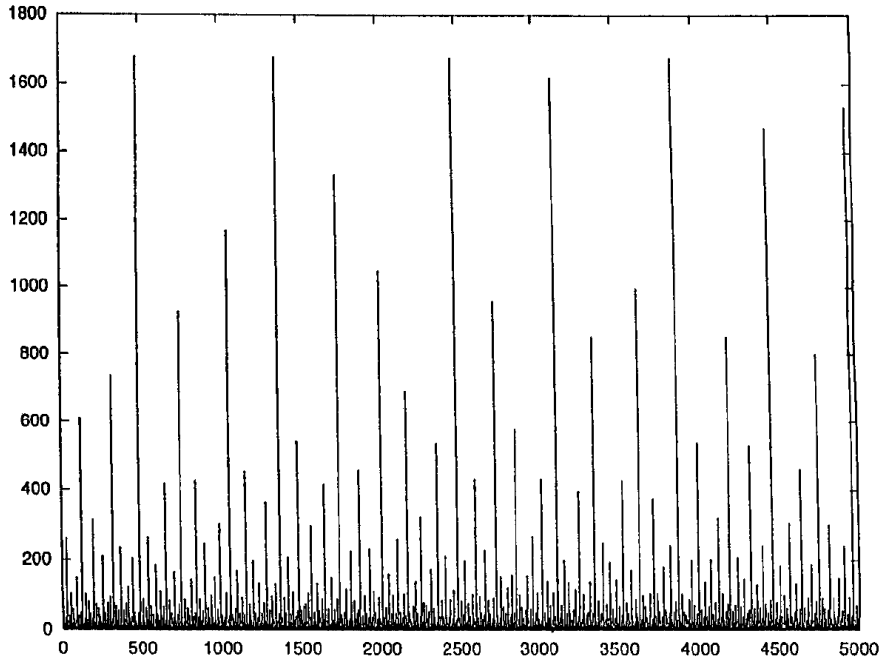

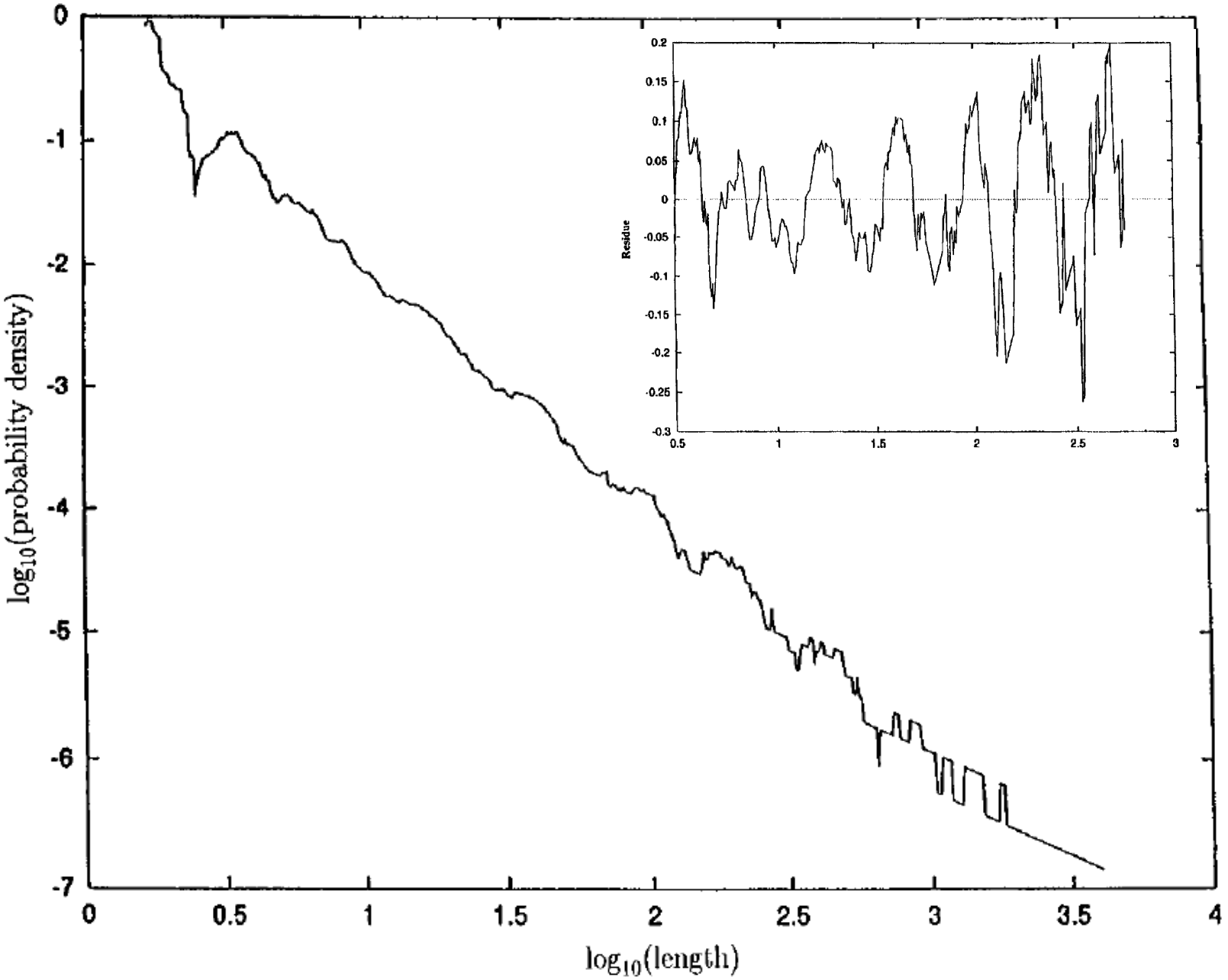
0
-1
-2
-3
-4
-5
-6
-7
0
0.5
1
1.5
2
2.5
3
3.5
4
log10(probability density)
log10(length)
Residue
0.2
0.15
0.1
0.05
0
-0.05
-0.1
-0.15
-0.2
-0.25
-0.3
0.5
1
1.5
2
2.5
3

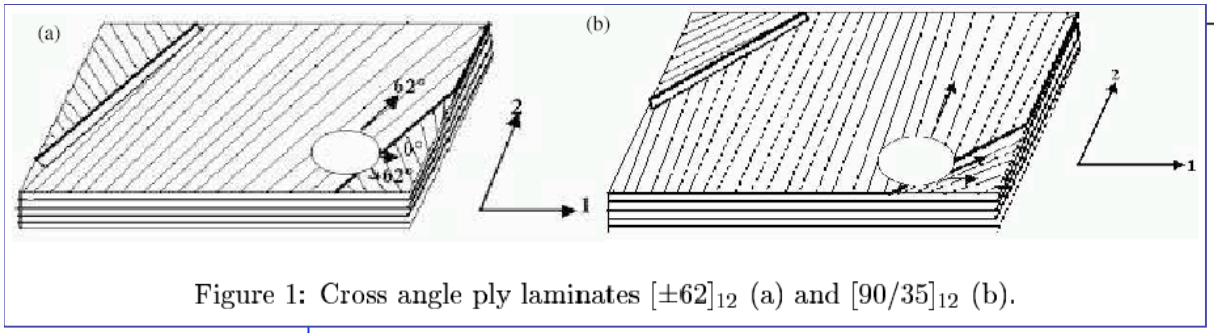

Figure 1: Cross angle ply laminates $[\pm 62]_{12}$ (a) and $[90/35]_{12}$ (b).

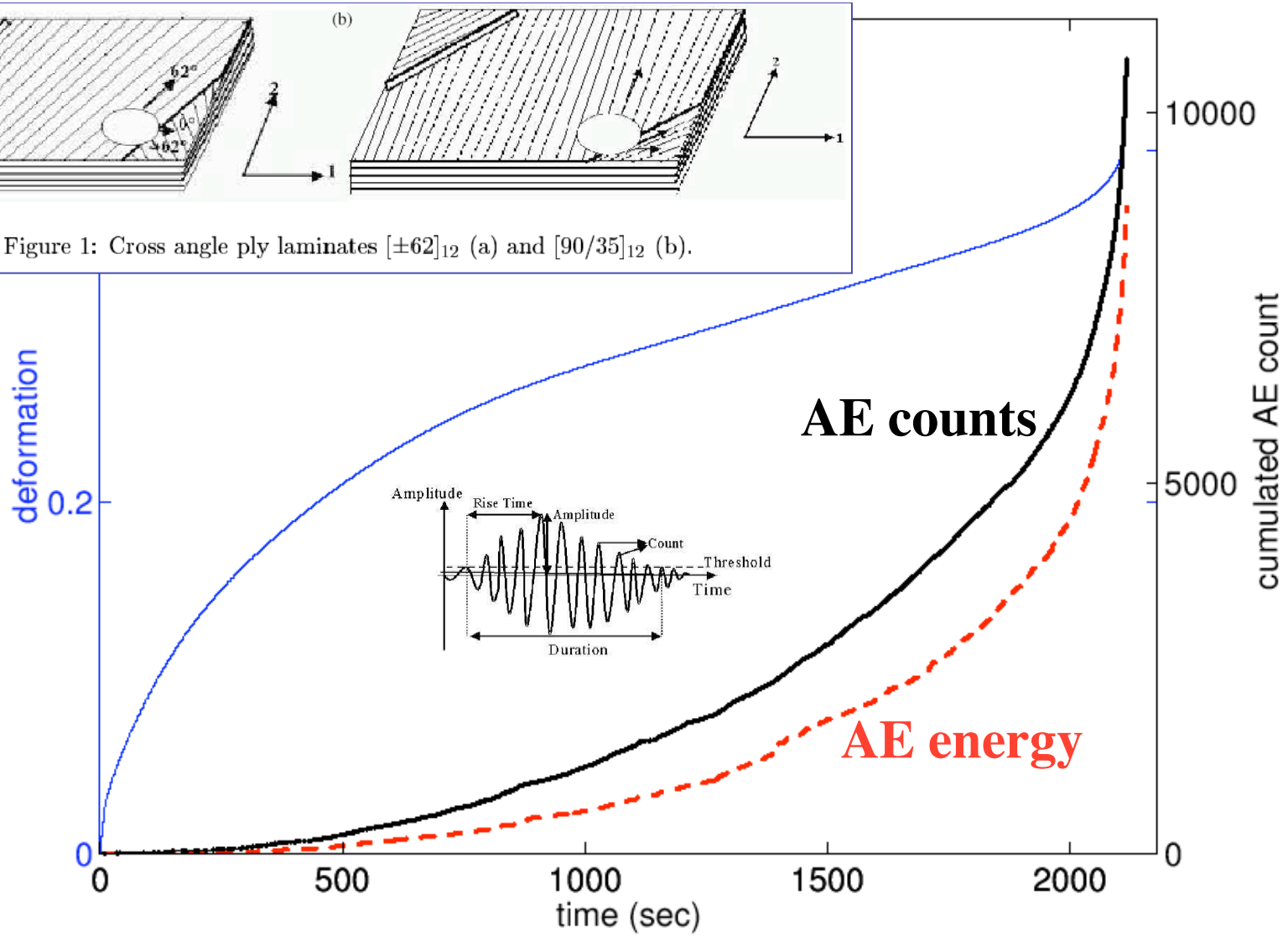

Figure 4: Creep strain and AE response for [90/35] angle ply composite #3. The thin solid line is the deformation (left axis), the heavy black line is the cumulated AE count (right axis) and dashed line is the cumulated energy (arbitrary units).

H. Nechad, A. Helmstetter, R. El Guerjouma and D. Sornette, Phys. Rev. Lett. 94, 045501 (2005)

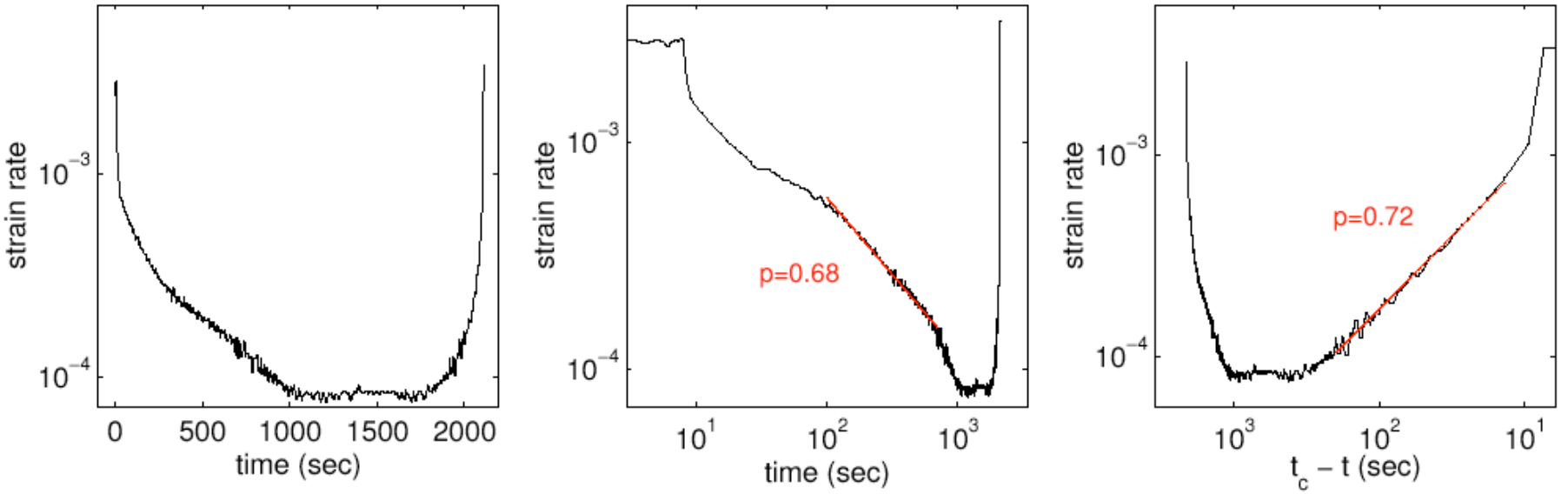

Figure 6: Creep strain rate for [90/35] angle ply composite #3

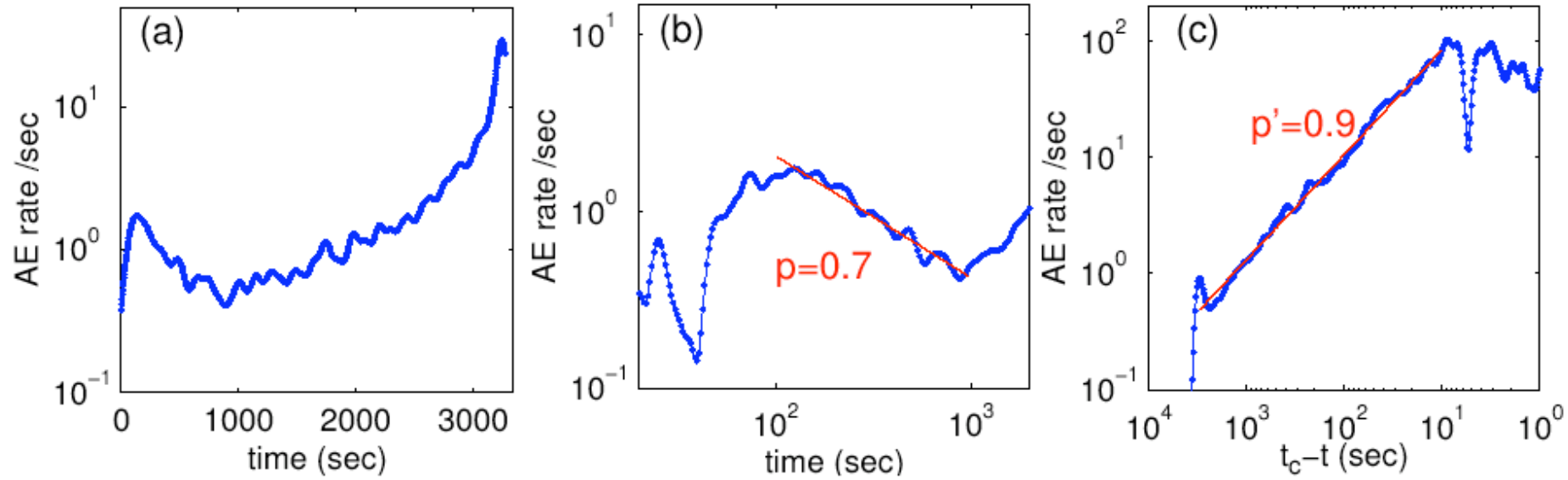

Figure 8: Rate of AE events for [90/35] angle ply composite #3. We use different axes to illustrate Andrade law in the primary creep regime $dN/dt \sim 1/t^p$ (b) and the power-law singularity of the AE rate before failure $dN/dt \sim 1/(t_c - t)^{p'}$. H. Nechad, A. Helmstetter, R. El Guerjouma and D. Sornette (2004)

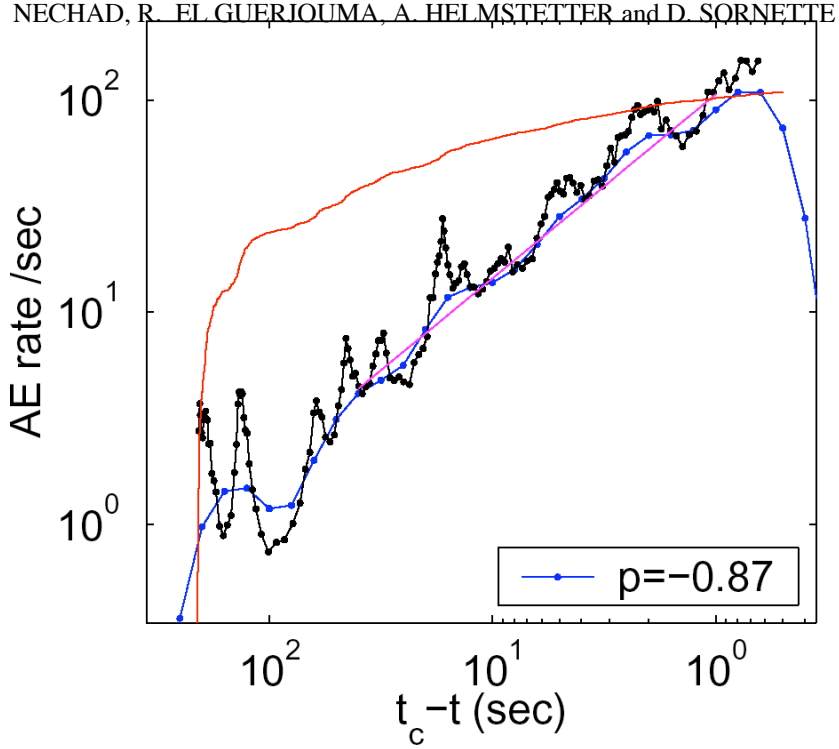
AE rate /sec
10^2
10^1
10^0
p=−0.87
10^2
10^1
10^0
$t_c - t$ (sec)

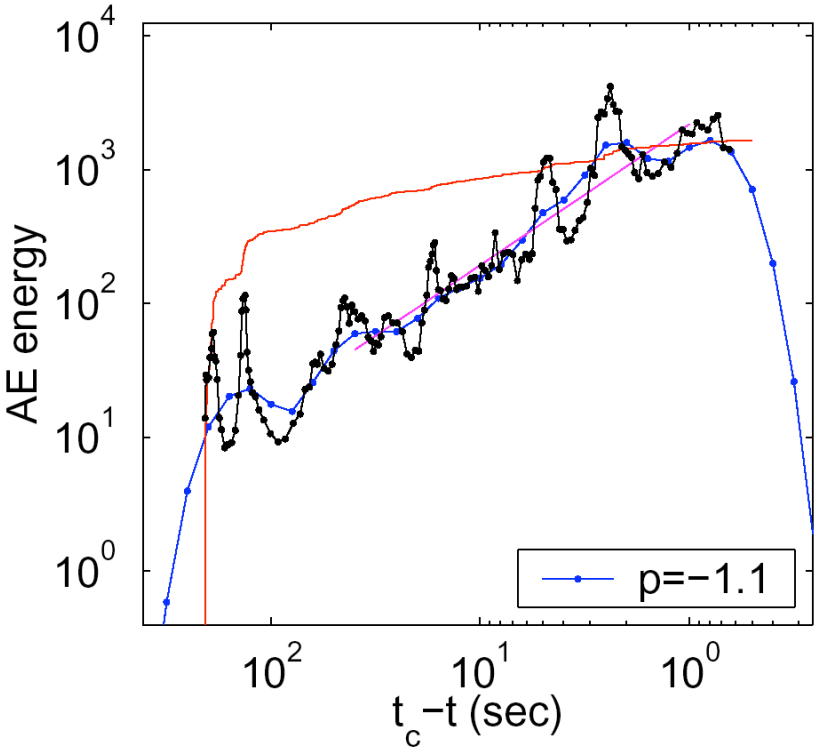
AE energy
10^4
10^3
10^2
10^1
10^0
p=−1.1
10^2
10^1
10^0
$t_c - t$ (sec)

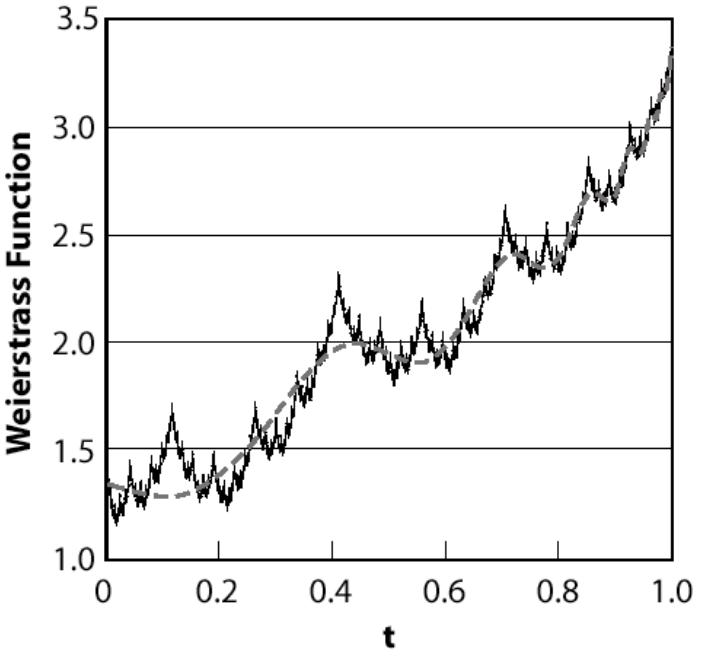
Weierstrass Function
3.5
3.0
2.5
2.0
1.5
1.0
0
0.2
0.4
0.6
0.8
1.0
t

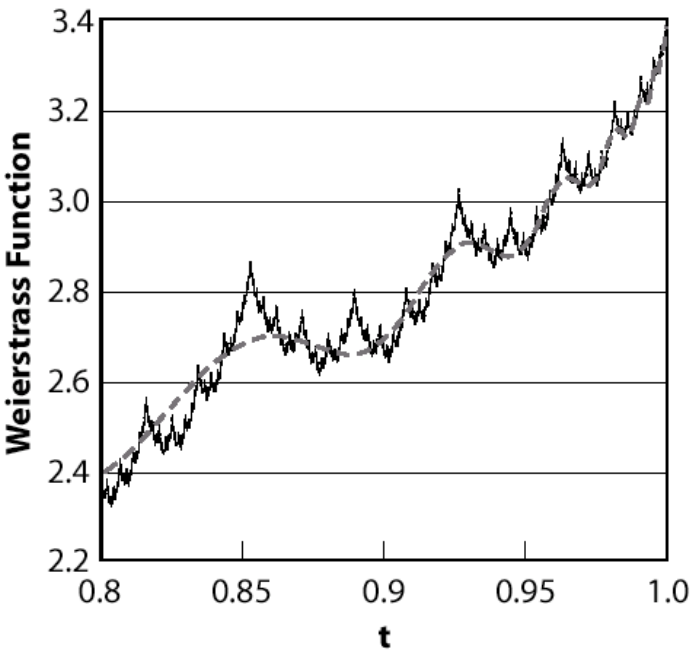
Weierstrass Function
3.4
3.2
3.0
2.8
2.6
2.4
2.2
0.8
0.85
0.9
0.95
1.0
t

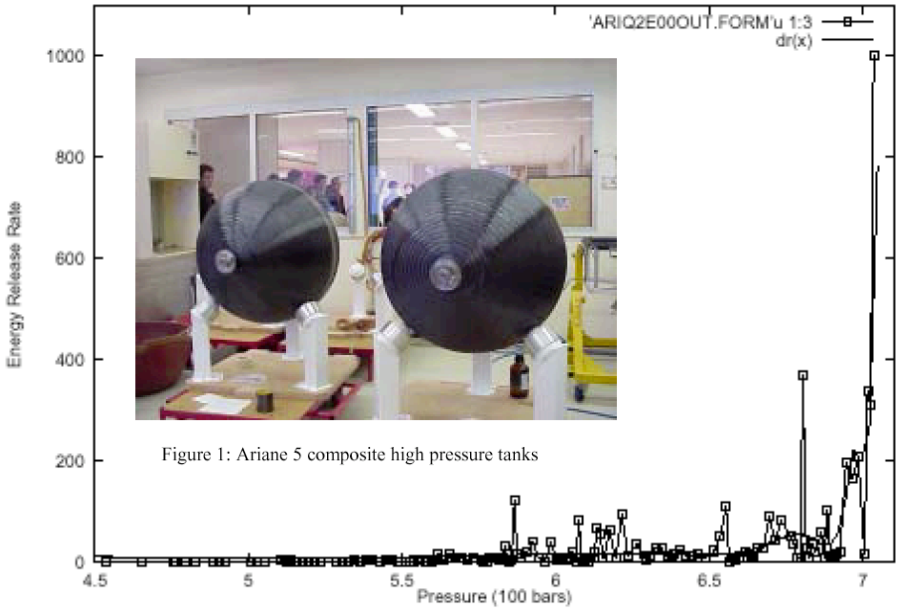

Figure 1: Ariane 5 composite high pressure tanks

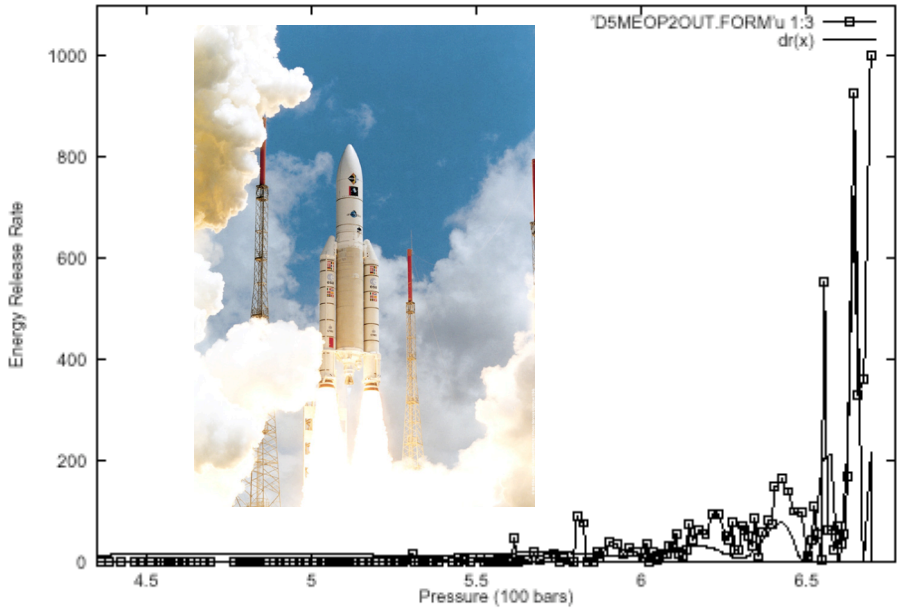

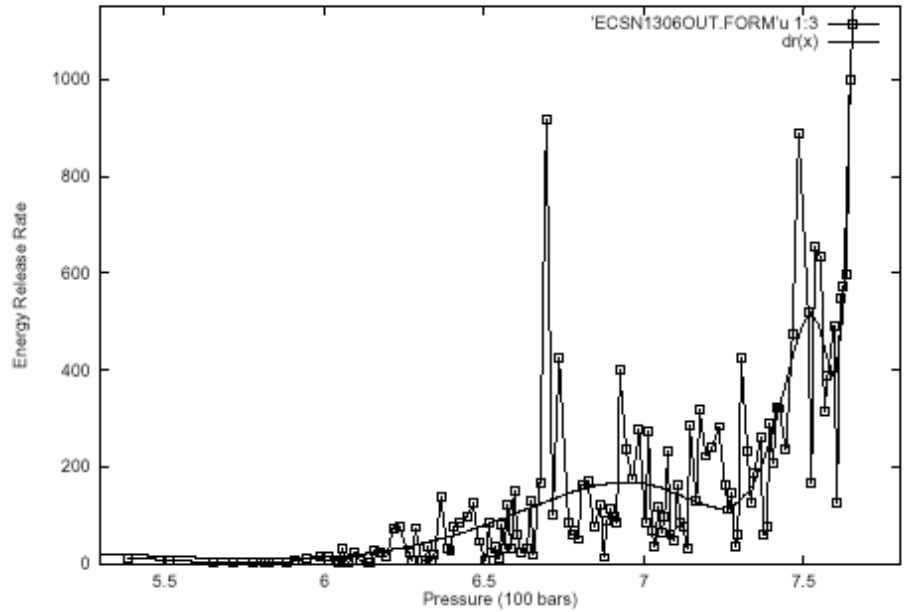

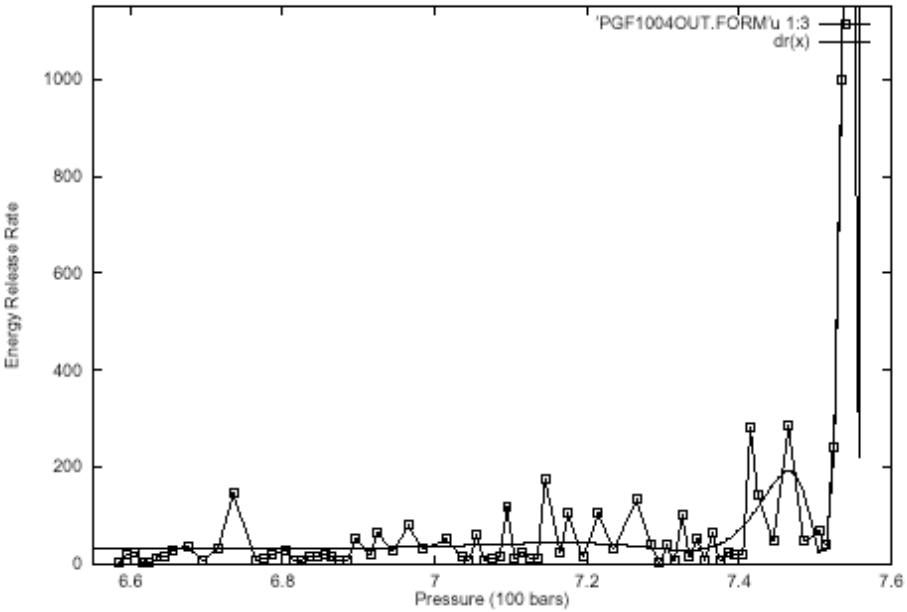

Critical ruptures

A. Johansen[1] and D. Sornette[1] Eur. Phys. J. B **18**, 163–181 (2000)

Figure 1: Ariane 5 composite high pressure tanks

Our prediction system is now used in the industrial phase as the standard testing procedure.

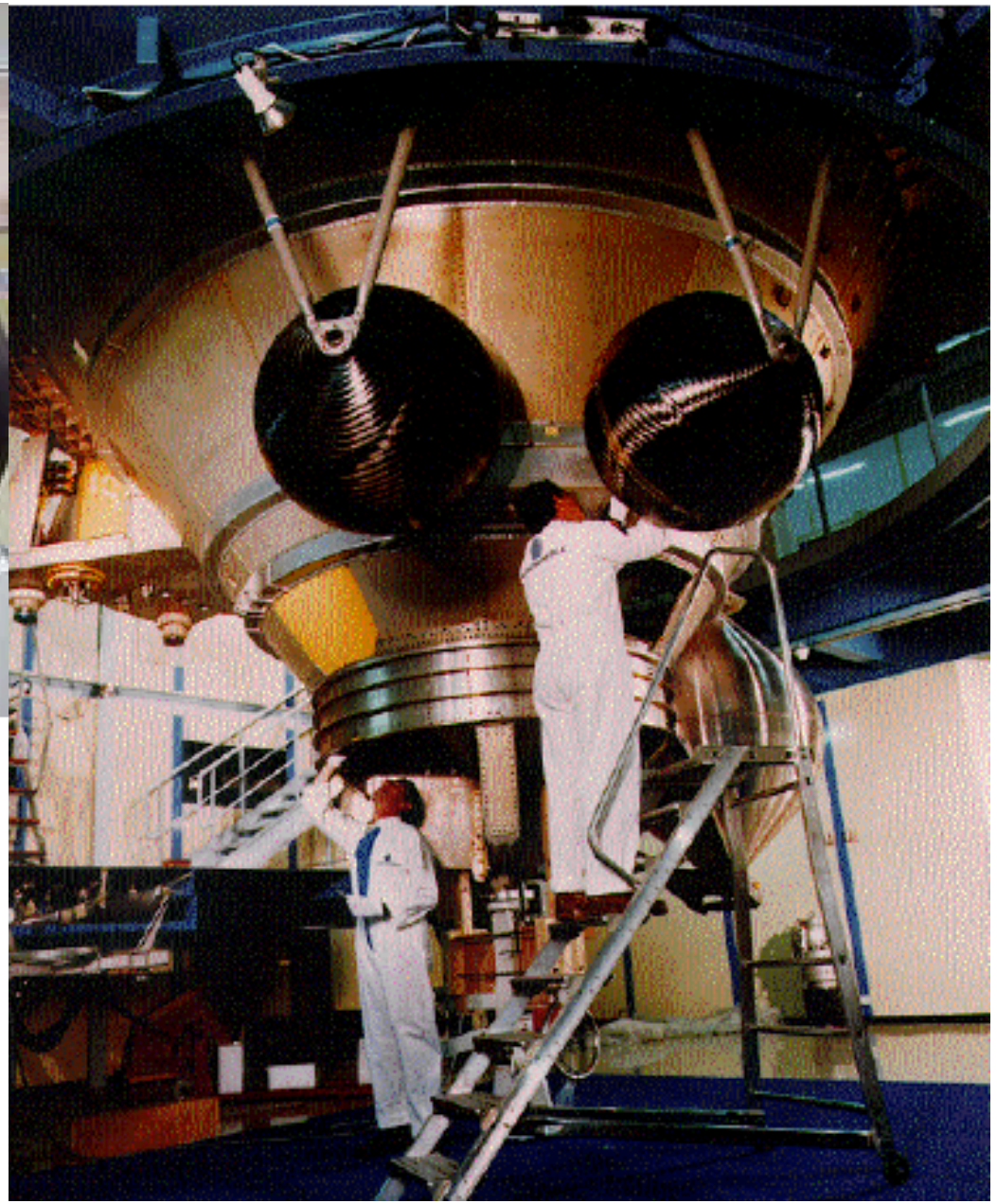

EADS LAUNCH VEHICLES

J.-C. Anifrani, C. Le Floc'h, D. Sornette and B. Souillard
"Universal Log-periodic correction to renormalization group scaling for rupture stress prediction from acoustic emissions", J.Phys.I France 5, n°6, 631-638 (1995)

predictability of ice avalanches

Nonlinear Processes in Geophysics, 12, 849–861, 2005

A. Pralong, C. Birrer,W. A. Stahel, and M. Funk

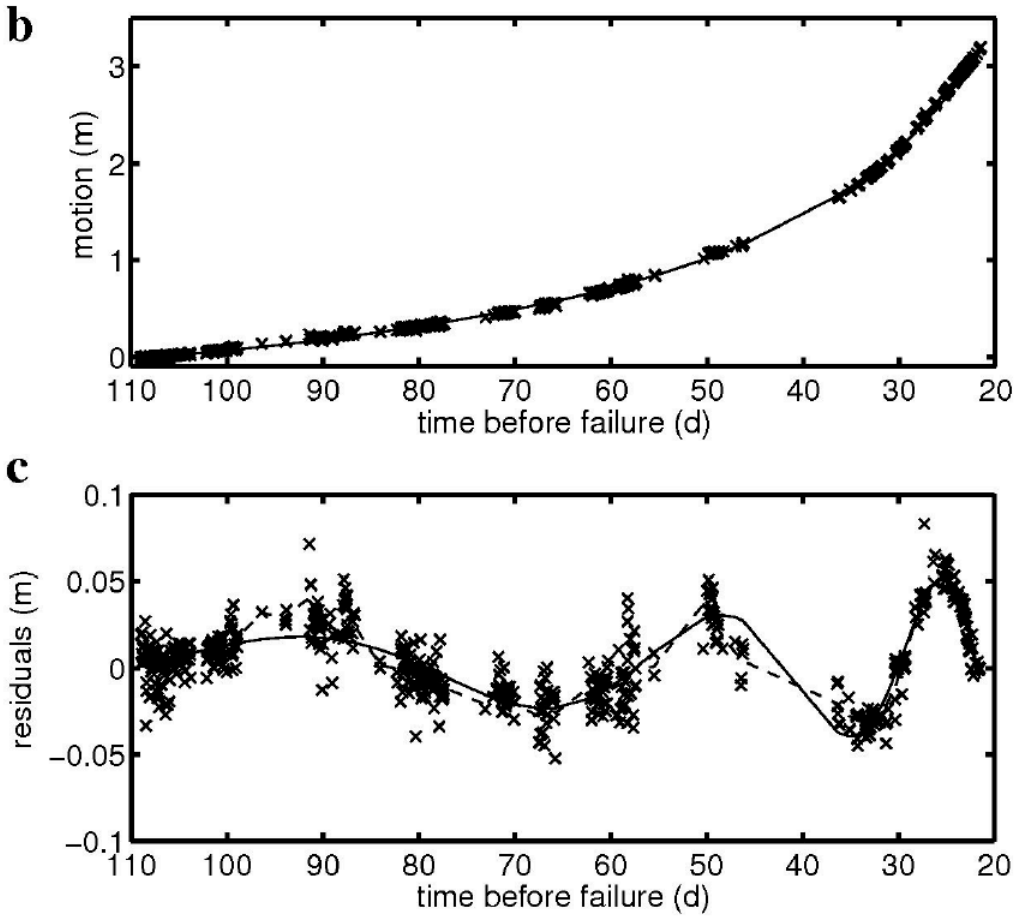

Fig. 3. Data set of Mönch glacier, Switzerland. (**a**) Photo of the measured unstable ice mass. The numbers indicate the location of the measured points. The unstable mass is approximately 50 m high, 300 m long (direction normal to the ice flow) and 40 m wide. The distance between points 1, 2 and 3 amounts to approximately 30 m. (**b**) Motion $Y^{a}-\theta_5 t$ versus time (crosses) of point 1 and its associated fit (solid line) based on Eq. (7). The estimated parameters $\hat{\theta}_i$ of Eq. (7) are listed in Table 1. The predicted failure time (corresponding to abscissa zero) was July 4, 2003. (**c**) Residuals of the fit. The solid line indicates the fit of the log-periodic oscillations (see Sect. 5). The dashed line shows the smooth cruve of the residu-**als**

Diffusion Limited Aggregation

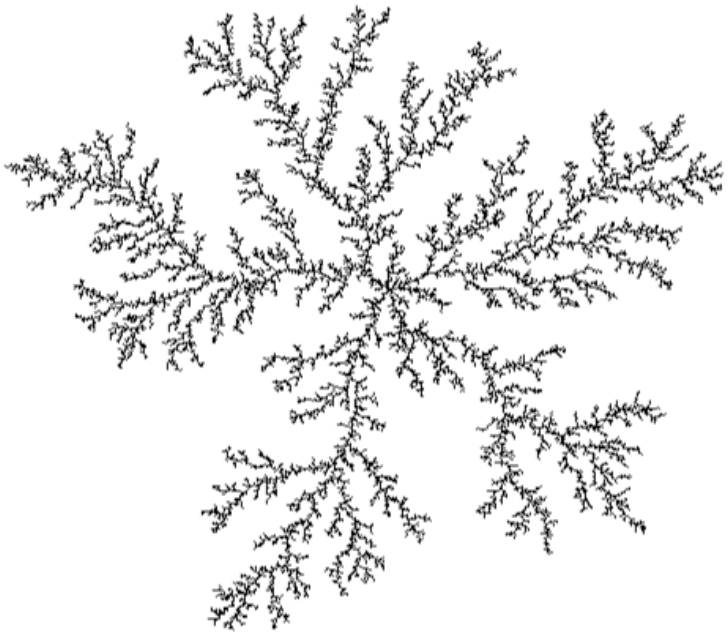

(Arneodo et al, 1992)

$$M(r) = \lambda M x\left(\frac{r}{\lambda}\right) + \lambda^2 M\left(\frac{r}{\lambda^2}\right)$$

$$M(r) = \sum_{n=-\infty}^{+\infty} c_n r^{D_n}$$

Log-periodic sub-dominant correction to scaling

$$D_n = 1 + (-1)^n \frac{\log\phi}{\log\lambda} + i\frac{n\pi}{\log\lambda}$$

$$D_0 = 1 + \log\phi / \log\lambda \simeq 1.65$$

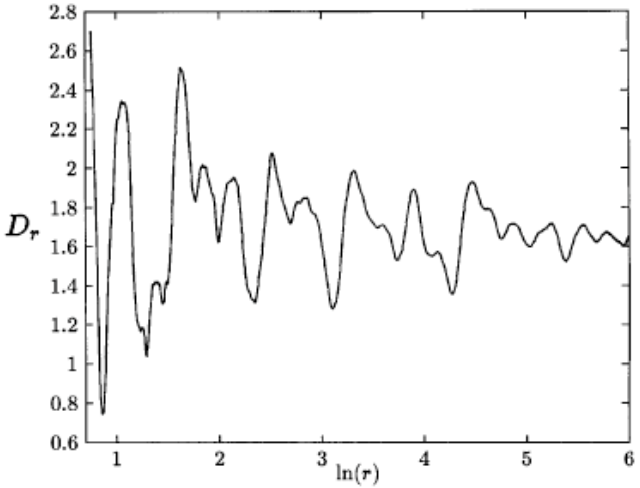

FIG. 1. Example of the local dimension $D_r(\log r) = d\log M(r)/d\log r$ as a function of $\log r$ for a typical DLA cluster. The numerical estimate of the derivative has been obtained with a Savitsky-Golay smoothing filter.

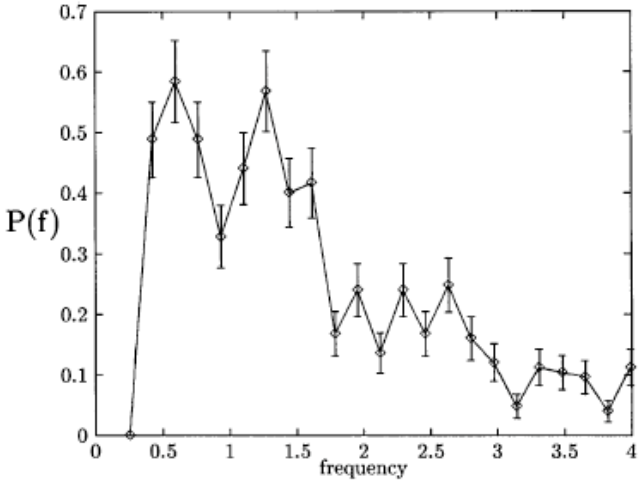

FIG. 2. Histogram of the frequencies found in the local dimension $D_r(\log r) = d\log M(r)/d\log r$ as a function of $\log r$, as illustrated in Fig. 1. The frequencies have been obtained by calculating Lomb's periodogram on D_r.

(Sornette et al., 1996)

TURBULENCE AND DISCRETE SCALE INVARIANCE

• Barenblatt's classification leads to the possibility of *Incomplete similarity* in the variable r/L. This would require the non-existence of a finite and non-zero limit of $F(\mathrm{Re}, r/L)$ as $r/L \to 0$, and leads in the simplest case to the form

$$D_{LL}(r) = C_K(\bar{\epsilon}r)^{2/3}\left(\frac{r}{L}\right)^{\alpha} \ ,$$

where α is the so-called intermittency exponent, believed to be small and non-negative.

D. Sornette, Discrete scale invariance in turbulence? U. Frisch (ed.), Advances in Turbulence VII, 251-254 (Kluwer Academic Publishers, The Netherlands, 1998) (http://xxx.lanl.gov/abs/cond-mat/9802121)

1. if α is real $\to$ similarity of the second kind;
2. if α is complex,

$$D_{LL}(r) = C_K(\bar{\epsilon}r)^{2/3}\left(\frac{r}{L}\right)^{\alpha_R} \cos[\alpha_I \log(r/L)] \ .$$

There is no limit of $F(\mathrm{Re}, r/L)$ but rather accelerated oscillations. (Dubrulle, 1997)

Averaging : grand canonical versus canonical

• Randomness introduces a sensitive dependence of the phase in the cos log formula : different realizations have a different phase and averaging will produce a "destructive interference" that makes vanish the log-periodic oscillations.

• No averaging : log-periodic oscillations are *specific* fingerprints of the specific system one is looking at.

F. Pazmandi, R.T. Scalettar and G.T. Zimanyi, Phys. Rev. Lett. 79, 5130 (1997).

• "Grand canonical" averaging introduces a spurious noise of relative amplitude proportional to $L^{-d/2}$.

• "canonical" averaging consists in identifying, for each realization, the corresponding specific value of the critical control parameter K_c^R. The natural control parameter then becomes

$$\Delta = (K - K_c^R)/K_c^R$$

and the act of averaging can then be performed for the samples with the same Δ.

A. Johansen and D. Sornette, Evidence of discrete scale invariance by canonical averaging, Int. J. Mod. Phys. C 9 (3), 433-447 (1998)

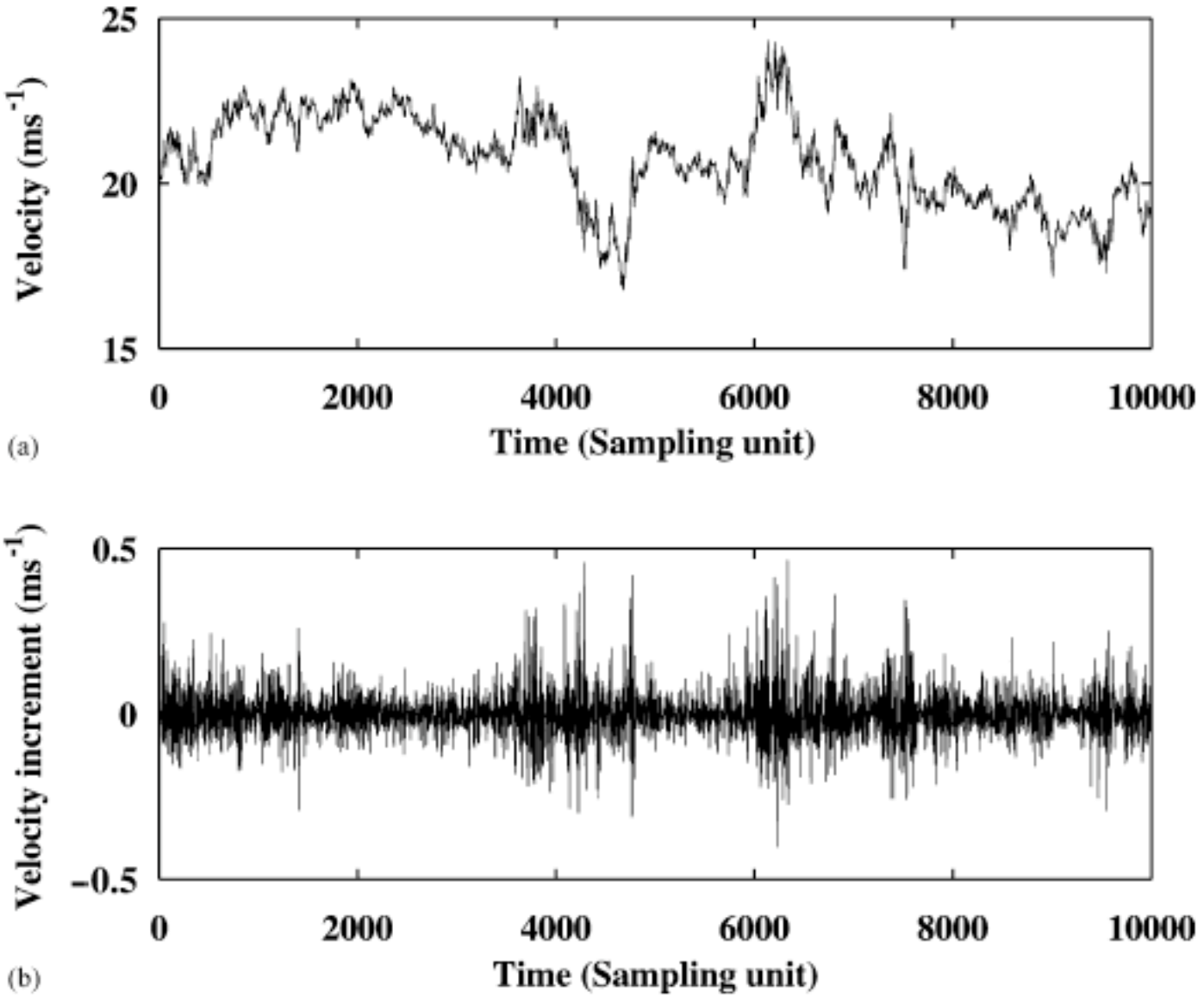

Fig. 11. (a) A typical streamwise velocity time series recorded by hot-wire anemometry in the S1 ONERA wind tunnel. (b) Corresponding time series of the velocity increments.

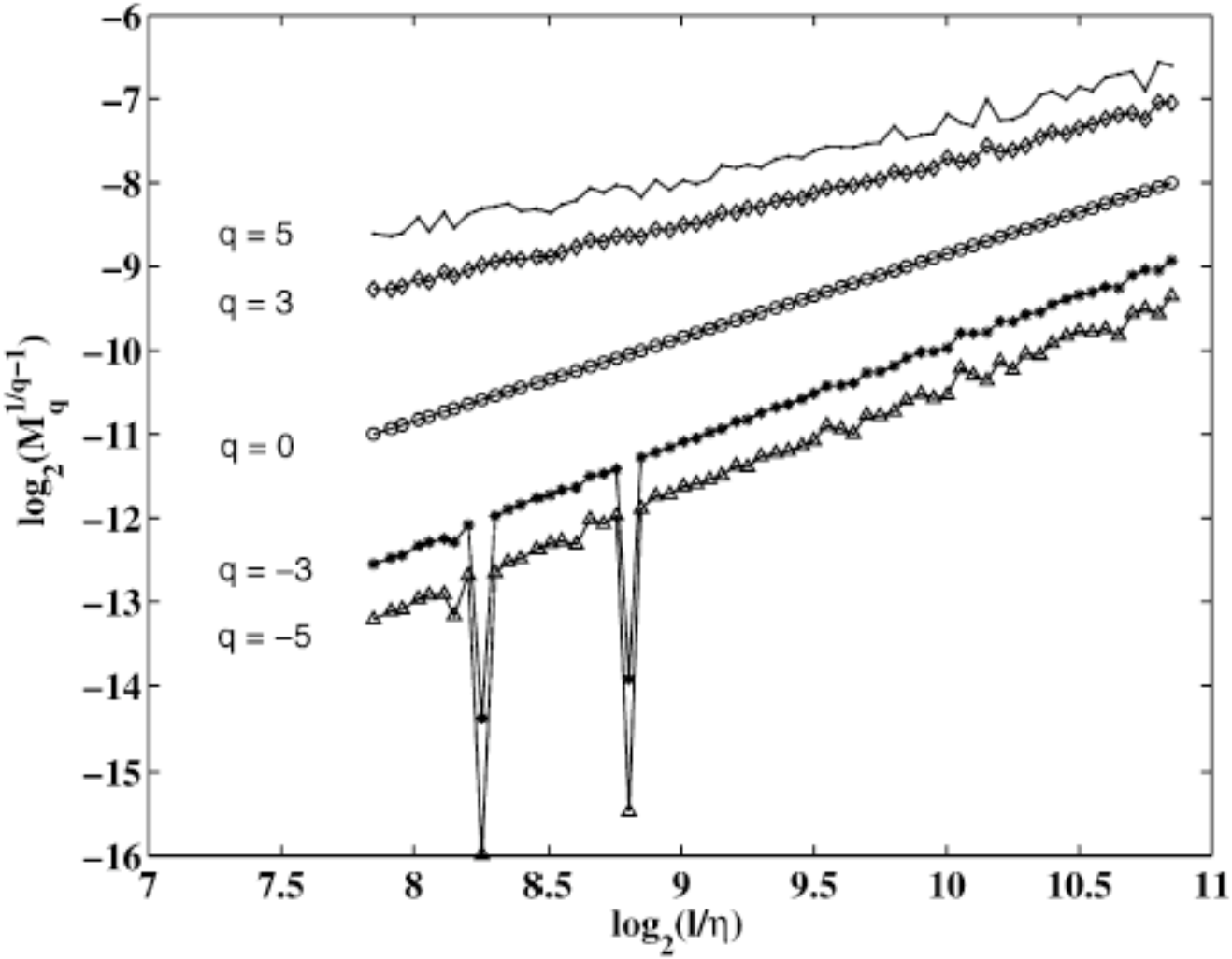

Fig. 12. Double logarithmic plots of $[M_q(\ell)]^{1/(q-1)}$ versus ℓ/η for $q = 5, 3, 0, -3, -5$. We use the usual ("grand-canonical") averaging which scramble any possible log-periodic oscillations.

$$\tau\left(q, \ln(\ell/\eta)\right) = \frac{d\ln[M_q(\ell/\eta)]}{d\ln(\ell/\eta)}$$

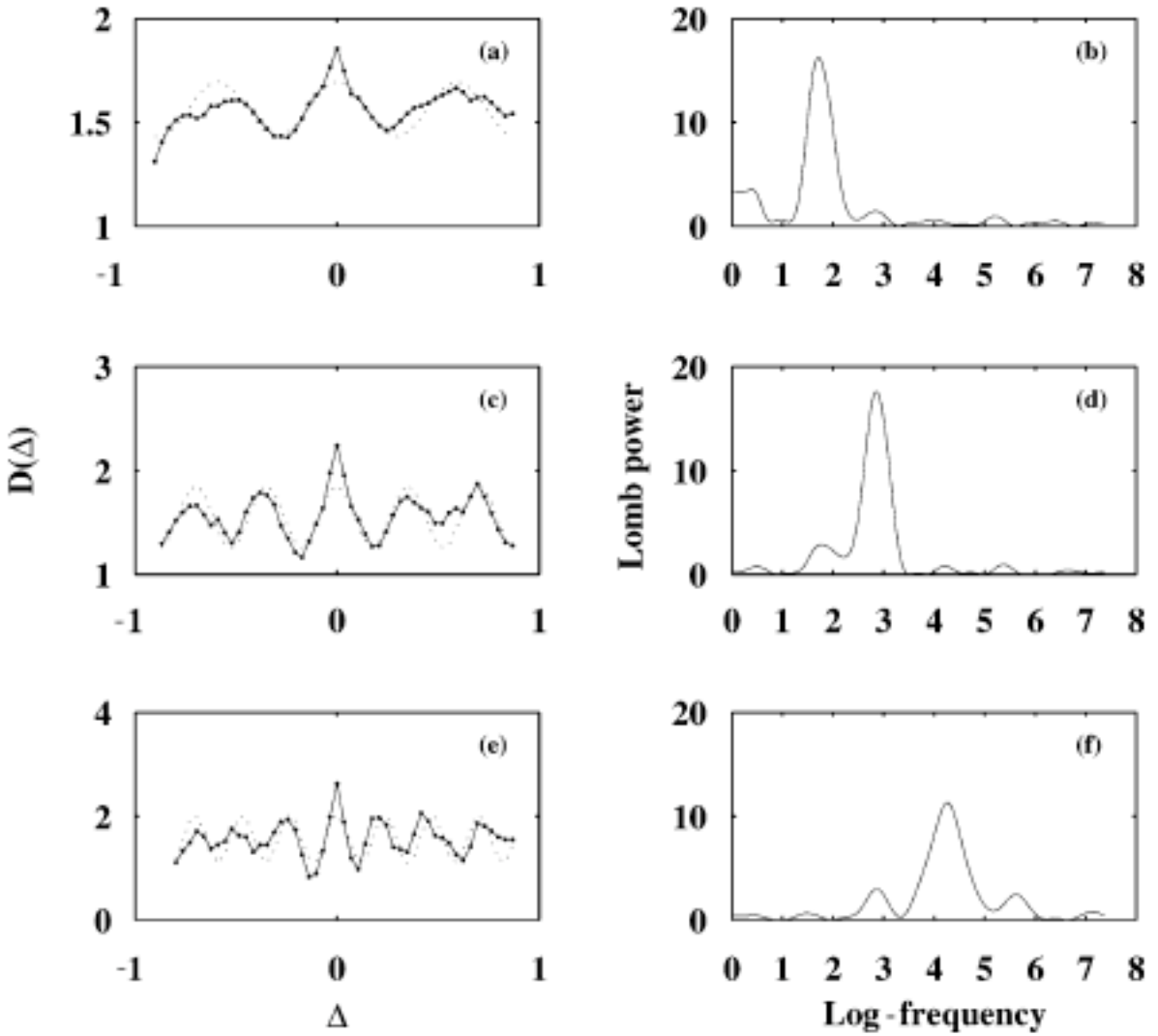

Fig. 14. Local log-derivative $D(\Delta)$ defined in (12), canonically averaged over the 64 samples of a single record of length $L = 2^{17}$ points, as a function of Δ (left panels) and their corresponding Lomb periodograms (right panels) for three choices of the Savitzky–Golay filter parameters N_L and M. (a, b) $M = 4$ and $N_L = 10$; (c, d) $M = 5$ and $N_L = 9$; (e, f) $M = 7$ and $N_L = 8$. The dotted line in the left panels are pure cosine functions $D(\Delta) = \langle D \rangle + \sqrt{2}\sigma_D \cos(2\pi f \Delta)$.

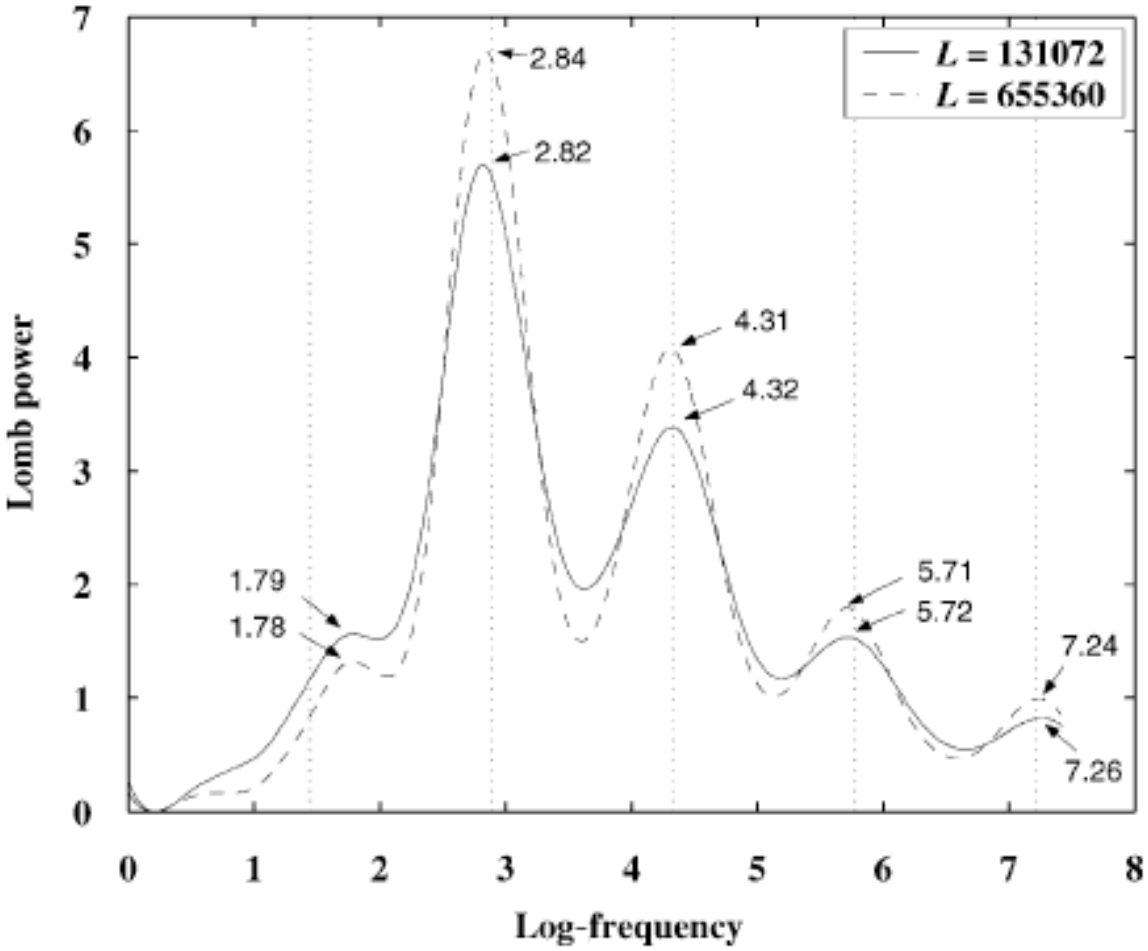

Fig. 22. Average of all 2400 (continuous line) (resp. 480 (dashed line)) Lomb periodograms shown in Figs. 18–21 over all 24 filters and all records. The vertical dashed lines correspond to log-frequencies equal, respectively, to $f_1 = 1.44$, $f_2 = 2f_1 = 2.89$, $f_3 = 3f_1 = 4.33$ and $f_4 = 4f_1 = 5.77$. These values correspond, respectively, to increasing harmonics of a fundamental frequency $f_1 = 1/\ln \gamma$ associated with the scale ratio $\gamma = 2$.

Wei-Xing Zhou and Didier Sornette
Statistical Significance of Periodicity and Log-Periodicity with Heavy-Tailed Correlated Noise, Int. J. Mod. Phys. C 13 (2), 137-170 (2002)

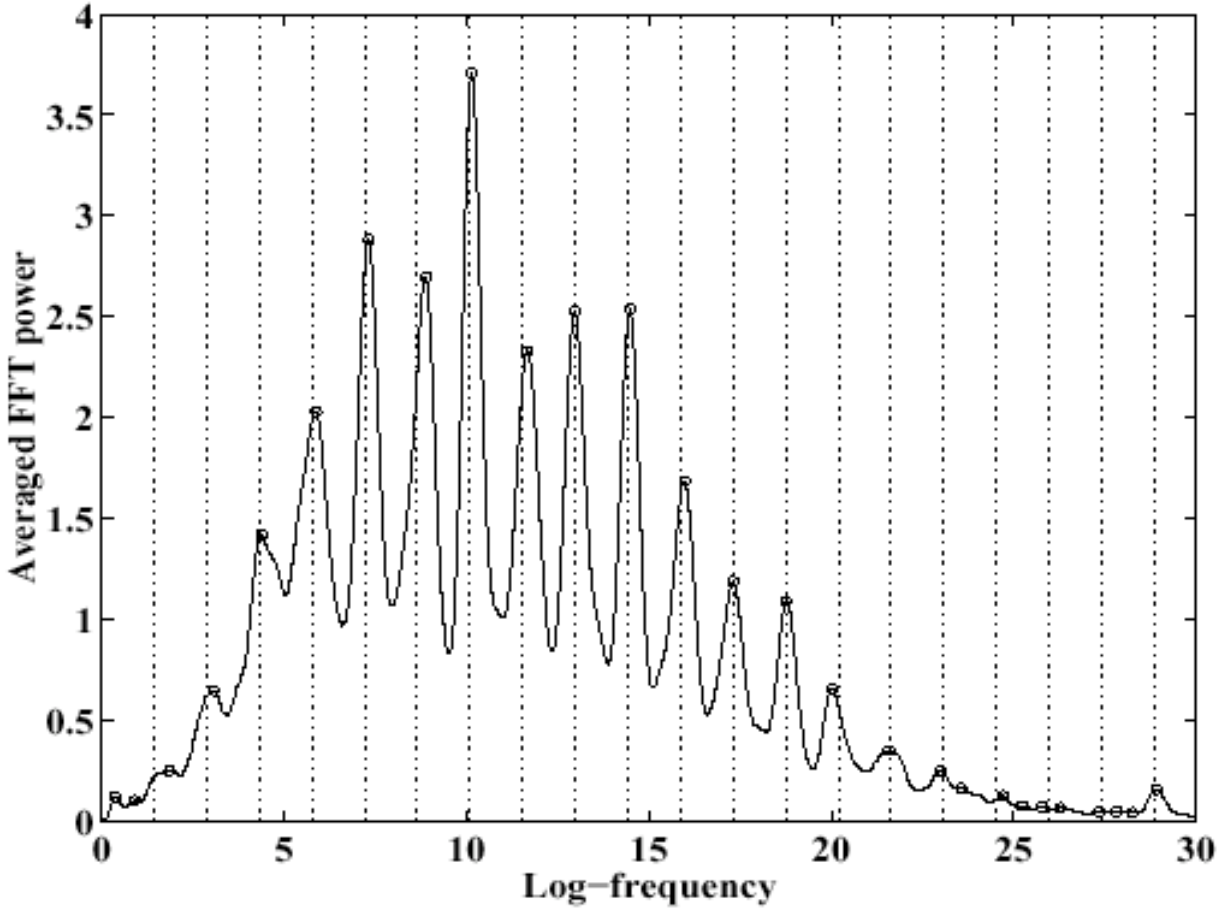

FIG. 7: Average of all Fourier periodograms over 320 samples. The vertical dashed lines correspond to log-frequencies equal to $f_k = k/\ln 2$ with $k = 1, \cdots, 21$. The peaks are indicated with open circles. Most of the peaks are very close to the vertical dotted lines which can be interpreted as harmonics of $f = 1/\ln 2$.

Wei-Xing Zhou, Didier Sornette and Vladilen Pisarenko, New Evidence of Discrete Scale Invariance in the Energy Dissipation of Three-Dimensional Turbulence: Correlation Approach and Direct Spectral Detection, Int. J. Mod. Phys. C in press (http://arXiv.org/abs/cond-mat/0208347)

Oscillatory Finite-Time Singularities in Finance, Population and Rupture

The balance between supply and demand determines the price variation from $p(t)$ to $p(t+\delta t)$ over the time interval δt according to [Farmer, 1998]

$$\ln p(t+\delta t) - \ln p(t) = \frac{1}{L}[\Omega_{\text{value}}(t) + \Omega_{\text{tech}}(t)] \quad (10)$$

Fundamental value strategies

$$\Omega_{\text{value}}(t) = -c \ \ln[p(t)/p_f] \ |\ln[p(t)/p_f]|^{n-1}$$

Technical analysis strategies

$$\Omega_{\text{tech}}(t) = a_1[\ln p(t) - \ln p(t-\delta t)]$$
$$+a_2[\ln p(t) - \ln p(t-\delta t)]|\ln p(t) - \ln p(t-\delta t)|^{m-1}$$

The theory becomes critical when the "mass" term vanishes, i.e., when $a_1 = L$. Rescaling t and y_1 by α and posing $y_2 = dY_1/dt$ and $\gamma = \alpha^{-(n+1)} c/L(\delta t)^2$ where $\alpha \equiv a_2(\delta t)^{m-2}/L$, we obtain

$$\frac{dy_1}{dt} = y_2 \ ,$$
$$\frac{dy_2}{dt} = \alpha y_2 |y_2|^{m-1} - \gamma y_1 |y_1|^{n-1}$$

or

$$\frac{d^2 y_1}{dt^2} = -\gamma y_1 |y_1|^{n-1} + \alpha \frac{dy_1}{dt} \left|\frac{dy_1}{dt}\right|^{m-1}$$

Inertia + NL negative feedback + NL positive feedback

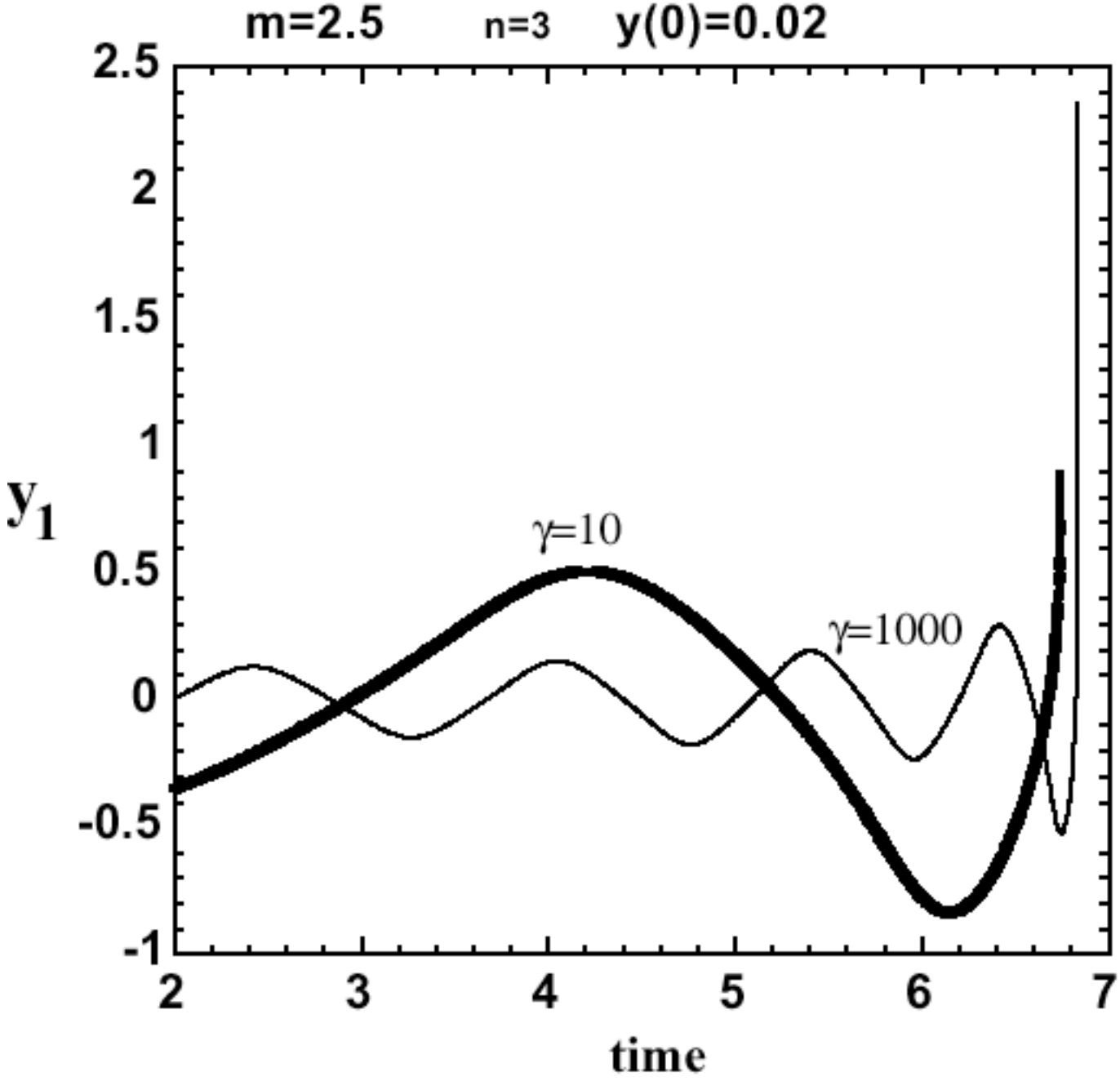
m=2.5 n=3 y(0)=0.02
2.5
2
1.5
1
0.5
0
-0.5
-1
y1
γ=10
γ=1000
2
3
4
5
6
7
time

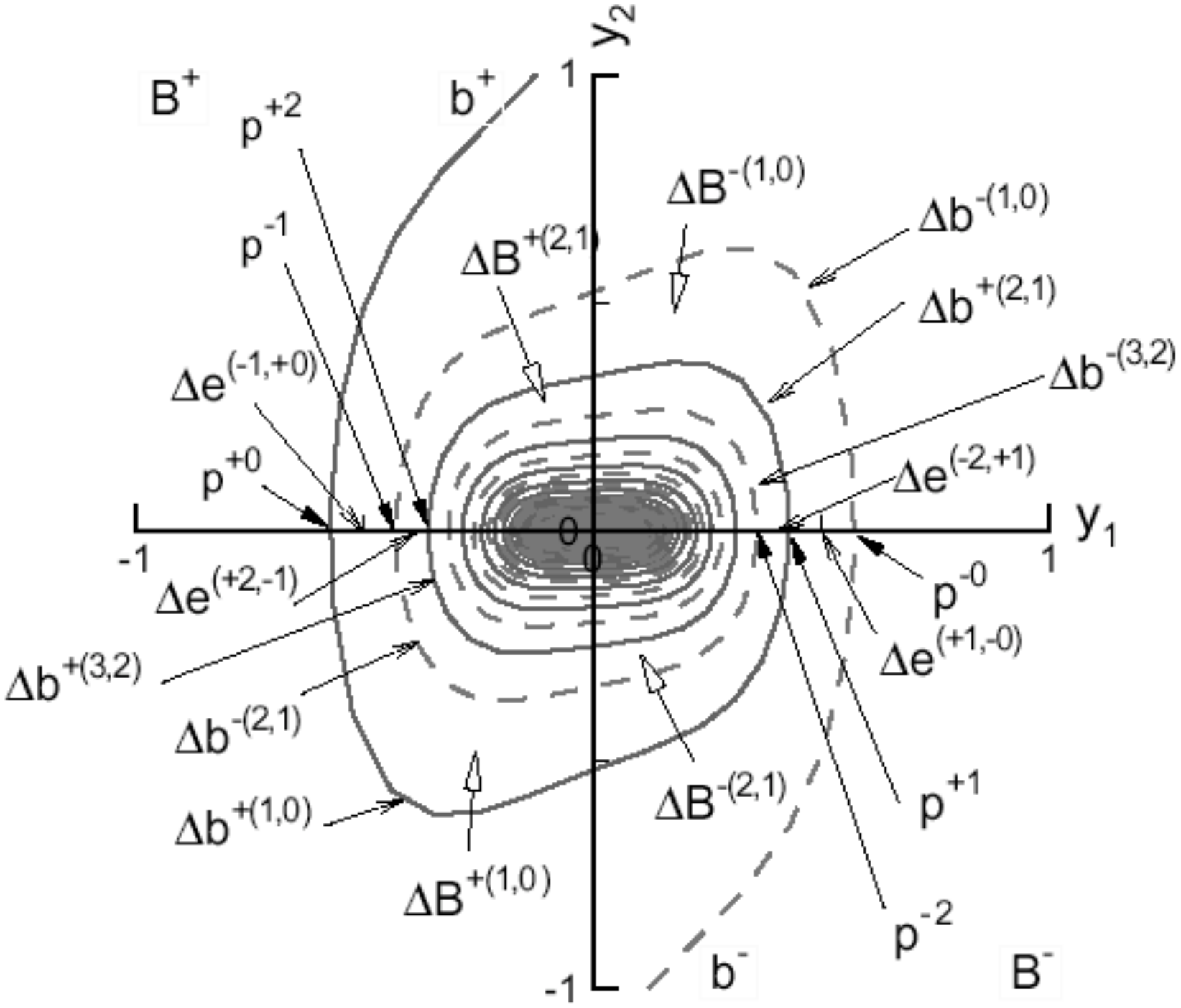
B+
b+
y2
1
p+2
p-1
ΔB-(1,0)
Δb-(1,0)
ΔB+(2,1)
Δb+(2,1)
Δb-(3,2)
Δe(-1,+0)
p+0
Δe(-2,+1)
y1
-1
0
0
1
Δe(+2,-1)
p-0
Δe(+1,-0)
Δb+(3,2)
Δb-(2,1)
p+1
Δb+(1,0)
ΔB-(2,1)
ΔB+(1,0)
p-2
b-
B-
-1

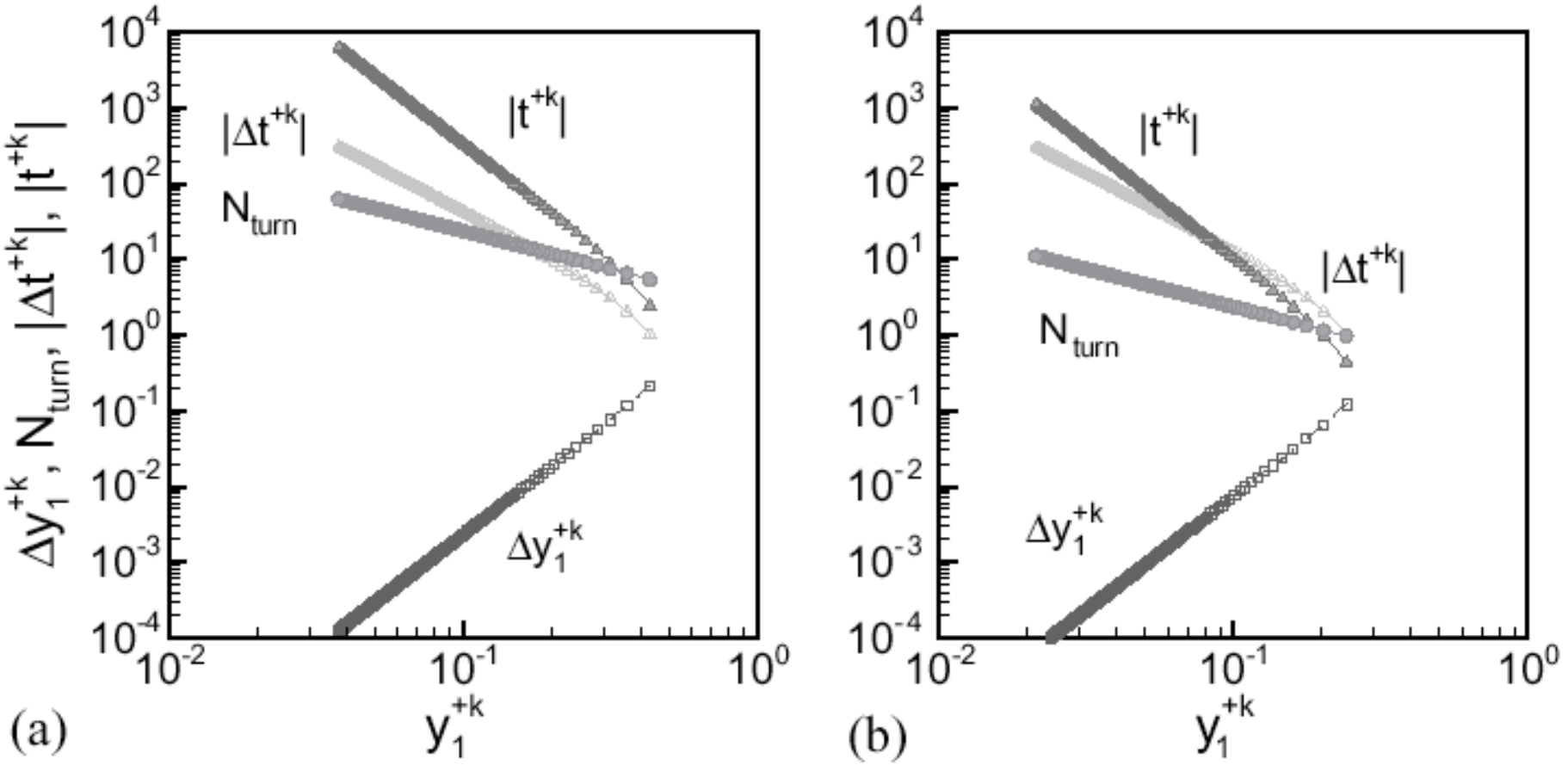

Fig. 13. Scaling laws associated with the fractal properties as a function of the initial condition at the turn points $\mathbf{y}_0 = (y_{10}^{+k}, 0)$ of b^+ for $y_1 > 0$ on the y_1-axis for $(n, m) = (3, 2.5)$: (a) $\gamma = 10$ as in Fig. 9 and (b) $\gamma = 1000$. The notations are: $\Delta y_1 = |y_{10}^{+(k+2)} - y_{10}^{+k}|$, $\Delta t_e = t_e(\mathbf{p}^{+(k+2)}) - t_e(\mathbf{p}^{+k})|$, $t_e = t^{\pm k}(\mathbf{p}^{+k})$, and $N_{turn} = k$.

$N_{turn} \sim y_{10}^{-a}$ where $a > 0$,

$t_c \sim y_{10}^{-b}$ where $b > 0$,

$\Delta y_1 \sim y_{10}^{c}$ where $c > 0$,

$\Delta t_c \sim y_{10}^{-d}$ where $d > 0$.

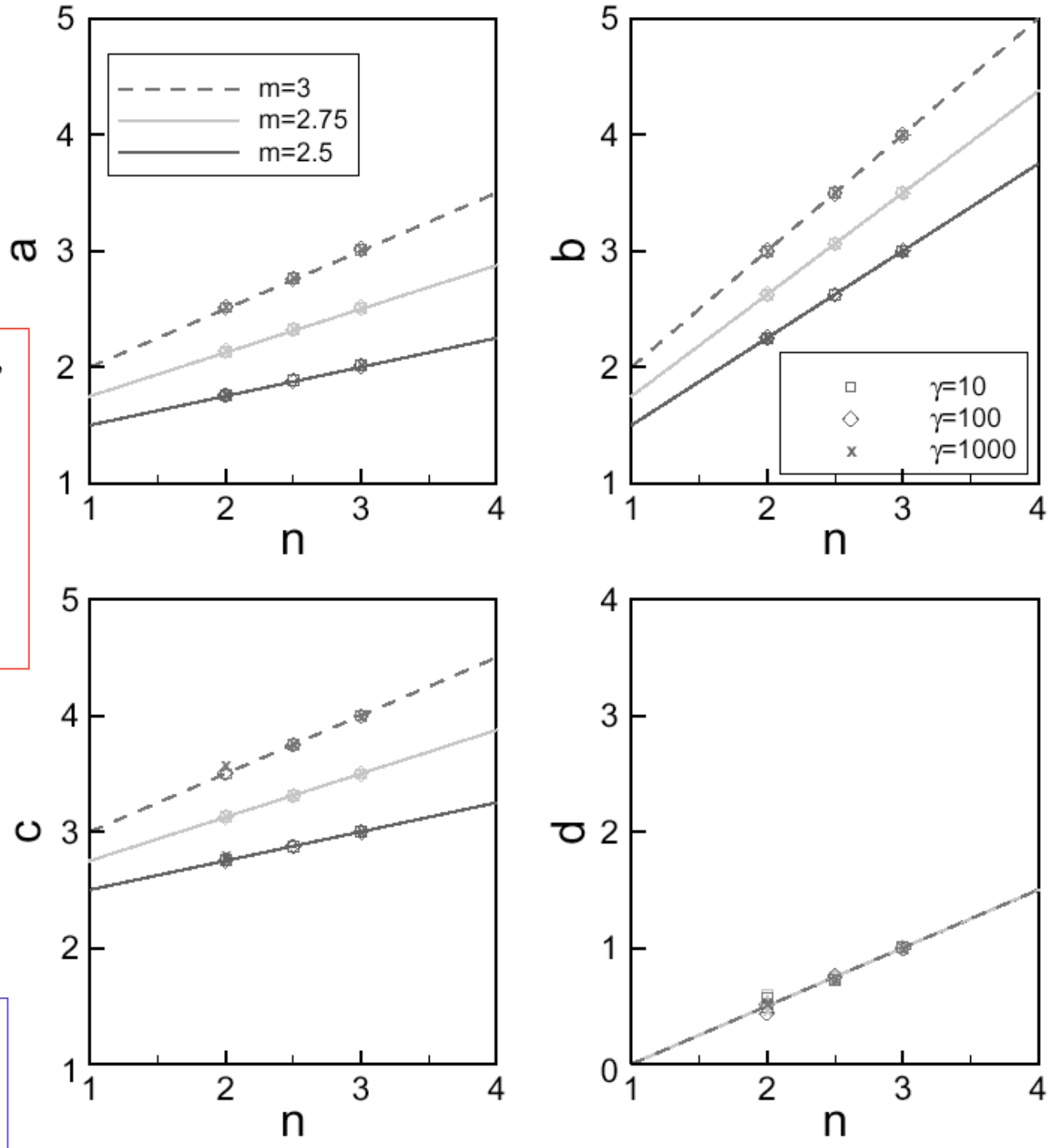

K. Ide and D. Sornette
Oscillatory Finite-Time Singularities in Finance, Population and Rupture, Physica A 307 (1-2), 63-106 (2002)

Hong-Kong

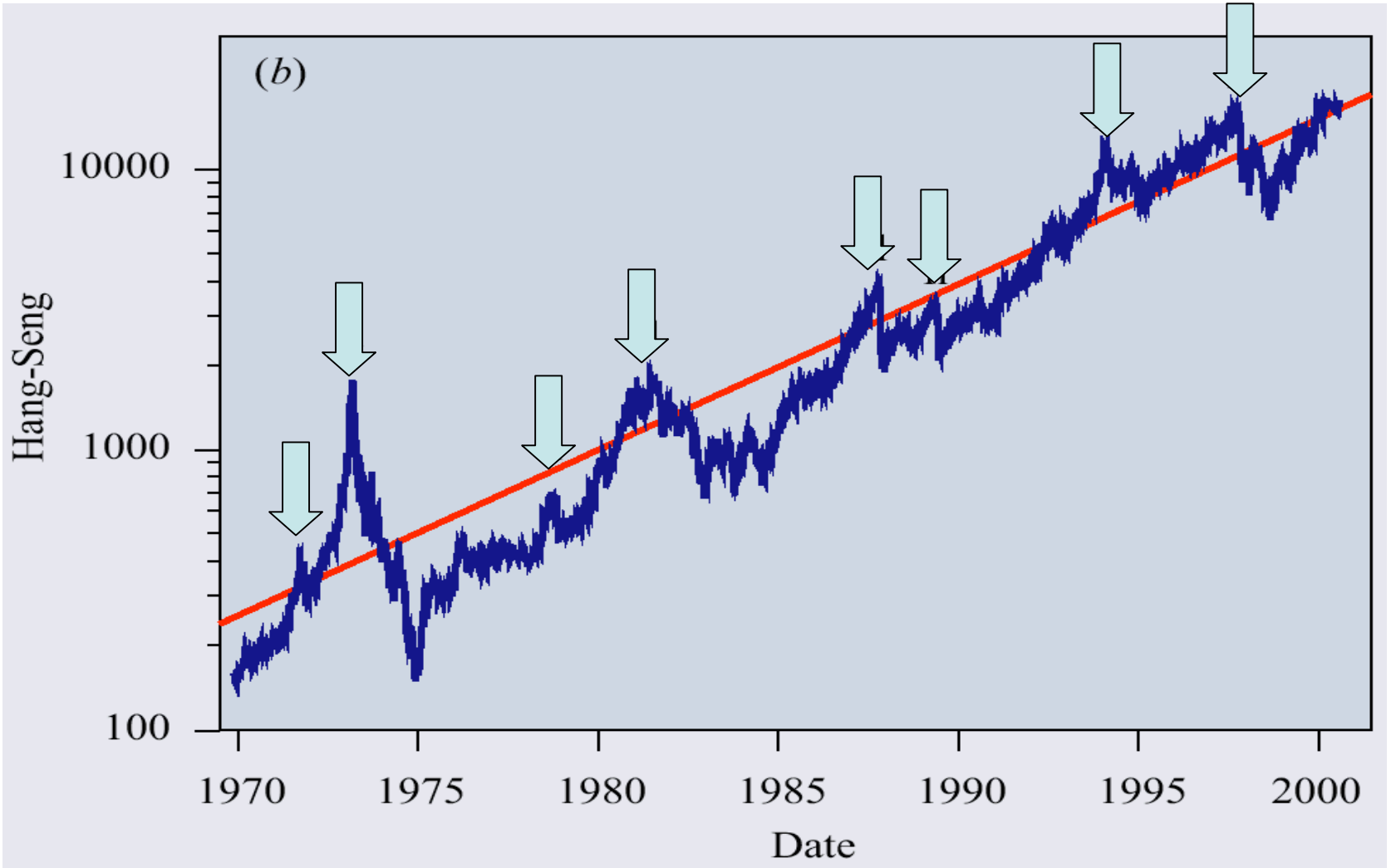

Figure 12. Hong Kong crash of 1971. The parameter values of the fit with equation (3) are $A \approx 569$, $B \approx -340$, $C \approx 17$, $\beta \approx 0.20$, $t_c \approx 1971.73$, $\phi \approx -0.5$ and $\omega \approx 4.3$.

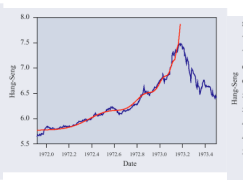

Figure 11. Hong Kong crash of 1973. The parameter values of the fit with equation (3) are $A \approx 10.8$, $B \approx -5.0$, $C \approx -0.05$, $\beta \approx 0.11$, $t_c \approx 1973.19$, $\phi \approx -0.05$ and $\omega \approx 8.7$. Note that for this bubble, it is the logarithm of the index which is used in the fit.

Figure 10. Hong Kong crash of 1978. The parameter values of the fit with equation (3) are $A \approx 824$, $B \approx -538$, $C \approx -28.0$, $\beta \approx 0.40$, $t_c \approx 1978.69$, $\phi \approx -0.17$ and $\omega \approx 5.9$.

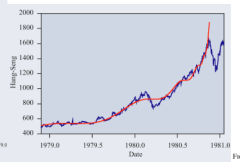

Figure 9. Hong Kong crash of 1980. The parameter values of the fit with equation (3) are $A \approx 2006$, $B \approx -1286$, $C \approx -55.5$, $\beta \approx 0.29$, $t_c \approx 1980.88$, $\phi \approx 1.8$ and $\omega \approx 7.2$.

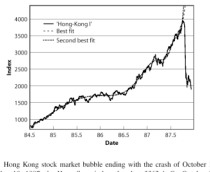

Fig. 7.9. Hong Kong stock market bubble ending with the crash of October 1987. On October 19, 1987, the Hang Seng index closed at 3362.4. On October 26, it closed at 2241.7, corresponding to a loss of 33.3%. See Table 7.1 for the parameter values of the fit with equation (15). Note that the two fits are almost indistinguishable except at the very end of the bubble. Reproduced from [218].

Figure 8. Hong Kong crash of 1989. The parameter values of the fit with equation (3) are $A \approx 3515$, $B \approx -1072$, $C \approx 225$, $\beta \approx 0.57$, $t_c \approx 1989.46$, $\phi \approx 0.5$ and $\omega \approx 4.9$.

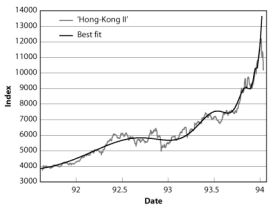

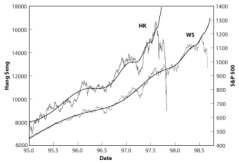

Fig. 7.17. The Hang Seng index prior to the October 1997 crash on the Hong Kong Stock Exchange already shown in Figure 7.13 and the S&P 500 stock market index prior to the crash on Wall Street in August 1998. The fit to the S&P 500 index is equation (15) with $A_1 \approx 1321$, $B_1 \approx -402$, $B_2/C \approx 19.7$, $m_2 \approx 0.60$, $t_c \approx 98.72$, $\phi \approx 0.75$, and $\omega \approx 6.4$. Reproduced from [221].

THE CRASH OF OCTOBER 1987

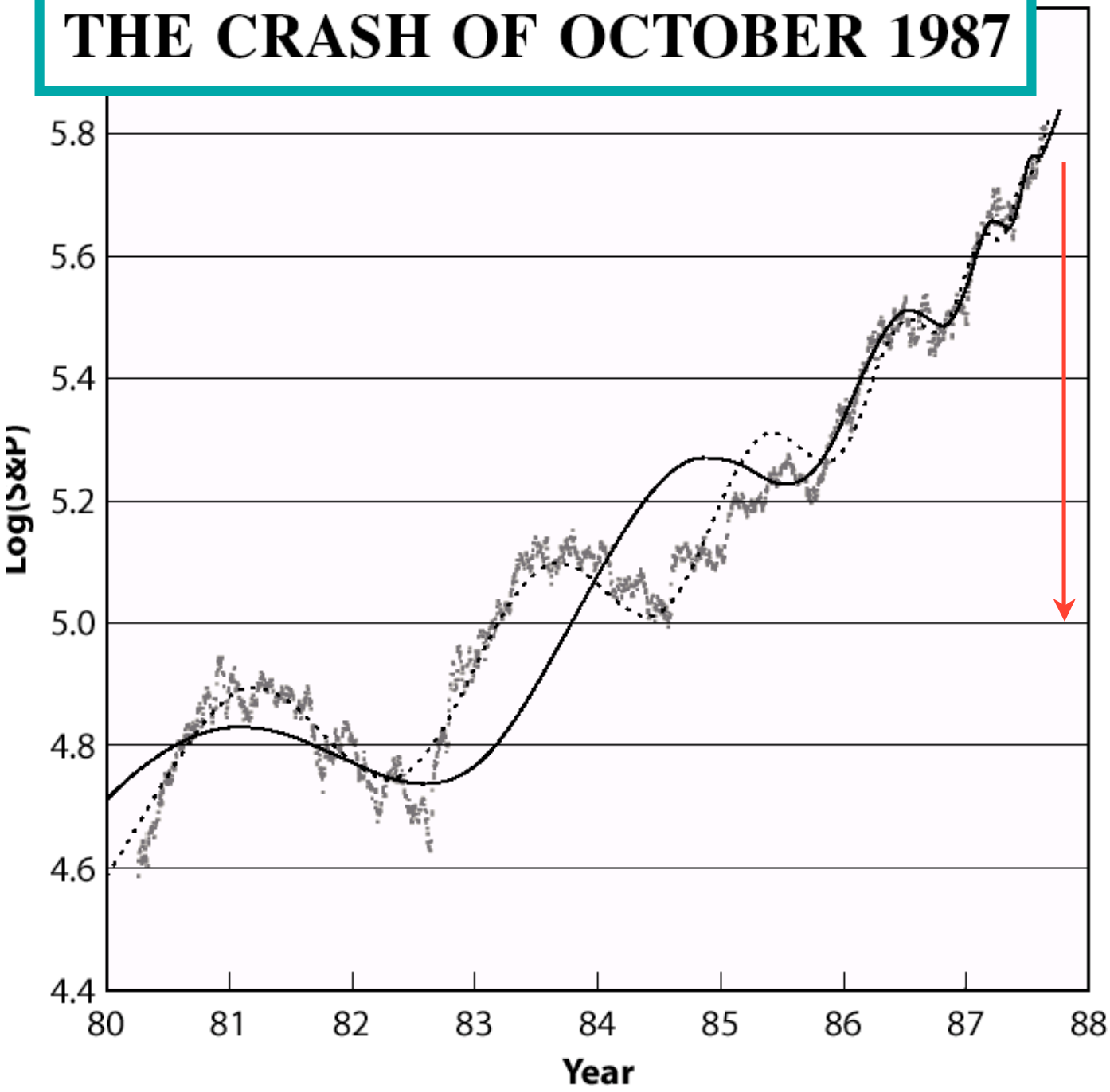

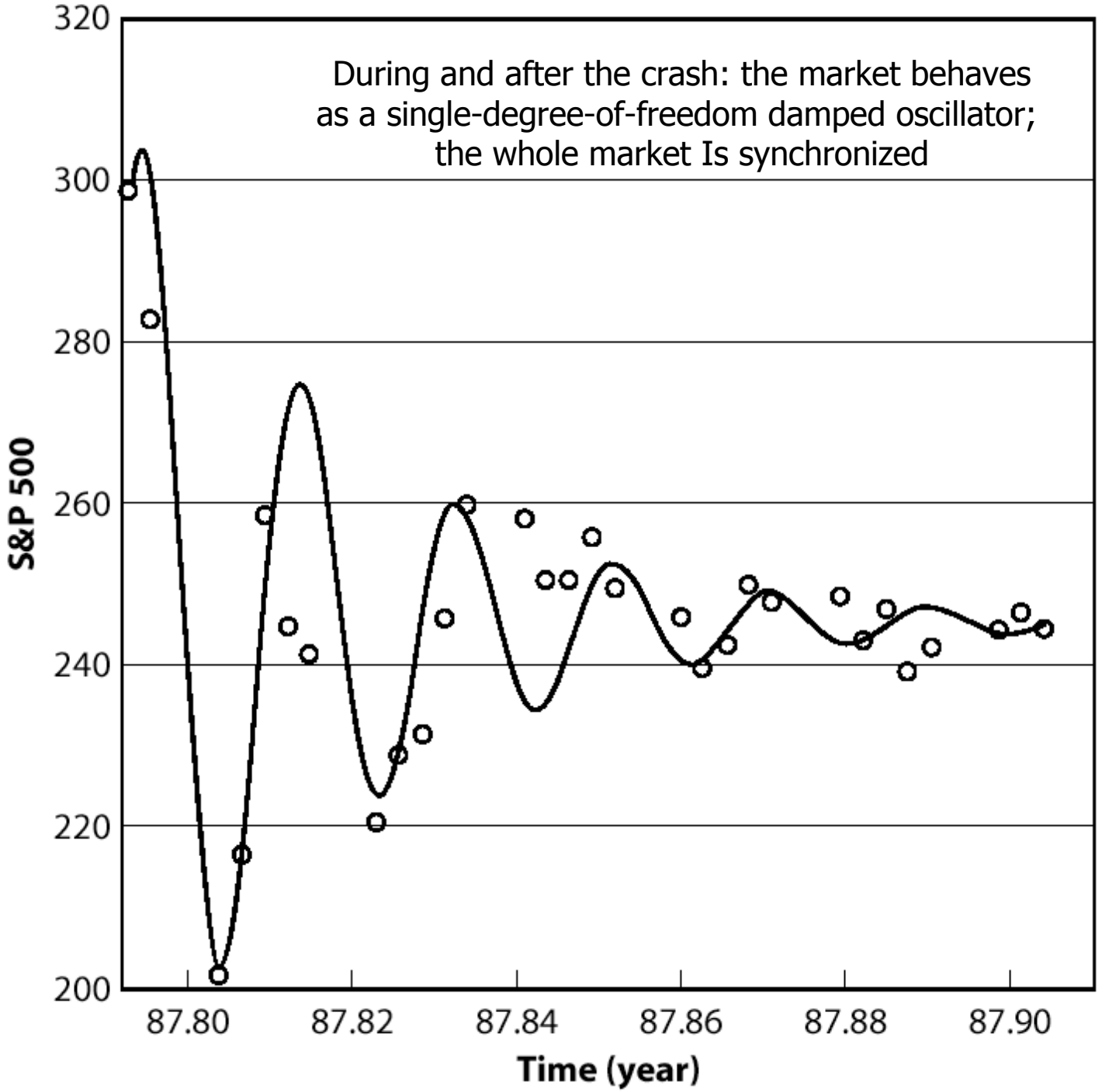
During and after the crash: the market behaves
as a single-degree-of-freedom damped oscillator;
the whole market Is synchronized
320
300
280
260
240
220
200
S&P 500
87.80
87.82
87.84
87.86
87.88
87.90
Time (year)

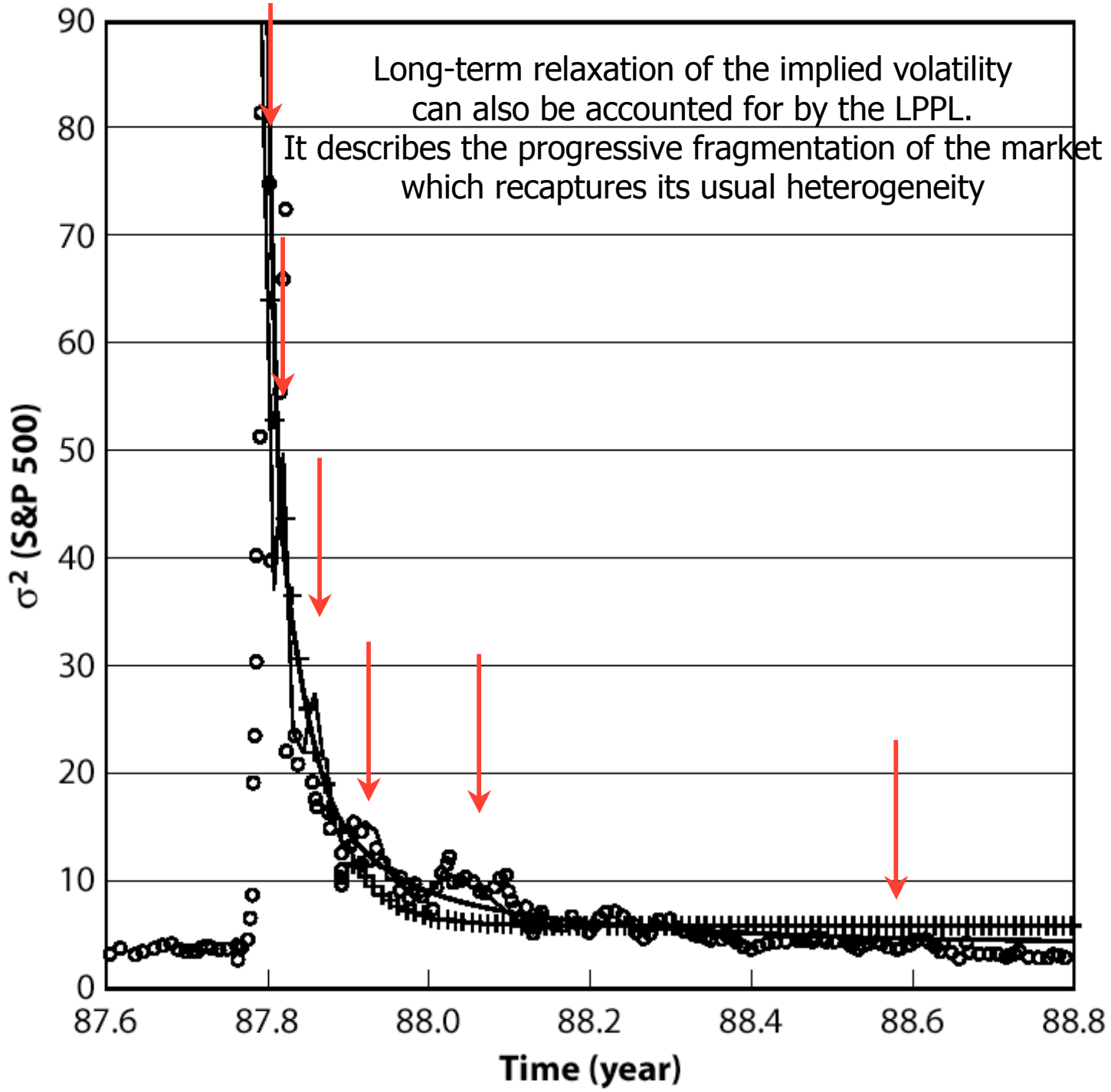
Long-term relaxation of the implied volatility
can also be accounted for by the LPPL.
It describes the progressive fragmentation of the market
which recaptures its usual heterogeneity
σ² (S&P 500)
Time (year)
90
80
70
60
50
40
30
20
10
0
87.6
87.8
88.0
88.2
88.4
88.6
88.8

THE NASDAQ CRASH OF APRIL 2000

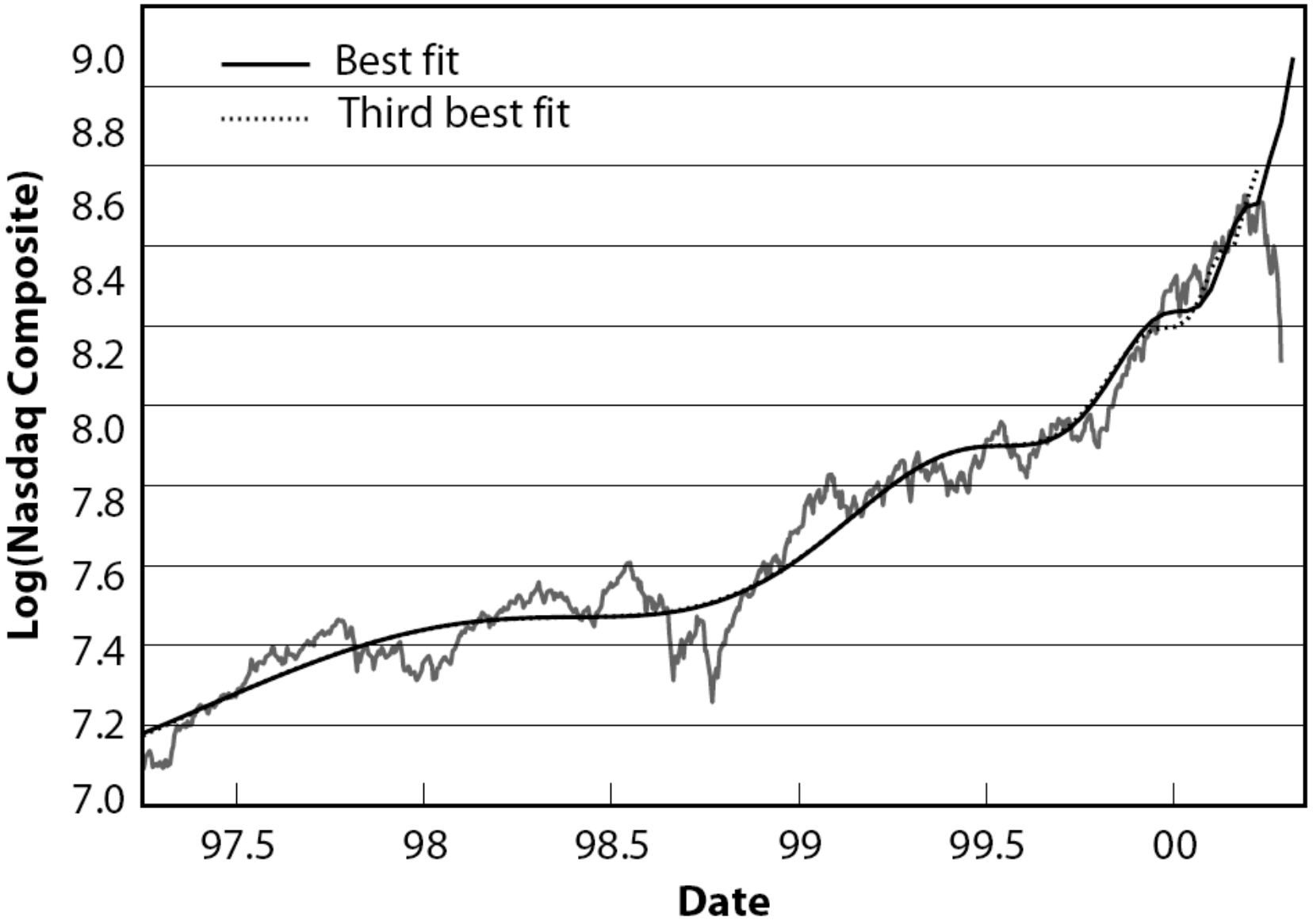

Various Bubbles and Crashes

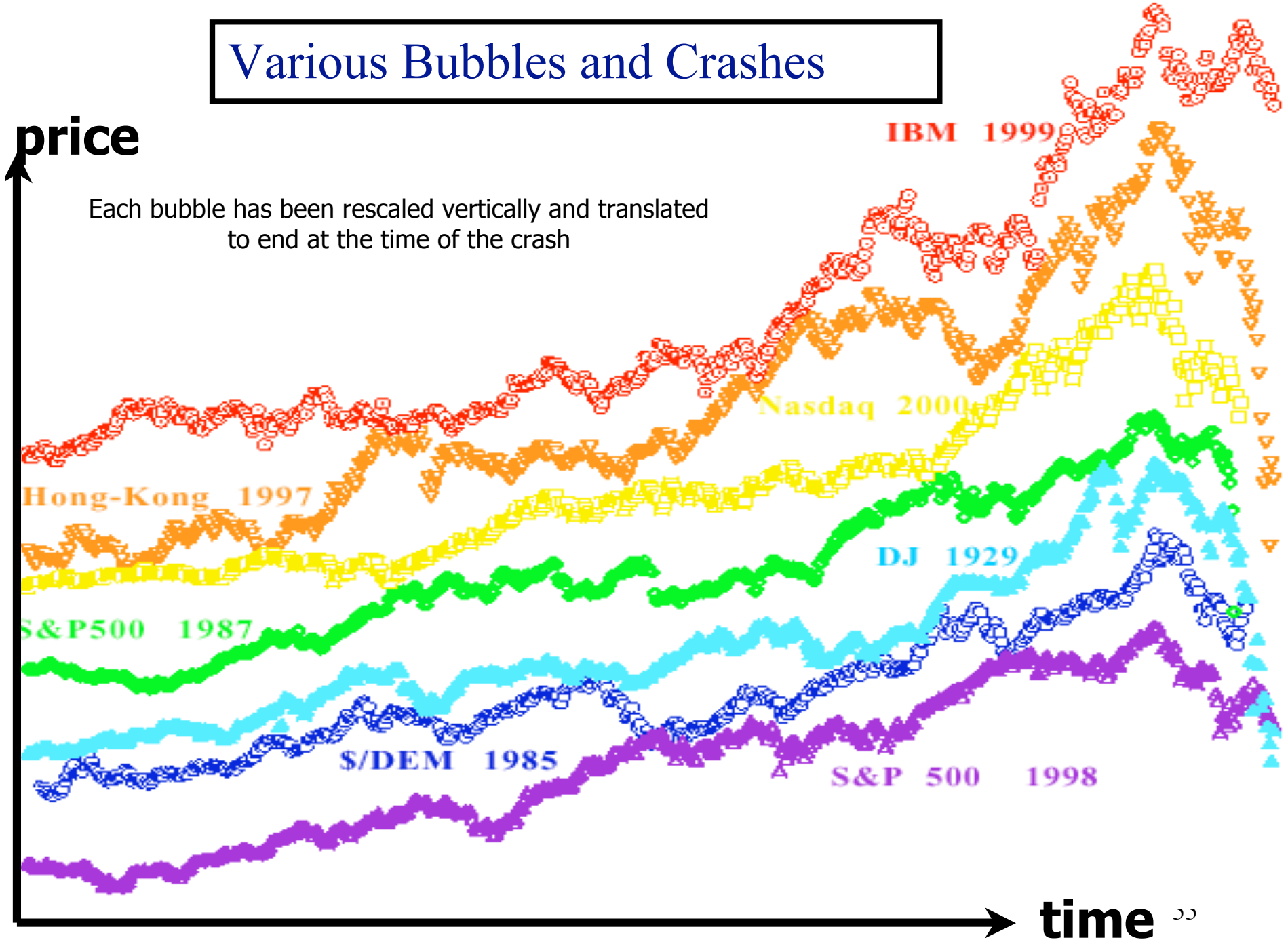

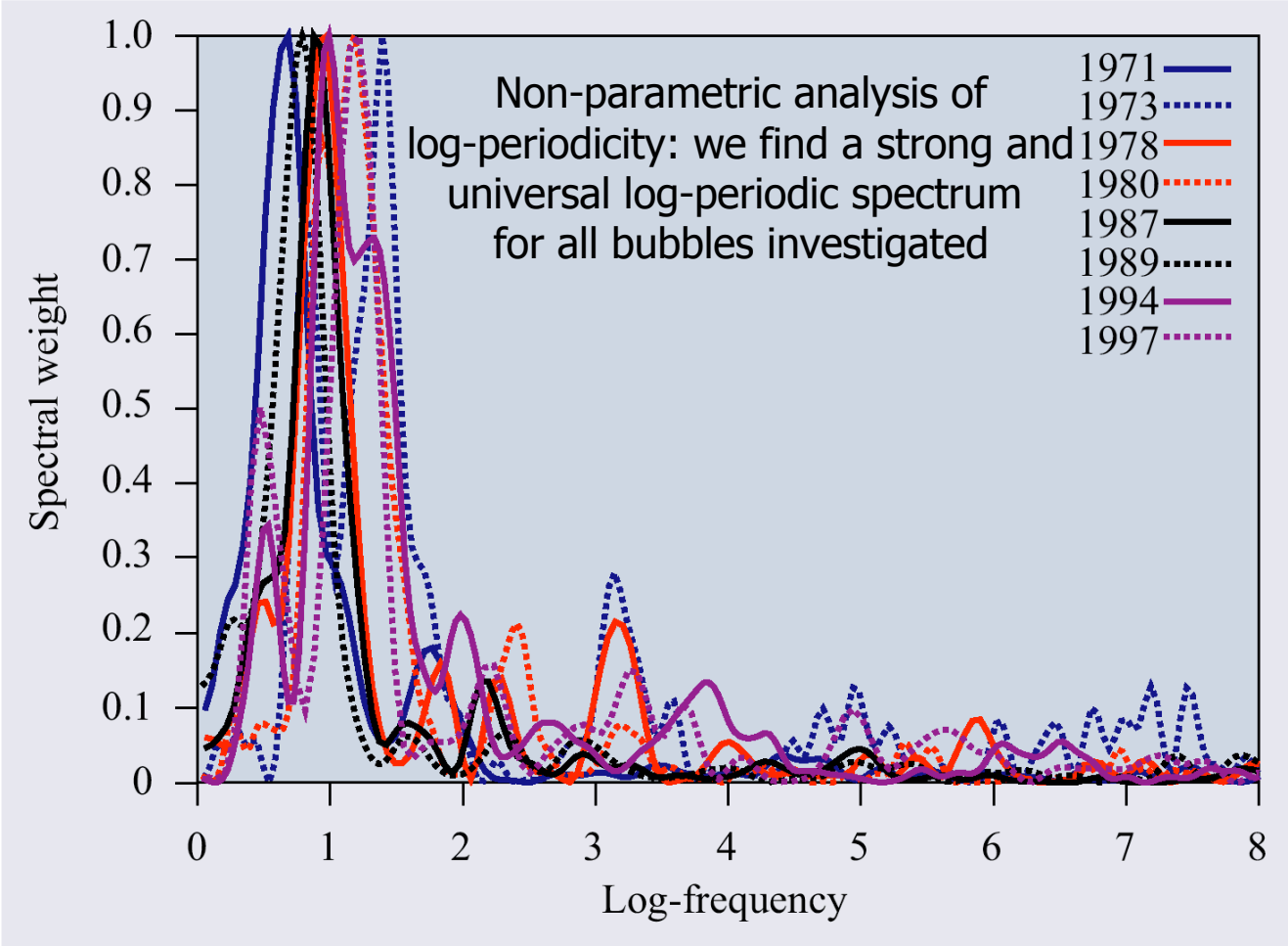

Figure 1. The Lomb periodogram of the log-periodic component of the Hang-Seng price index (Hong Kong) for the eight bubbles followed by crashes observed in figure 13, ending in October 1971, in February 1973, in September 1978, in October 1980, in October 1987, in April 1989, in January 1994 and in October 1997. See Johansen *et al* (1999) for details on how to calculate the Lomb periodogram.

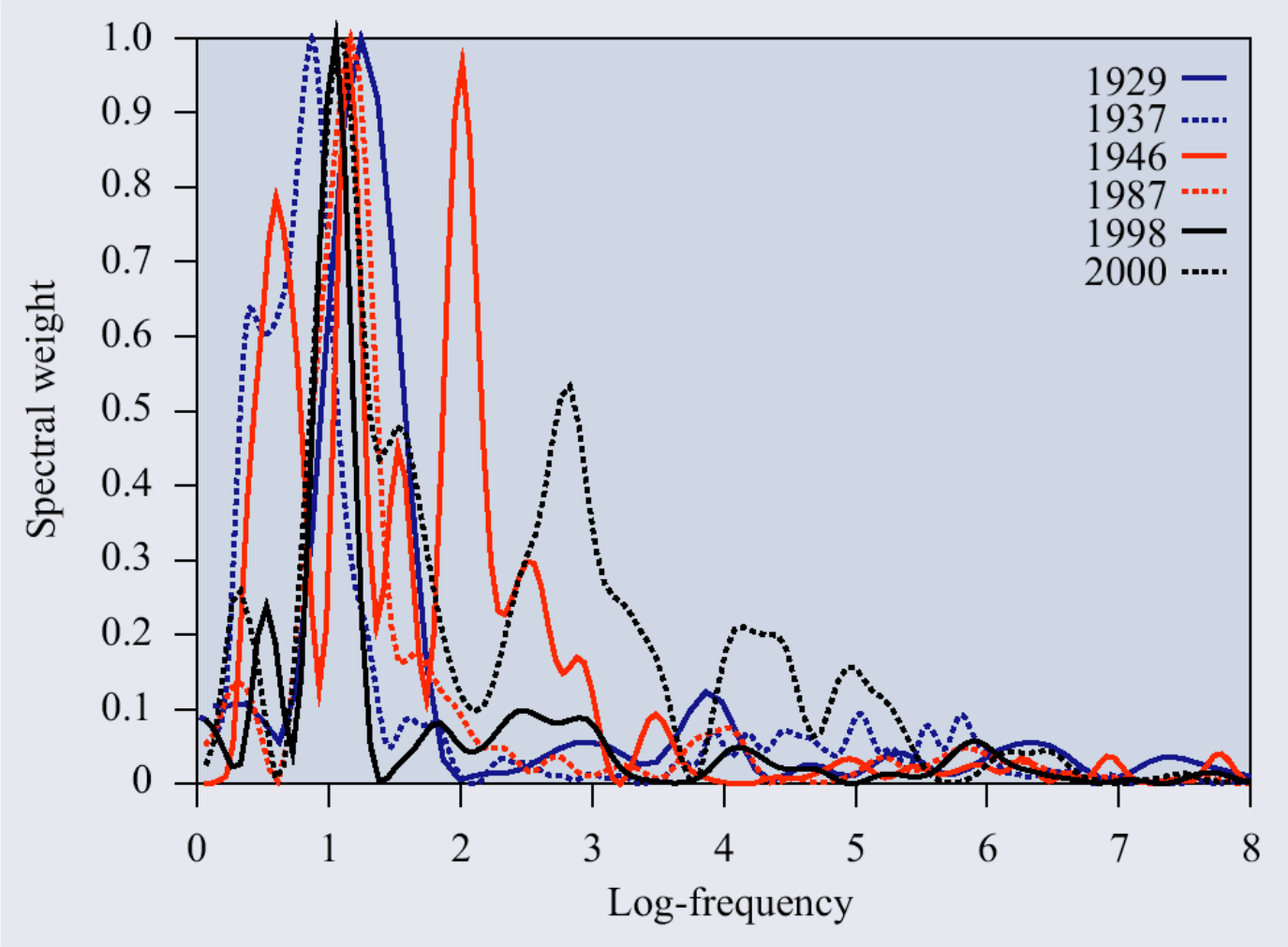

Figure 2. Log-periodic spectra for all the major bubbles ending in crashes on the Dow Jones and SP500 index in the twentieth century as well as the NASDAQ crash of 2000. Observe that the sub-harmonics (half log-frequency) and two harmonics $2f$ and $3f$ are quite strong in some of the data sets. See Johansen *et al* (1999) for details on how to calculate the Lomb periodogram.

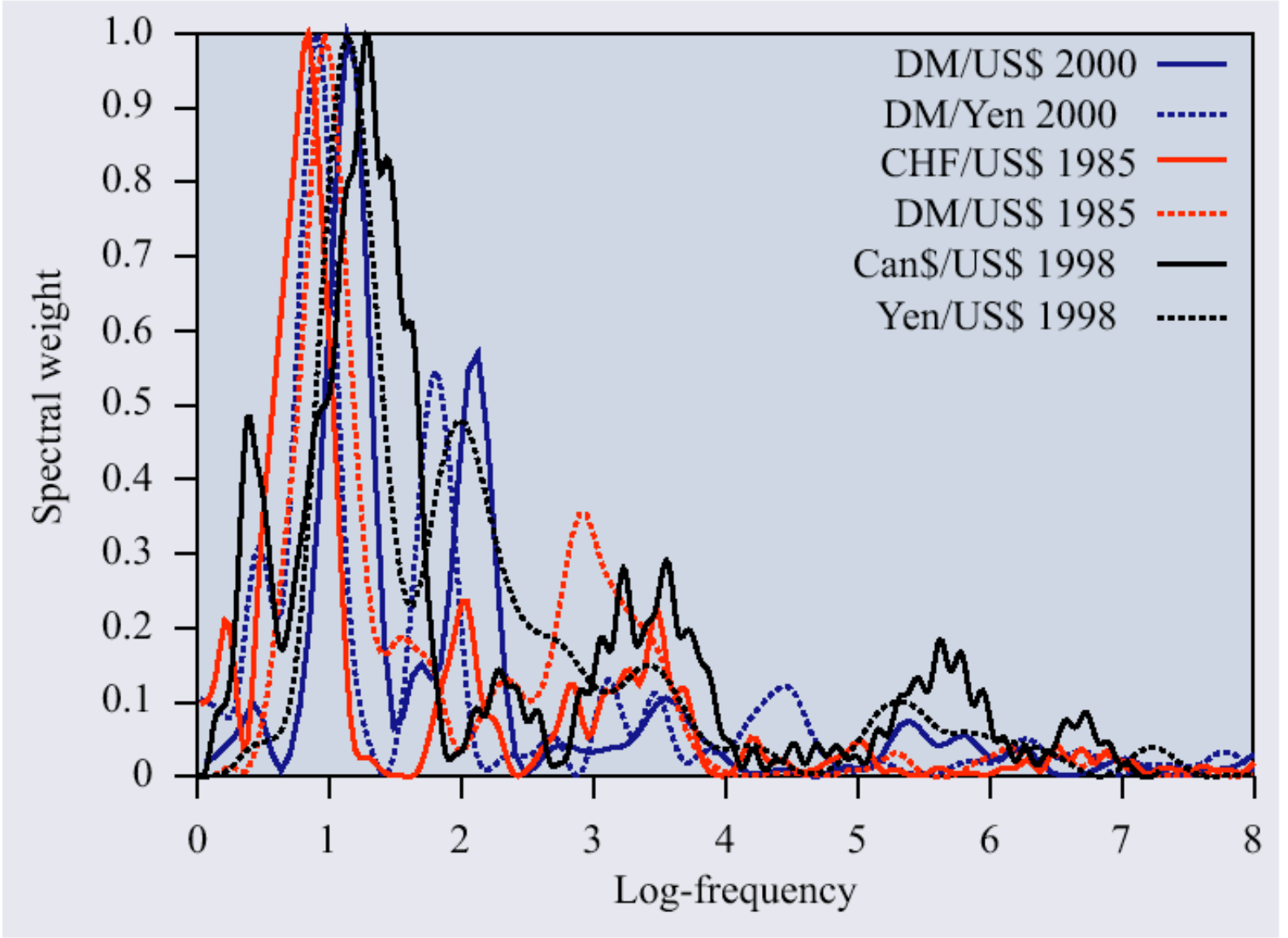

Figure 3. Log-periodic spectra for the major recent bubbles on currencies. See Johansen *et al* (1999) for details on how to calculate the Lomb periodogram.

Crash	t_c	t_{max}	t_{min}	*% drop*	m_2	ω	λ
1929 (DJ)	30.22	29.65	29.87	47%	0.45	7.9	2.2
1985 (DM)	85.20	85.15	85.30	14%	0.28	6.0	2.8
1985 (CHF)	85.19	85.18	85.30	15%	0.36	5.2	3.4
1987 (S&P)	87.74	87.65	87.80	30%	0.33	7.4	2.3
1987 (HK)	87.84	87.75	87.85	50%	0.29	5.6	3.1
1994 (HK)	94.02	94.01	94.04	17%	0.12	6.3	2.7
1997 (HK)	97.74	97.60	97.82	42%	0.34	7.5	2.3
1998 (S&P)	98.72	98.55	98.67	19.4%	0.60	6.4	2.7
1999 (IBM)	99.56	99.53	99.81	34%	0.24	5.2	3.4
2000 (P&G)	00.04	00.04	00.19	54%	0.35	6.6	2.6
2000 (Nasdaq)	00.34	00.22	00.29	37%	0.27	7.0	2.4

t_c is the critical time predicted from the fit of the financial time series to the equation (15). The other parameters m_2, ω, and λ of the fit are also shown. The fit is performed up to the time t_{max} at which the market index achieved its highest maximum before the crash. t_{min} is the time of the lowest point of the market before rebound. The percentage drop is calculated from the total loss from t_{max} to t_{min}. Reproduced from [218].

$$I(t) = A + B(t_c - t)^z + C(t_c - t)^z \cos(\omega \log(t_c - t) - \phi)$$

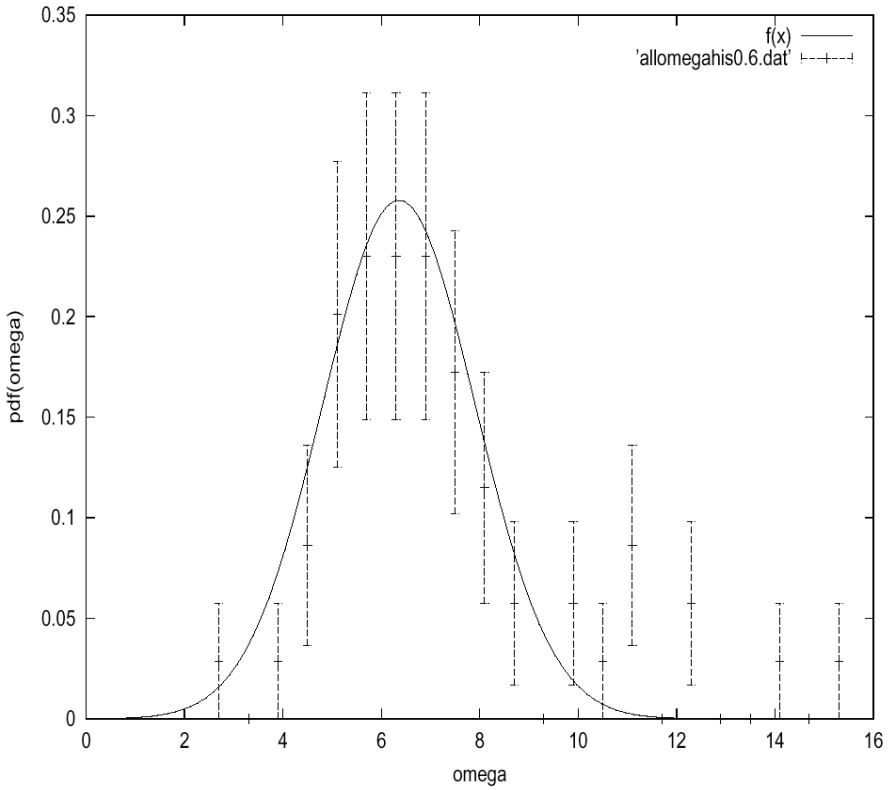

Figure 5: Empirical distribution of the log-periodic angular frequency ω in eq. (1) for over thirty case studies. The fit with a Gaussian distribution gives $\omega \approx 6.36 \pm 1.55$. The smaller peak centered on $11-12$ suggests the existence of a second discernable harmonics at $2\omega \approx 12$.

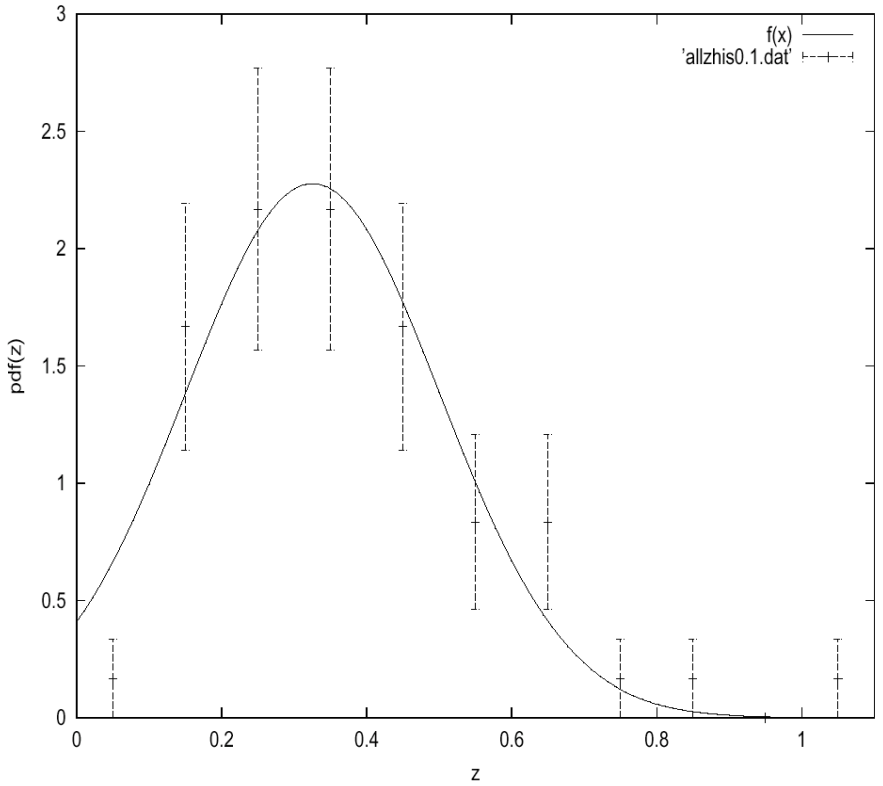

Figure 6: Empirical distribution of the exponent z of the power law in eq. (1) for over thirty case studies. The fit with a Gaussian distribution gives $\beta \approx 0.33 \pm 0.18$.

Demonstration of universal values of z and omega across many different bubbles at different epochs and different markets

A. Johansen and D. Sornette, Endogenous versus Exogenous Crashes in Financial Markets, (http://arXiv.org/abs/cond-mat/0210509)

Why do we have a big brain?
Discrete Hierarchical Organization of Social Group Sizes

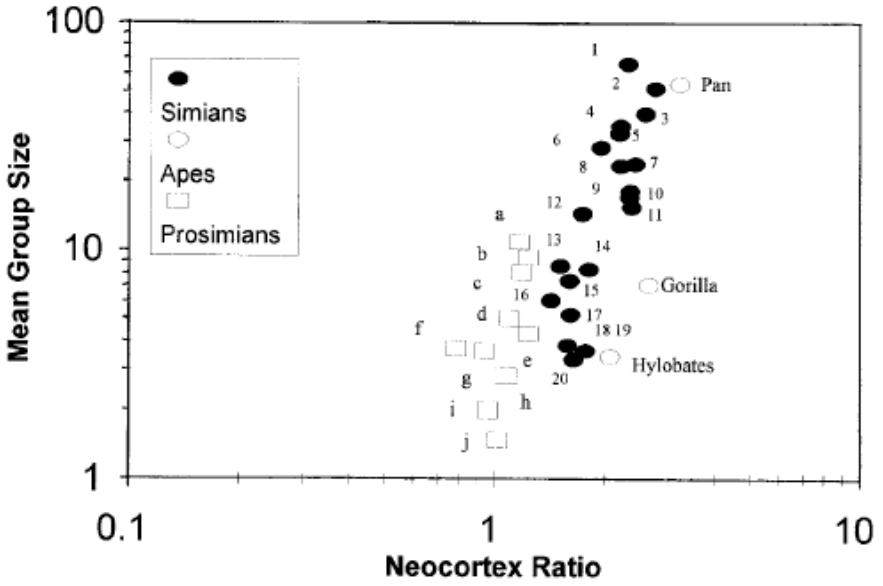

Figure 3. Mean group size plotted against neocortex ratio for individual genera, shown separately for prosimian, simian, and hominoid primates. Prosimian group size data, from Dunbar and Joffe,[25] include species for which neocortex ratio is estimated from total brain volume. Anthropoid data are from Dunbar.[24] Simians: 1, *Miopithecus;* 2, *Papio;* 3, *Macaca;* 4, *Procolobus;* 5, *Saimiri;* 6, *Erythrocebus;* 7, *Cercopithecus;* 8, *Lagothrix;* 9, *Cebus;* 10, *Ateles;* 11, *Cercocebus;* 12, *Nasalis;* 13, *Callicebus;* 14, *Alouatta;* 15, *Callimico;* 16, *Cebuella;* 17, *Saguinus;* 18, *Aotus;* 19, *Pithecia;* 20, *Callicebus.* Prosimians: a, *Lemur;* b, *Varecia;* c, *Eulemur;* d, *Propithecus;* e, *Indri;* f, *Microcebus;* g, *Galago;* h, *Hapalemur;* i, *Avahi;* j, *Perodictus.*

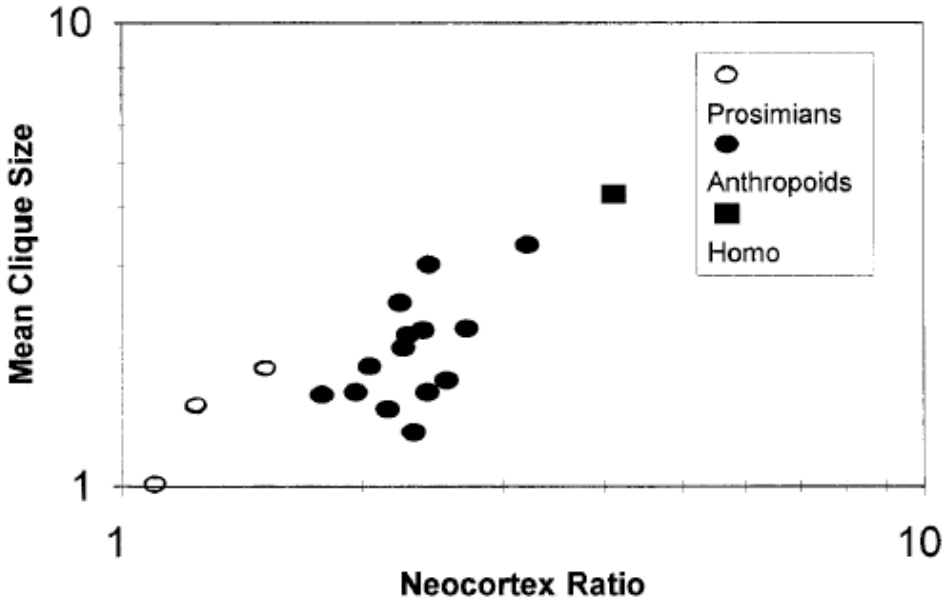

Figure 6. Mean grooming clique size plotted against mean neocortex ratio for individual primate genera. The square is *Homo sapiens.* Species sampled are *L. catta, L. fulvus, Propithecus, Indri, S. sciureus, C. apella, C. torquatus, A. geoffroyi, A. fusciceps, P. badius, P. entellus, P. pileata, P. johnii, C. campbelli, C. diana, C. aethiops, C. mitis, E. patas, M. mulatta, M. fuscata, M. arctoides, M. sylvana, M. radiata, P. anubis, P. ursinus, P. cynocephalus, P. hamadryas, T. gelada, P. troglodytes, P. paniscus.* (Redrawn from Kudo, Lowen, and Dunbar,[51] Fig. 4a.)

W.-X. Zhou, D. Sornette, R.A. Hill and R.I.M. Dunbar Proc. Nat. Acad. Sci. (USA) 272, 439-444 (2005)

Source	Support Clique	Sympathy group	Camp	Village	Tribe
[11]	3.01				
[12]	3.3				
[13]	4.47	11.6			
[14]	3.30				
[15]		10.9			
[16]		14.0/15.1/13.5/13.8			
[17]		$8 \sim 9$			
[18]		14.5			
[19]		10.2			
[20, 21]		15			
[22, 23]		15.0/14.3/14.8/14.2			
[24]		14.4			
[25]			25-30	221.5	886
[26]			27.3	202.5	1237.3
[27]			48	90	2290
[28]			26.5	53-159	450
[29]			60	109.1	1200
[30]			26.8/40-50	90-120	471/1625
[31]			21-85		2000
[32]			18.6	152.3	2693
[33]			25-35	60-100	1050
[34]			31.8/62.7		413
[35]			10-60	60-250	
[36]			50-75		
[37]			40-120		
[38]				128.7/180	
[39, 40]				60-150	
[41]				150	483
[42]				100	600
[43]				101.9	663

circle (support clique), triangle (sympathy group), diamond (bands), stars (cognitive groups),

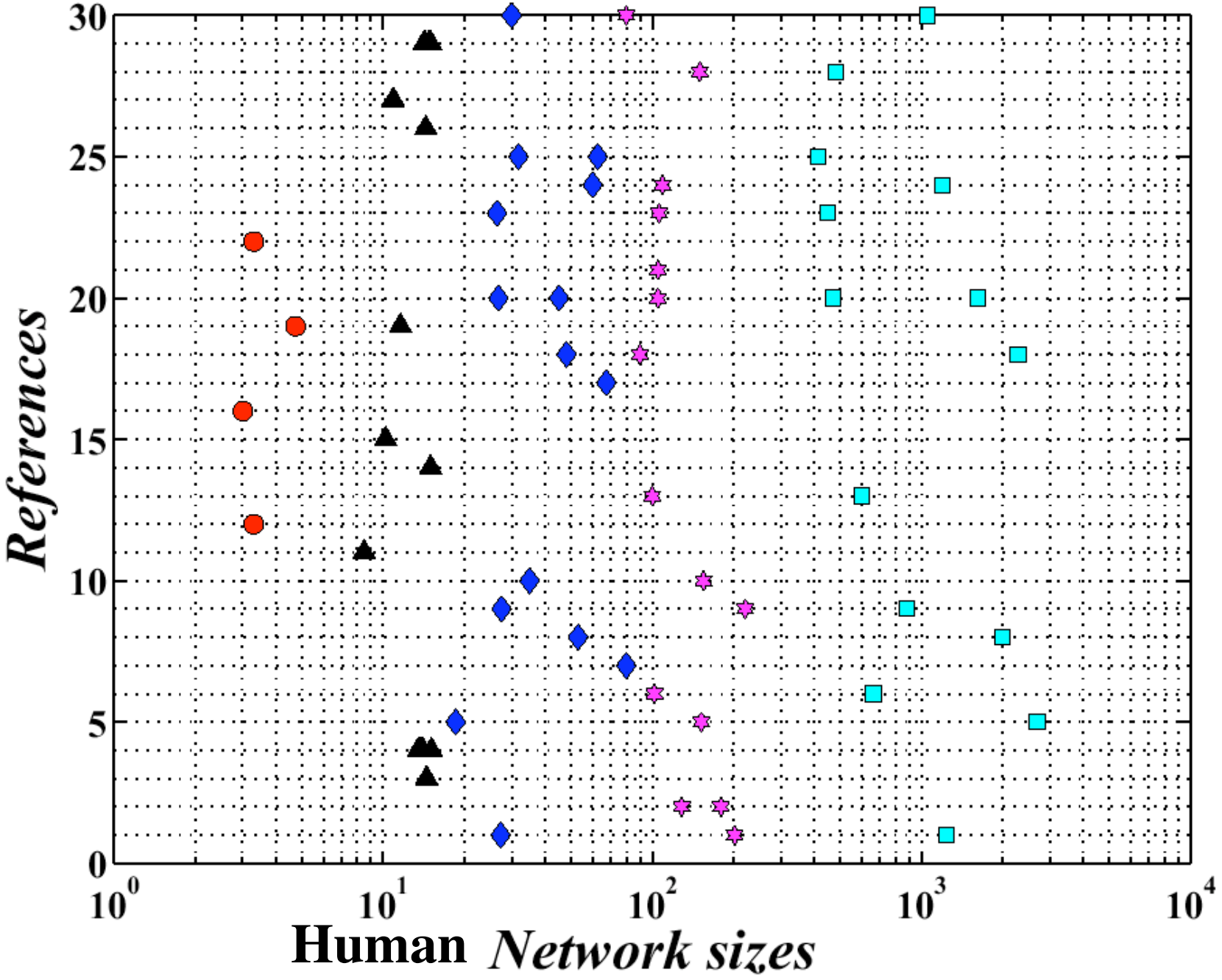

Method 1: Average sizes of different network layers. To summarize the previously cited data, we denote S_1 as the mean support clique size, S_2 the mean sympathy group, S_3 the mean band size, S_4 the mean cognitive group size, and S_5 and S_6 the size of small and large tribes. Here, we do not address the relevance of this classification (which will be done below) but only characterize it quantitatively. The previously cited data gives $S_0 = 1$ (individual or ego), $S_1 = 4.6$, $S_2 = 14.3$, $S_3 = 42.6$, $S_4 = 132.5$, $S_5 = 566.6$, and $S_6 = 1728$. In order to determine the possible existence of a discrete hierarchy, we construct the series of ratios S_i/S_{i-1} of successive mean sizes:

$$S_i/S_{i-1} = 4.58, 3.12, 2.98, 3.11, 4.28, 3.05\,, \quad \text{for } i = 1, \cdots, 6\,. \qquad (1)$$

This result suggests that humans form groups according to a discrete hierarchy with a prefered scaling ratio between 3 and 4: the mean of S_i/S_{i-1} is 3.50.

Method 2

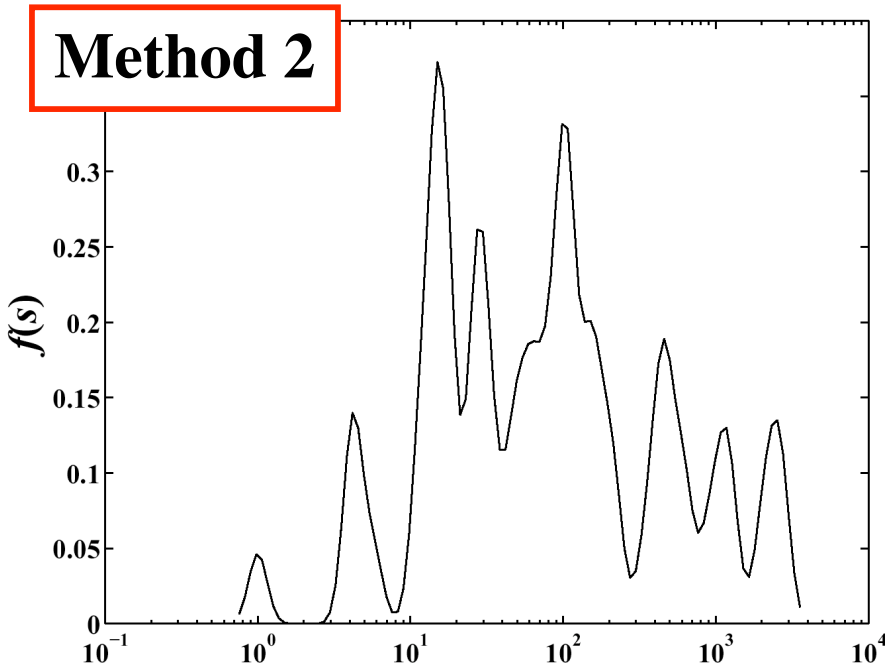

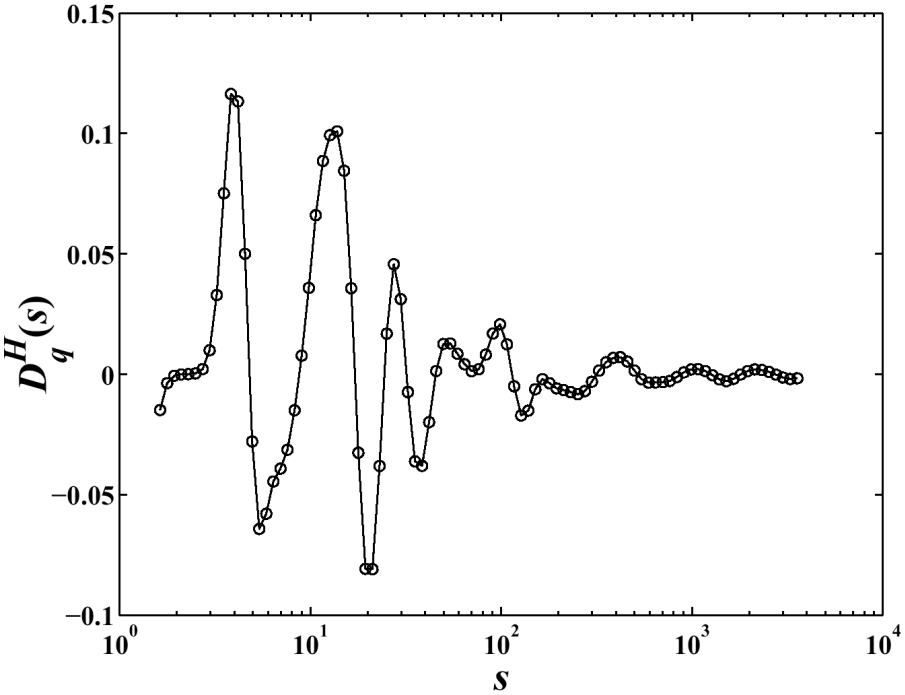

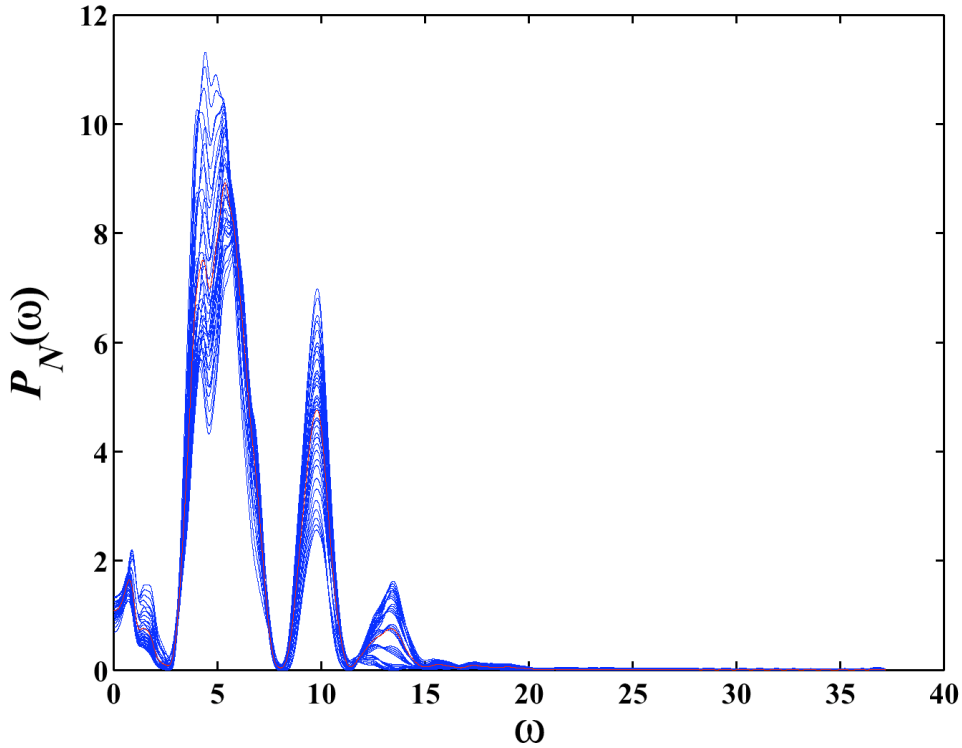

Preferred scaling ratio close to 3

Discrete Hierarchical Organization of Social Group Sizes

W.-X. Zhou[1], D. Sornette[1,2,3], R.I.M. Dunbar[4] and R. Hill[5]

Proc. Nat. Acad. Sci. (USA) 272, 439-444 (2005)

Method 3: Probability density function and generalised q-analysis of individual networks. We apply the same analysis to individual social networks based upon the exchange of Christmas cards in contemporary Western Society.

Hill, R.A. and Dunbar, R.I.M., *Human Nature* **14**. 53-72 (2003).

$$D_q^H f(x) \stackrel{d}{=} \frac{f(x) - f(qx)}{[(1-q)x]^H}$$

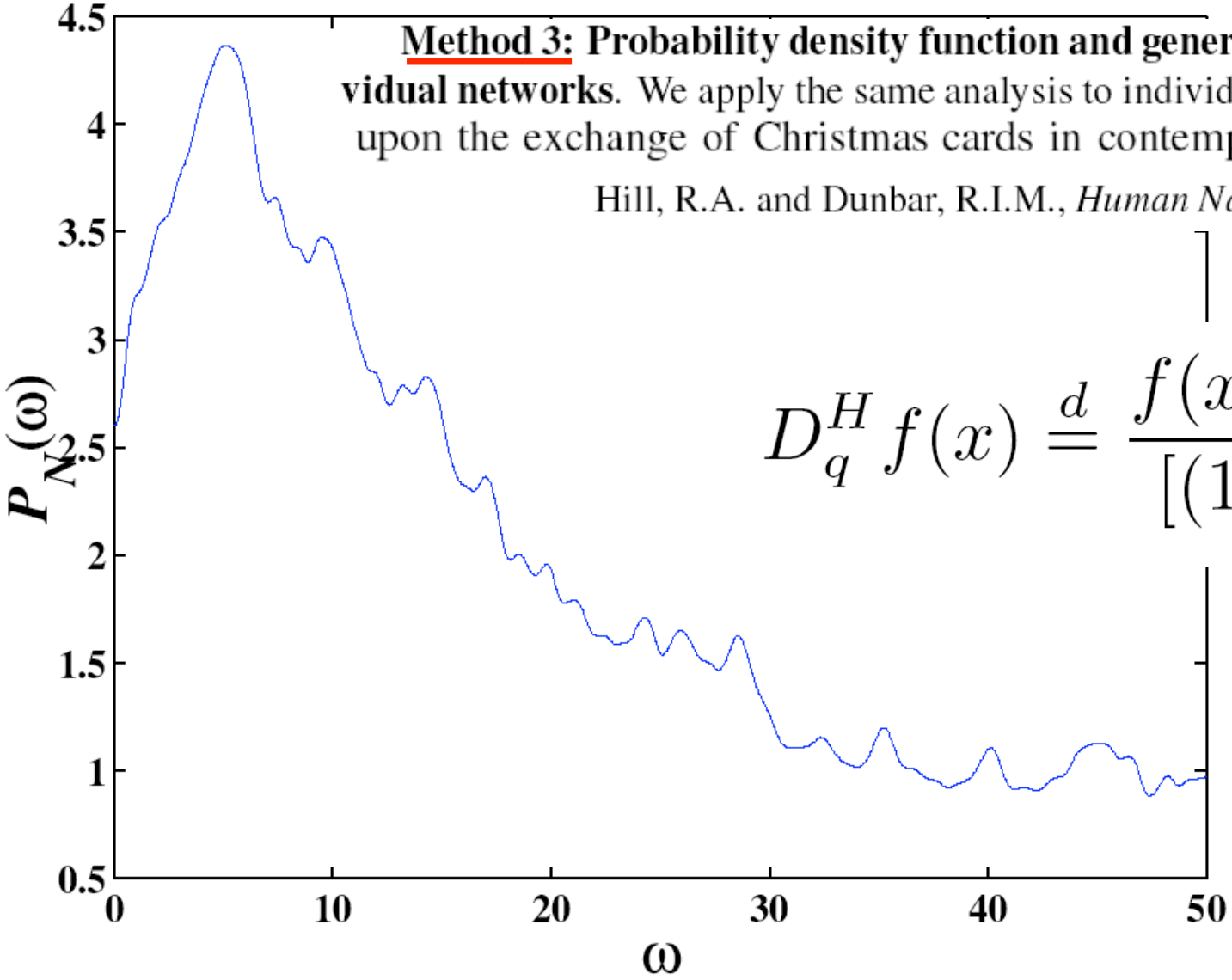

Figure 5: Average Lomb periodogram $P_N(\omega)$ of the (H,q)-derivative $D_q^H(s)$ with respect to the number of receivers of the residual contact frequency for each individual in the Christmas card experiment, as a function of the angular log-frequency ω of the (H,q)-derivative, over the 42 individuals and different pairs of (H,q) with $-1 \leq H \leq 1$ and $0.80 \leq q \leq 0.95$.

A real-life example of a hierarchical network

- **Sections (squads): 10-12 soldiers**
- **Platoons (of 3 sections, ≈ 35 soldiers)**
- **Companies (3-4 platoons, ≈ 120-150 soldiers)**
- **Battalions (3-4 companies plus support units, ≈ 550-800)**
- **Regiments (or brigades) (3 battalions plus support,2500+)**
- **Divisions (3 regiments)**
- **Corps (2-3 divisions)**
- **Armies**
- **Country**

Operational Unit Diagram

This diagram provides information on how Army operational units are organized - from the Theater Army, Field Army and Army Group level, down through Corps, Divisions, Brigades, Battalions, Companies, Platoons and ending with Squads & Sections - and the typical rank of the Commander of these type units. It also provides a listing of additional unit types that don't fall cleanly into this hierarchal structure. A short description of each organization is provided when you select a box, or when you select one of the additional unit types.

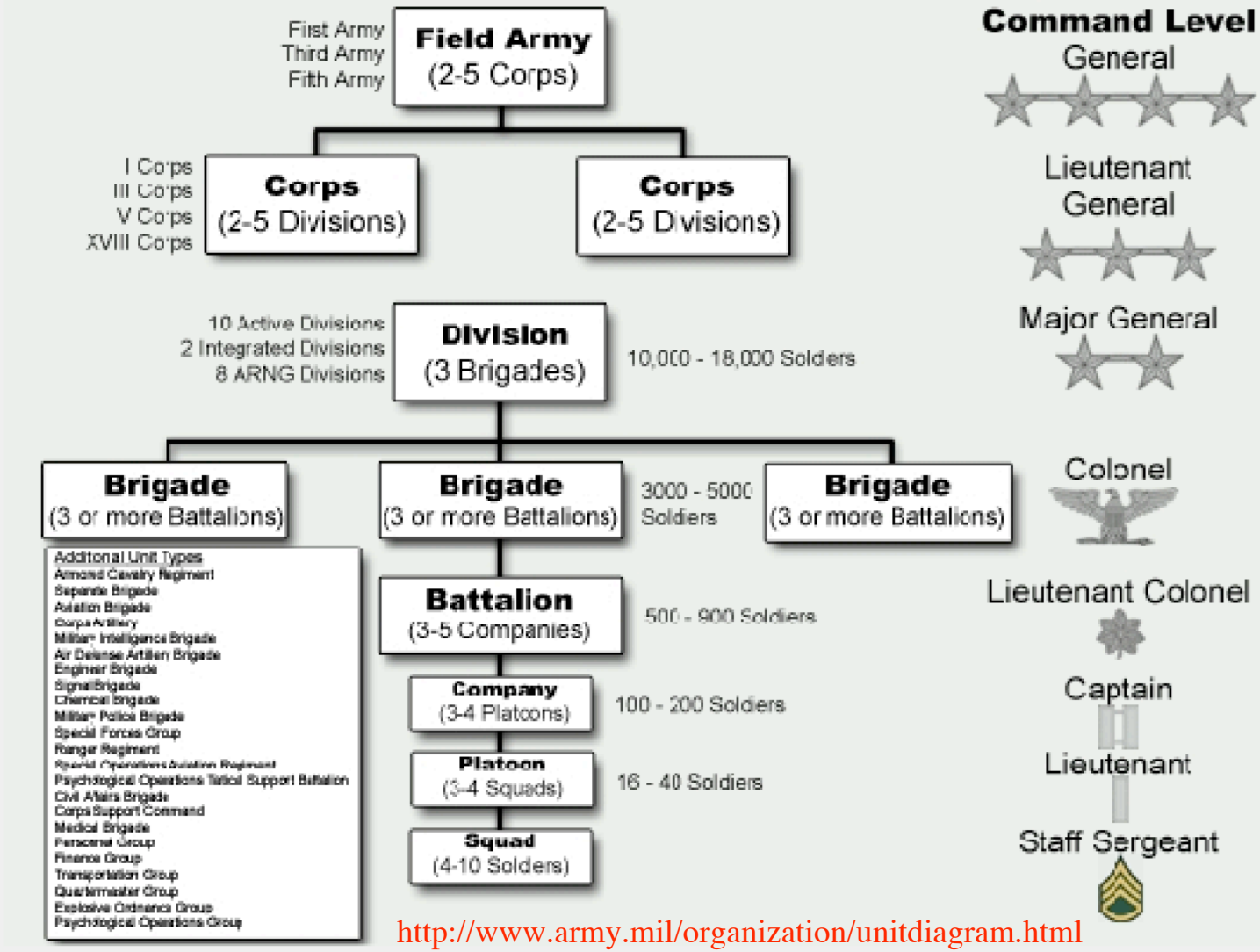

http://www.army.mil/organization/unitdiagram.html

Towards a methodology to identify and predict crash risks

- Development of methods to diagnose bubbles
- Crashes are not predictable
- Only the end of bubbles can be forecasted
- 2/3 ends in a crash
- Multi-time-scales
- Probability of crashes; alarm index
  - Successful advanced predictions: Oct. 1997; Aug. 1998, April 2000, real-estate bubble UK mid-2004, US mid-2006
  - False alarms: Oct. 1997

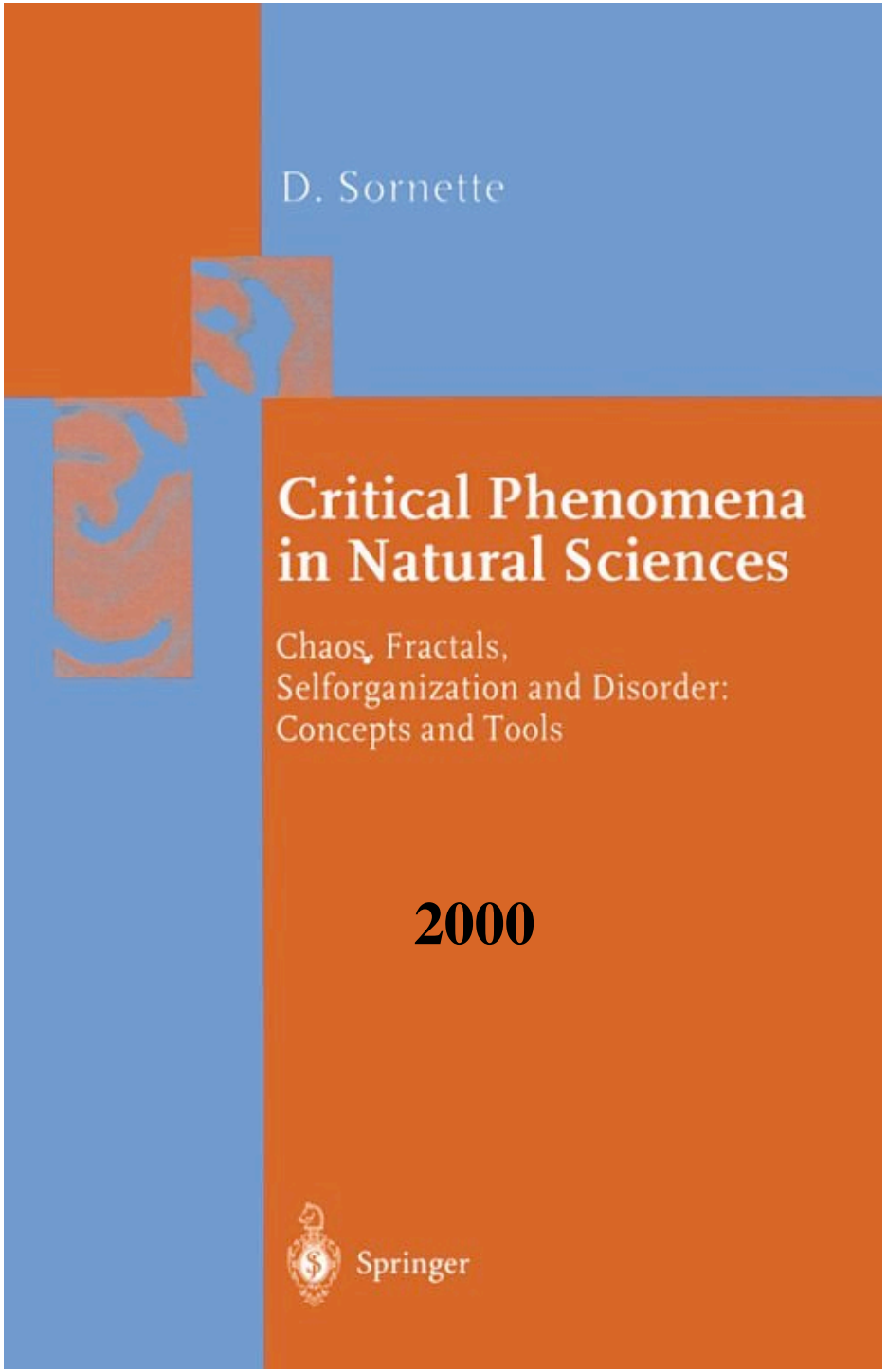
D. Sornette
Critical Phenomena in Natural Sciences
Chaos, Fractals, Selforganization and Disorder: Concepts and Tools
2000
Springer

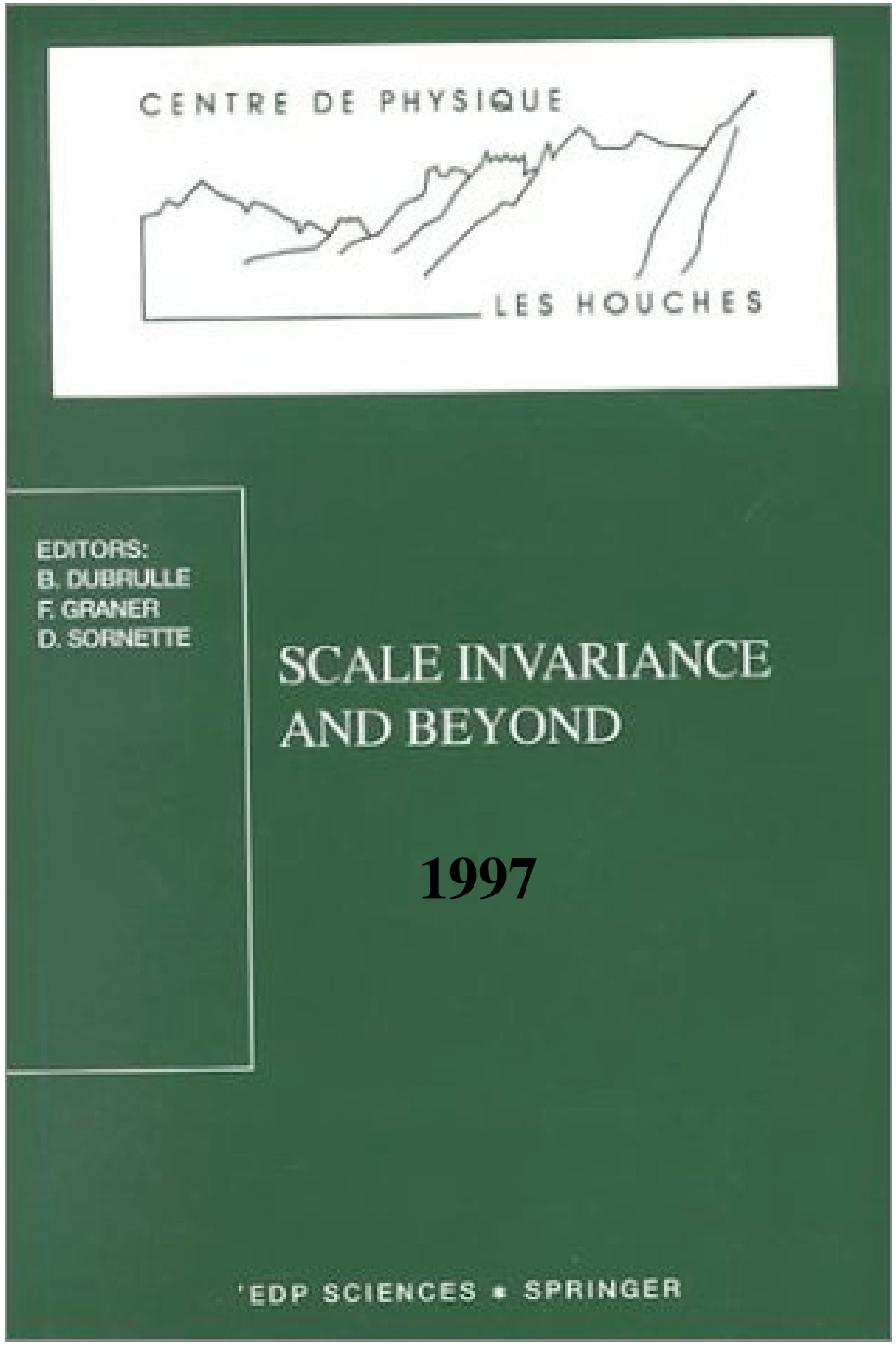
CENTRE DE PHYSIQUE
LES HOUCHES
EDITORS:
B. DUBRULLE
F. GRANER
D. SORNETTE
SCALE INVARIANCE AND BEYOND
1997
EDP SCIENCES • SPRINGER

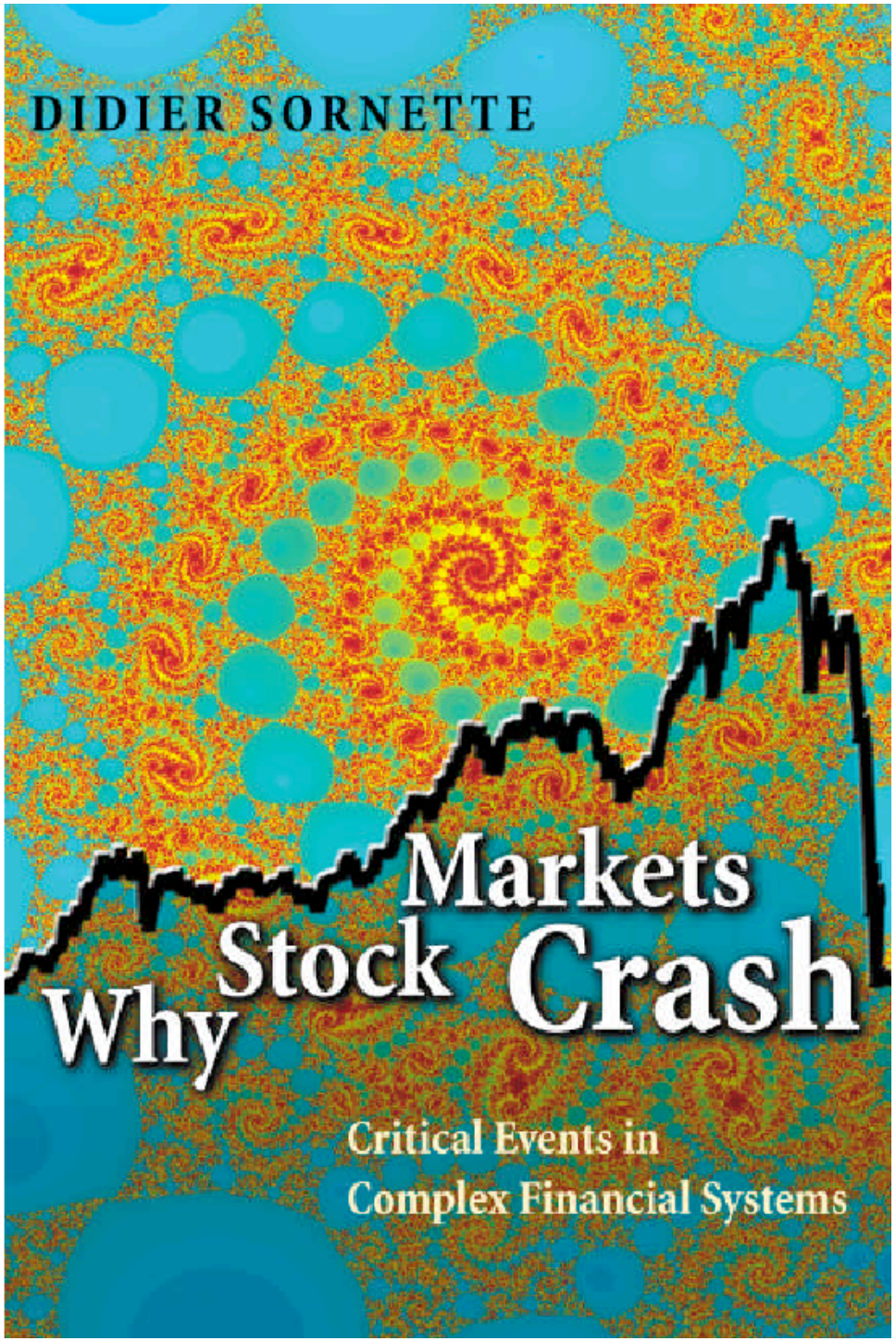

Princeton University Press
Jan. 2003

http://www.ess.ucla.edu/faculty/sornette/